Universidade do Estado do Rio de Janeiro
Centro de Tecnologia e Ciências
Instituto de Química

Julia Coelho Lemos

Global optimization of the design of shell-and-tube heat exchangers considering fouling modelling

Rio de Janeiro
2018

Julia Coelho Lemos

Global optimization of the design of Shell-and-Tube Heat Exchangers Considering fouling modelling

Tese apresentada, como requisito parcial para a obtenção do grau de Doutor, ao Programa de Pós-Graduação em Engenharia Química, da Universidade do Estado do Rio de Janeiro. Área de concentração: Processos Químicos, Petróleo e Meio Ambiente.

Orientadores: Prof. Dr. André Luiz Hemerly Costa

Prof. Dr. Miguel Jorge Bagajewicz

Rio de Janeiro

2018

CATALOGAÇÃO NA FONTE
UERJ/REDE SIRIUS/CTC/Q

L557 Lemos, Julia Coelho.
Global optimization of the design of shell-and-tube heat exchangers considering fouling modelling. / Julia Coelho Lemos. - 2018.
116 f.

Orientador: André Luiz Hemerly Costa.
Orientador: Miguel Jorge Bagajewicz
Tese (doutorado) – Universidade do Estado do Rio de Janeiro, Instituto de Química.

1. Permutadores térmicos - Teses. 2. Simulação e otimização – Teses. 3. Deposição - Teses. I. Costa, André Luiz Hemerly. II. Bagajewicz, Miguel Jorge. III. Universidade do Estado do Rio de Janeiro. Instituto de Química. IV. Título.

CDU 536.24

_____ _____

Assinatura Data

Julia Coelho Lemos

Global Optimization of the Design of Shell-and-Tube Heat Exchangers Considering Fouling Modelling

Tese apresentada, como requisito parcial para a obtenção do grau de Doutor, ao Programa de Pós-Graduação em Engenharia Química, da Universidade do Estado do Rio de Janeiro. Área de concentração: Processos Químicos, Petróleo e Meio Ambiente.

Aprovada em 30 de outubro de 2018.

Orientadores:

Prof. Dr. André Luiz Hemerly Costa
Instituto de Química – UERJ

Prof. Dr. Miguel Jorge Bagajewicz
Instituto de Química – UERJ

Banca Examinadora:

_____
Prof. Dr. André Luís Alberton
Instituto de Química – UERJ

_____
Prof. Dr. Eduardo Rocha de Almeida Lima
Instituto de Química – UERJ

_____
Prof.ª Dra. Heloísa Lajas Sanches
Escola de Química – UFRJ

_____
Prof. Dr. Eduardo Mach Queiroz
Escola de Química – UFRJ

_____
Dr. Sérgio Gregório de Oliveira
CENPES– PETROBRAS

Rio de Janeiro

2018

DEDICATÓRIA

Dedico esta tese à minha família por todo o apoio e incentivo em todos os momentos.

AGRADECIMENTOS

Ao meu orientador, Professor André Luiz Hemerly Costa, por todo o apoio, por acreditar em mim e por sempre estar disponível quando preciso. Tenho imensa admiração por seu trabalho e pela forma como o conduz.

Ao meu orientador, Professor Miguel Bagajewicz, por todas as suas ideias e seu amplo conhecimento na área, que ajudaram no desenvolvimento desta tese, e por me ensinar a lutar pelas minhas próprias ideias.

Ao meu marido, Marcelo, por todo o apoio e compreensão nesta fase da minha formação. Obrigada por sempre apoiar as minhas escolhas e contribuir para que eu tenha tranquilidade suficiente para continuar seguindo o caminho que escolhi.

Aos meus pais, Luiz e Lucia, que sempre me mostraram o quanto era importante buscar conhecimento e me apoiaram em todas as minhas escolhas, sei que sem eles provavelmente não estaria concluindo esta tese.

À minha avó, Zelia, que sempre esteve ao meu lado e infelizmente faleceu em 2009, mas com certeza foi fundamental na minha formação como ser humano.

À Babi, por tornar minha vida mais feliz e tranquila só com um olhar e sempre que possível estar ao meu lado.

À minha amiga desde a graduação, Erika, por sempre ter estado ao meu lado nesta longa caminhada.

À Universidade do Estado do Rio de Janeiro, por ter feito parte de toda a minha vida até então, desde criança até hoje.

À CAPES, pelo apoio financeiro.

RESUMO

LEMOS, Julia Coelho. *Global Optimization of the Design of Shell-and-Tube Heat Exchangers Considering Fouling Modelling*, 2018. 116 f. Tese (Doutorado em Engenharia Química) - Instituto de Química, Universidade do Estado do Rio de Janeiro, Rio de Janeiro, 2018.

Trocadores de calor são equipamentos responsáveis pela alteração da temperatura e/ou estado físico de correntes materiais. Durante a sua operação, estes equipamentos estão sujeitos ao fenômeno da deposição, o que causa a diminuição na transferência de calor, levando a um aumento nos custos operacionais e de manutenção. A abordagem usualmente adotada para lidar com este problema durante o projeto dos trocadores de calor é inserir resistências térmicas adicionais no cálculo do coeficiente global de transferência de calor. Entretanto, estas resistências adicionais, representadas na forma de resistências de depósito, ignoram o fato que a taxa de deposição é afetada pelas condições termofluidodinâmicas presentes no interior do equipamento. Por esta razão, cada alternativa de solução para o problema de projeto está associada a uma taxa de deposição diferente. Desta forma, a presente tese apresenta uma investigação de como os modelos de deposição podem ser inseridos no projeto de trocadores de calor na forma de um problema de otimização. Através da aplicação de técnicas de programação matemática, são propostas formulações do problema levando em conta dois tipos de modelos de deposição: (i) um modelo onde a resistência de depósito depende da velocidade de escoamento, tipicamente aplicável a sistemas envolvendo correntes de água de resfriamento e (ii) um modelo de taxa de deposição dependente da velocidade e da temperatura, característico de correntes de óleo cru em baterias de pré-aquecimento em unidades de destilação atmosférica em refinarias. A primeira formulação resulta em um problema de programação linear inteira (ILP) e a segunda formulação corresponde a um problema de programação linear inteira mista (MILP). O caráter linear de ambas as formulações permite a identificação do ótimo global, mesmo utilizando algoritmos de otimização convencionais. As formulações propostas obtiveram resultados compatíveis com o esperado, gerando soluções melhores que as obtidas através da formulação convencional, que considera resistências de depósito constantes.

Palavras-chave: Trocador de calor. Otimização. Deposição.

ABSTRACT

LEMOS, Julia Coelho. *Global Optimization of the Design of Shell-and-Tube Heat Exchangers Considering Fouling Modelling*, 2018. 116 f. Tese (Doutorado em Engenharia Química) - Instituto de Química, Universidade do Estado do Rio de Janeiro, Rio de Janeiro, 2018.

Heat exchangers are equipment responsible for altering the temperature and/or physical state of process streams. During the operation, these equipment are subjected to fouling phenomenon, what causes a decrease in heat transfer, increasing the operational and maintenance costs. The approach used to deal with this problem during the heat exchanger design is to insert additional thermal resistances when calculating the overall heat transfer coefficient. However, these additional resistances, represented as fouling resistances, ignore the fact that the fouling rate is affected by the thermo-fluid dynamic conditions in the interior of the equipment. Therefore, each alternative for the design solution is associated to a different fouling rate. Concluding, the present thesis presents an investigation of how the fouling models can be inserted in the heat exchanger design optimization problem. Through applying mathematical programming techniques, formulations of the problem are proposed considering two types of fouling models: (i) a model in which the fouling resistance depends on the flow velocity, typically applied to systems involving water streams and (ii) a fouling rate model that depends on flow velocity and temperature, applied to crude oil streams in preheat trains in atmospherically distillation units in refineries. The first formulation results in an integer linear programming problem (ILP) and the second one in a mixed integer linear programing problem (MILP). The linear nature of both formulations allows the identification of the global optimum, even when using conventional optimization algorithms. The formulations proposed are able to identify the feasible solutions for the heat exchanger design with lower cost than those obtained through the conventional design considering constant fouling resistances.

Keywords: Heat Exchanger. Optimization. Fouling.

LISTA DE ILUSTRAÇÕES

LISTA DE TABELAS

LISTA DE ABREVIATURAS E SIGLAS

TEMA	Tubular Exchangers Manufacturers Association
PSO	particle swarm optimization
SA	simulated annealing
LP	linear programing
ILP	integer linear programing
MILP	mixed integer linear programing
MINLP	mixed integer nonlinear programing
GAMS	General algebraic modeling system

LISTA DE SÍMBOLOS

- Latin letters

A	area ,m^2
$\widehat{Aexc}$	excess area, %
$Areq$	required area, m^2
$\widehat{Af}$	fouling model parameter, m^2K/J
Ar	area between adjacent baffles, m^2
$\widehat{Bf}$	fouling model parameter, m^2K/J
dte	outer tube diameter, m
dti	inner tube diameter, m
Deq	equivalent diameter, m
Ds	shell diameter, m
Ea	activation energy, J/mol
fs	Darcy friction factor for shell-side
ft	Darcy friction factor for tube-side
F	LMTD correction factor
FAR	free area ratio
FR	formation rate on fouling model, m^2K/J
FR_{min}	fouling formation rate for minimum surface temperature, m^2K/J
FR_{max}	fouling formation rate for clean surface, m^2K/J
$\hat{g}$	gravity acceleration, m/s^2
hs	convective heat transfer coefficient for shell-side, W/m^2K
ht	convective heat transfer coefficient for tube-side, W/m^2K
$\widehat{kRfs}$	shell-side fouling model parameter
$\widehat{kRft}$	tube-side fouling model parameter
$\widehat{ks}$	thermal conductivity of the fluid on shell-side, W/m·K
$\widehat{kt}$	thermal conductivity of the fluid on tube-side, W/m·K
lay	layout of the heat exchanger
lbc	baffle spacing, m
ltp	tube pitch, m
L	tube length, m
$\widehat{ms}$	mass flow rate on shell-side, kg/s

$\widehat{mt}$	mass flow rate on tube-side, kg/s
Nb	number of baffles
Npt	number of tube passes
Ntp	number of tubes per pass
Ntt	total number of tubes
Nus	Nusselt number for shell-side
Nut	Nusselt number for tube-side
$\widehat{PDs}_{srow}$	standard shell diameter, m
$\widehat{Pdte}_{srow}$	standard outer tube diameter, m
$\widehat{Pdti}_{srow}$	standard inner tube diameter, m
$\widehat{PL}_{srow}$	standard tube length, m
$\widehat{Play}_{srow}$	tube layout
$\widehat{PNb}_{srow}$	number of baffles
$\widehat{PNpt}_{srow}$	number of tube passes
$\widehat{PNtt}_{srow}$	total number of tubes
$\widehat{Prp}_{srow}$	standard tube pitch ratio
$\widehat{Prs}$	Prandtl for shell-side
$\widehat{Prt}$	Prandtl for tube-side
$\hat{Q}$	heat load, W
R	ideal gas constant, J/mol K
rp	pitch ratio
Res	Reynolds number for shell-side
Ret	Reynolds number for tube-side
Rfs	fouling factor on shell-side, m^2K/W
Rft	fouling factor on tube-side, m^2K/W
$\widehat{Rf}^{MAX}$	maximum fouling resistance on the tube-side, m^2K/W
Rf^{∞}	asymptotic fouling resistance on tube-side, m^2K/W
SR	suppression rate on fouling model, m^2K/J
$\widehat{Tc}^{av}$	cold stream average temperature, K
$\widehat{Tci}$	cold stream inlet temperature, ºC
$\widehat{Tco}$	cold stream outlet temperature, ºC
$\widehat{Thi}$	hot stream inlet temperature, ºC
$\widehat{Tho}$	hot stream outlet temperature, ºC

Ts	surface temperature, K
Tw	wall temperature, K
U	overall heat transfer coefficient, W/m^2 K
vs	shell-side flow velocity, m/s
$\widehat{vsmax}$	maximum shell-side flow velocity, m/s
$\widehat{vsmin}$	minimum shell-side flow velocity, m/s
vt	tube-side flow velocity, m/s
$\widehat{vtmax}$	maximum tube-side flow velocity, m/s
$\widehat{vtmin}$	minimum tube-side low velocity, m/s
wRf	variable representing the fouling resistance, m^{2}K/W
$w1Rf^{\infty}$	variable representing the asymptotic resistance, m^{2}K/W
$w2Rf^{\infty}$	variablerepresenting the asymptotic resistance, m^{2}K/W
$w3Rf^{\infty}$	variablerepresenting the asymptotic resistance, m^{2}K/W
$y1$	binary variable to map the fouling resistance value
$y2$	binary variable to map the fouling resistance value
$y3$	binary variable to map the fouling resistance value
yd_{sd}	binary variable representing the tube diameter
yDs_{sDs}	binary variable representing the shell diameter
yL_{sL}	binary variable representing the tube length
$ylay_{slay}$	binary variable representing the tube layout
yNb_{sNb}	binary variable representing the number of baffles
$yNpt_{sNpt}$	binary variable representing the number of tube passes
yrp_{srp}	binary variable representing the tube pitch ratio
$yrow_{srow}$	binary variable that represents simultaneously all discrete variables

- Greek letters

α	fouling model parameter, m^{2}K/J
$\widehat{\alpha Rfs}$	shell-side fouling model parameter
$\widehat{\alpha Rft}$	tube-side fouling model parameter
ε	small value used in the additional constraints
γ	fouling model parameter, m^{2}K/J
ΔPs	pressure drop on shell-side, Pa
$\Delta\widehat{Psdisp}$	available pressure drop on shell-side, Pa

ΔPt	pressure drop on tube-side, Pa
$\Delta\widehat{Ptdısp}$	available pressure drop on tube-side, Pa
$\widehat{\Delta T}^{av}$	average temperature difference, K
$\widehat{\Delta Tlm}$	logarithmic mean temperature difference, ºC
$\widehat{\mu s}$	viscosity of the fluid on shell-side, Pa·s
$\widehat{\mu t}$	viscosity of the fluid on tube-side, Pa·s
$\widehat{\rho s}$	density of the fluid on the shell-side, kg/m^3
$\widehat{\rho t}$	density of the fluid on the tube-side, kg/m^3
$\widehat{\psi f}$	threshold model parameter, K

SUMÁRIO

INTRODUCTION

A very common phenomenon that happens in heat transfer equipment is the accumulation of deposits in heat transfer surfaces known as fouling. Those deposits decrease the overall heat transfer coefficient, therefore diminishing the heat recovery. The final impact is the increase in energy consumption, due to the augmentation of the utility consumption. Fouling is a big obstacle that the process plants face during operation.

The traditional approach to include fouling effects during the design of heat exchangers is the insertion of additional thermal resistances in the evaluation of the overall heat transfer coefficient. These thermal resistances are represented by fouling factors, parameters available in the literature, but associated to a considerable level of uncertainty (SHILLING, 2012). The utilization of fixed values of fouling resistances for a given thermal task ignores the fact that the fouling phenomenon depends on the thermo-fluid dynamic conditions inside the equipment. Therefore, different heat exchanger solutions for a design task can be affected by fouling differently, but are associated to the same set of fouling factors during the traditional design approach.

Aiming to contribute to the fouling mitigation issue, this work presents a new approach to address the heat exchanger design problem. Using mathematical programming techniques, the design task is represented by an optimization problem where fouling modelling equations are present. Therefore, this approach can consider, during the design, the relation between the thermo-fluid dynamic conditions associated to each individual configuration and the fouling impact during the future operation of the unit. Previous attempts proposed in the literature in order to consider the fouling models along with the design problem used graphical methods or simplifications that are not very practical or rigorous (BUTTERWORTH, 2002; POLLEY et al. 2002b; SHILLING, 2012).

The proposed investigation explores two different fouling models. The first fouling model describes the fouling resistance in relation to the flow velocity, approach suitable for cooling water streams (NESTA; BENNETT, 2004). The second fouling model investigated explores a model where the fouling rate depends on the flow velocity and temperature (POLLEY et al., 2002a), suitable for fouling prediction in crude oil streams flowing in crude preheat trains in atmospheric distillation units of petroleum refineries. Those two cases were chosen for their importance in the process industry and because the fouling models for them are discussed and detailed in the literature, however the basic ideas explored here can also be extended to other systems.

The approach developed here incorporates the fouling models available in the literature to a heat exchanger design model proposed by Gonçalves et al. (2016, 2017). This previous formulation describes the design problem (with fixed fouling resistances) as an integer linear programing (ILP) problem. The idea behind the development of the ILP model is to use the commercially available values for the geometric parameters and then use binary variables to model the heat exchanger design problem. Hence, the linear form of the optimization problem proposed is rigorously equivalent to the original nonlinear equations, which allows the identification of the global optimum of the corresponding design problem.

This thesis is organized as follows: Chapter 1 brings a brief review of literature with the works that have been developed around the subject of this thesis; Chapter 2 presents the development of the ILP heat exchanger design model, employed as starting point of the proposed approach; Chapter 3 encompasses the heat exchanger design optimization problem considering the fouling resistance as a function of velocity and its results; Chapter 4 presents the optimization problem with a fouling rate model function of velocity and temperature plus its results and conclusions.

1 REVIEW OF THE LITERATURE

The review of literature will encompass the following subjects: shell-and-tube heat exchangers and its geometric parameters, fouling models and the main works regarding heat exchanger design considering fouling models.

1.1. **Shell-and-tube heat exchangers**

Heat exchangers are static equipment that promote the heat transfer between a hot stream and a cold stream. The most common type of heat exchanger in the process industries is the shell-and-tube. This equipment is composed by a shell in which there is a tube bundle, with one stream flowing inside the tubes and another through the shell.

Figure 1 shows a scheme of a heat exchanger and its parts. The main building elements are numbered and their nomenclature is displayed in Table 1 (TEMA, 2007).

Figure 1 – Shell-and-tube heat exchanger scheme.

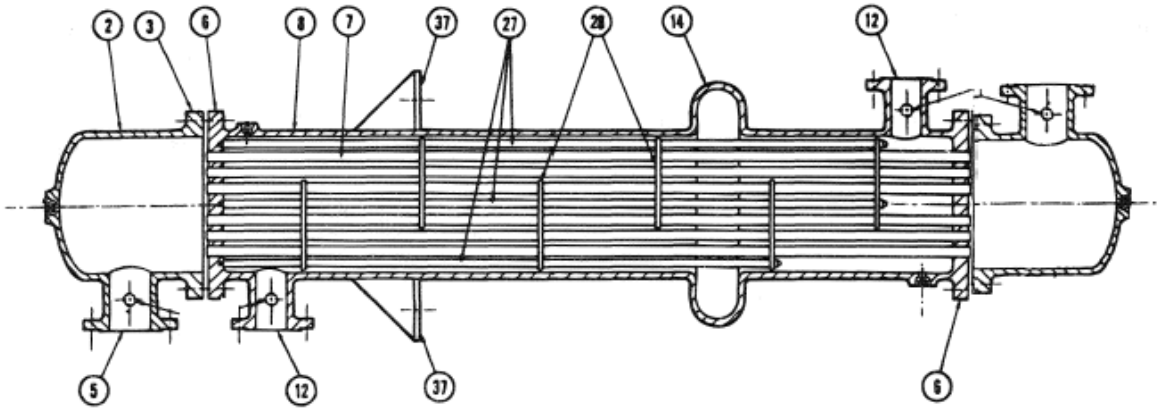

Fonte: TEMA, 2007

Table 1 – Main heat exchanger elements

NOMENCLATURE

2	Stationary head
3	Flange
5	Nozzle
6	Stationary tube sheet
7	Tubes
8	Shell
12	Shell nozzle
14	Expansion joint
27	Tie rods and spacers
28	Transverse baffles
37	Support saddle

The recommended values regarding the heat exchanger geometric variables that will appear during the thesis were based on what is proposed by Tubular Exchangers Manufacturers Association (TEMA, 2007).

1.1.1 Tubes

The tube bundle is a set of tubes made especially for heat transfer, where the material of the tubes will vary accordingly to the nature of the streams and operating conditions. Those tubes have different nominal sizes (external diameter) and the thickness will be expressed according to a BWG scale (SAUNDERS, 1988).

Those tubes are connected to metallic tube discs called tube sheets that will sustain them. Figure 2 shows a tube bundle being constructed, it is possible to observe that the tubes are tide in the tube sheet.

Figure 2 – Tube bundle under construction

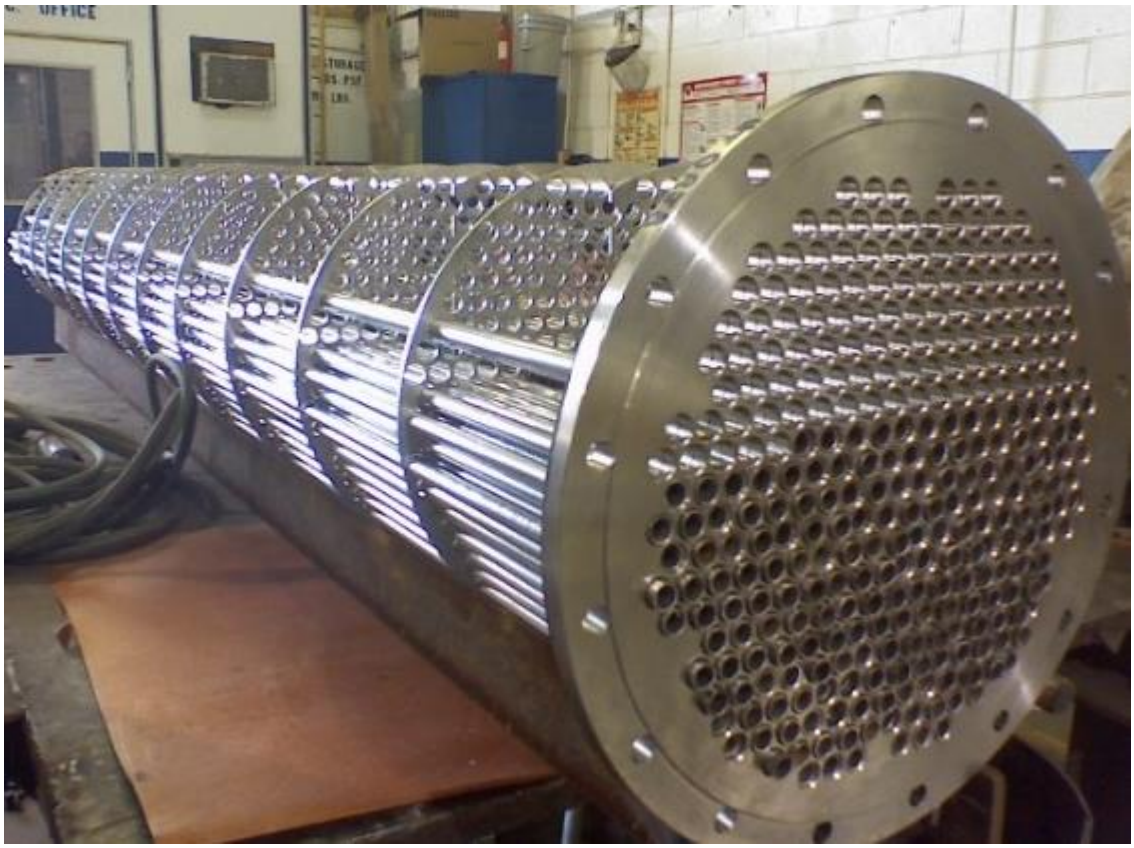

Fonte: https://www.indiamart.com/proddetail/ss-heat-exchanger-tube-bundle-10702114730.html – acesso 01/10/2018 às 15:22

1.1.2 Baffles

Baffles have two main goals; the first one is structural, allowing the tubes to be supported over several points along the heat exchanger, avoiding vibration problems (SAUNDERS, 1988). The second goal is to promote the transversal flow over the tube bundle, which favors the heat transfer. In this case, the most used baffle is the single segmental baffle, shown in Figure 3.

Figure 3 – Segmental baffle

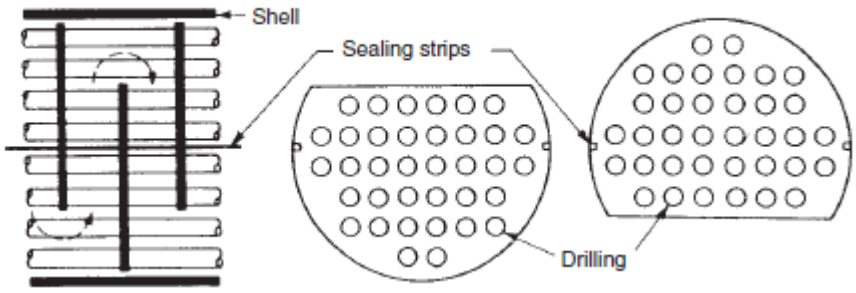

Fonte: SERTH, 2007.

The percentage of baffle cut (Figure 4) is one of the project variables in the heat exchanger design and it is defined as the ratio between the cut height and the shell inner diameter. The fixation of the baffles is made with the help of tie rods and spacers.

Figure 4 – Baffle cut ratio

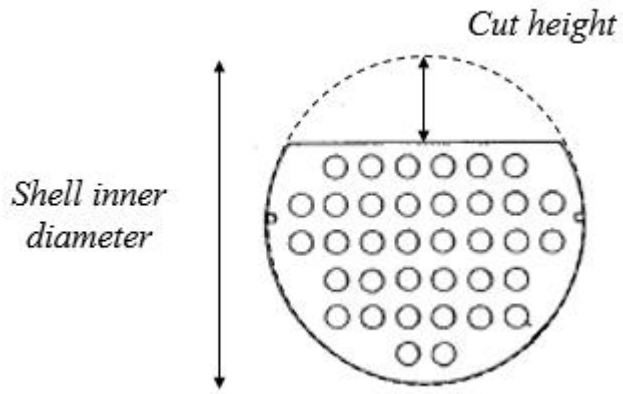

Fonte: A autora, 2018

The baffle spacing (*lbc*) is defined taking into account the turbulence promotion and the pressure drop limits, this is also a very important variable in heat exchanger design. However, a limit must be obeyed between the minimum and the maximum baffle spacing. Figure 5 illustrate the geometric nature of this variable.

Figure 5 – Baffle spacing

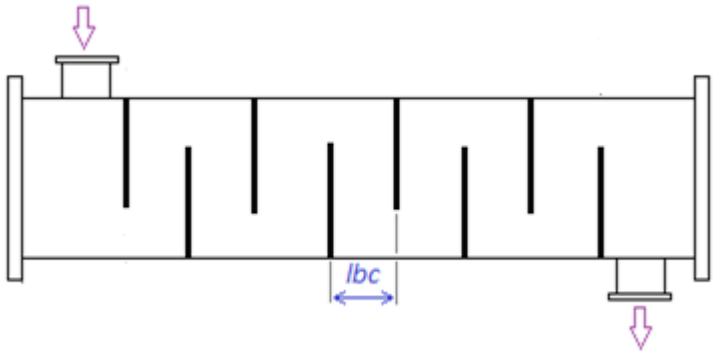

Fonte: A autora, 2018.

1.1.3 Layout and tube pitch

The distance between the centers of two adjacent tubes in a tube bundle is called pitch, and its configuration, that characterizes the unitary cell of a bundle, is called layout, both are geometric variables in the heat exchanger design. Figure 6 shown the types of tube layouts available.

Figure 6 – Tube layouts

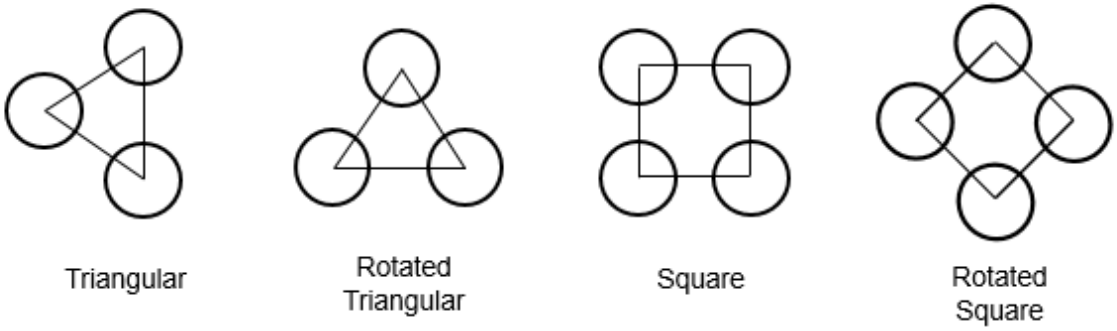

Fonte: A autora, 2018.

By analyzing the options, we realize that the triangular layouts are more compactthan the square ones (considering the same pitch); therefore, triangular layouts can lead to smaller shell diameters and higher convective coefficients, due to the turbulence caused by the tortuous path.

Comparing the square layouts, the same analysis is made. The rotated one will provide more turbulence and, therefore, a higher convective coefficient, favoring heat transfer. On the

other hand, one must keep in mind that once turbulence is increased, the pressure drop will also increase which in some cases is a determinant factor during the heat exchanger design.

1.1.4 Number of tube passes and shell passes

The number of tube passes is a very important variable in heat exchanger design. For example, comparing two heat exchangers with the same number of tubes, one with only one pass and the other with four passes, one can affirm that the velocity on the tube-side for the second one will be four times bigger than for the first, and the fluid will go through a distance four times bigger.

The shell has two passes maximum, and the tubes can have up until sixteen passes (but a limit of eight is usually applied). Typically, the number of tube passes is one or an even number.

Comparing exchangers with only one tube pass and one shell pass (countercurrent flow, Figure 7) with exchangers with, for example, one shell pass and two tube passes (1-2 heat exchanger, Figure 8), the last one will have one countercurrent pass and one parallel, therefore the effectiveness will be smaller than the one for a countercurrent exchanger. However, the use of more than one tube pass is very common when it is necessary to increase the tube-side flow velocity and the convective coefficient, improving the heat transfer.

Figure 7 – Countercurrent flow

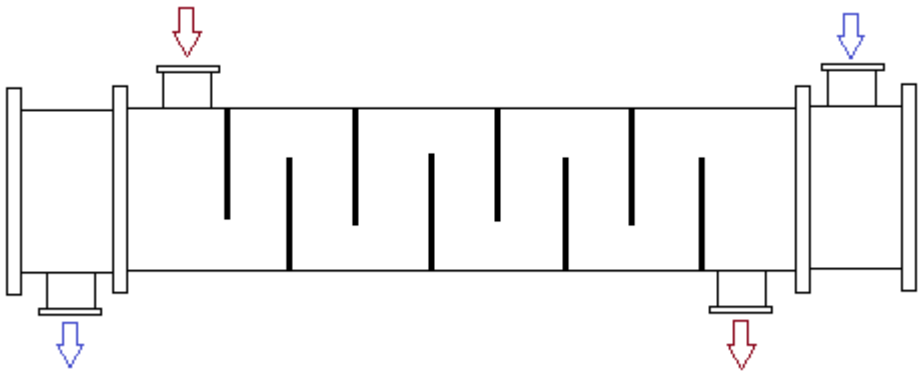

Fonte: A autora, 2018.

Figure 8 – 1-2 heat exchanger

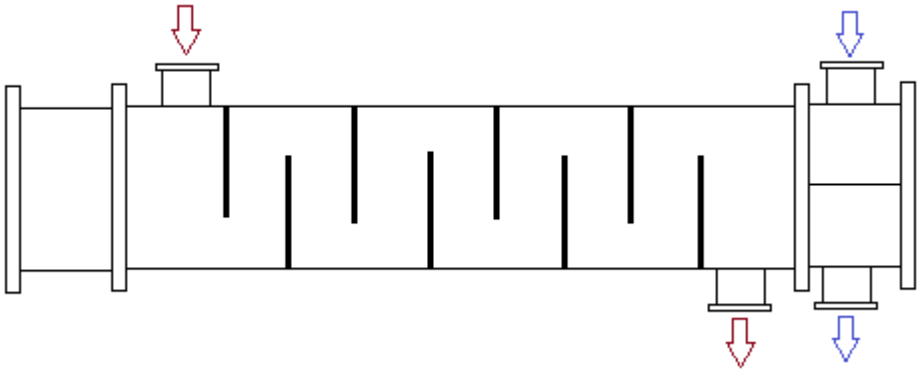

Fonte: A autora, 2018.

1.1.5 Shell and head types

TEMA classifies the shell and head types as shown in Figure 9, in which they are identified through a set of three letters (TEMA, 2007). The first letter identifies the nature of the front head, the second letter indicates the shell type and the last letter identifies the type of rear head.

Figure 9 – Shell and head types

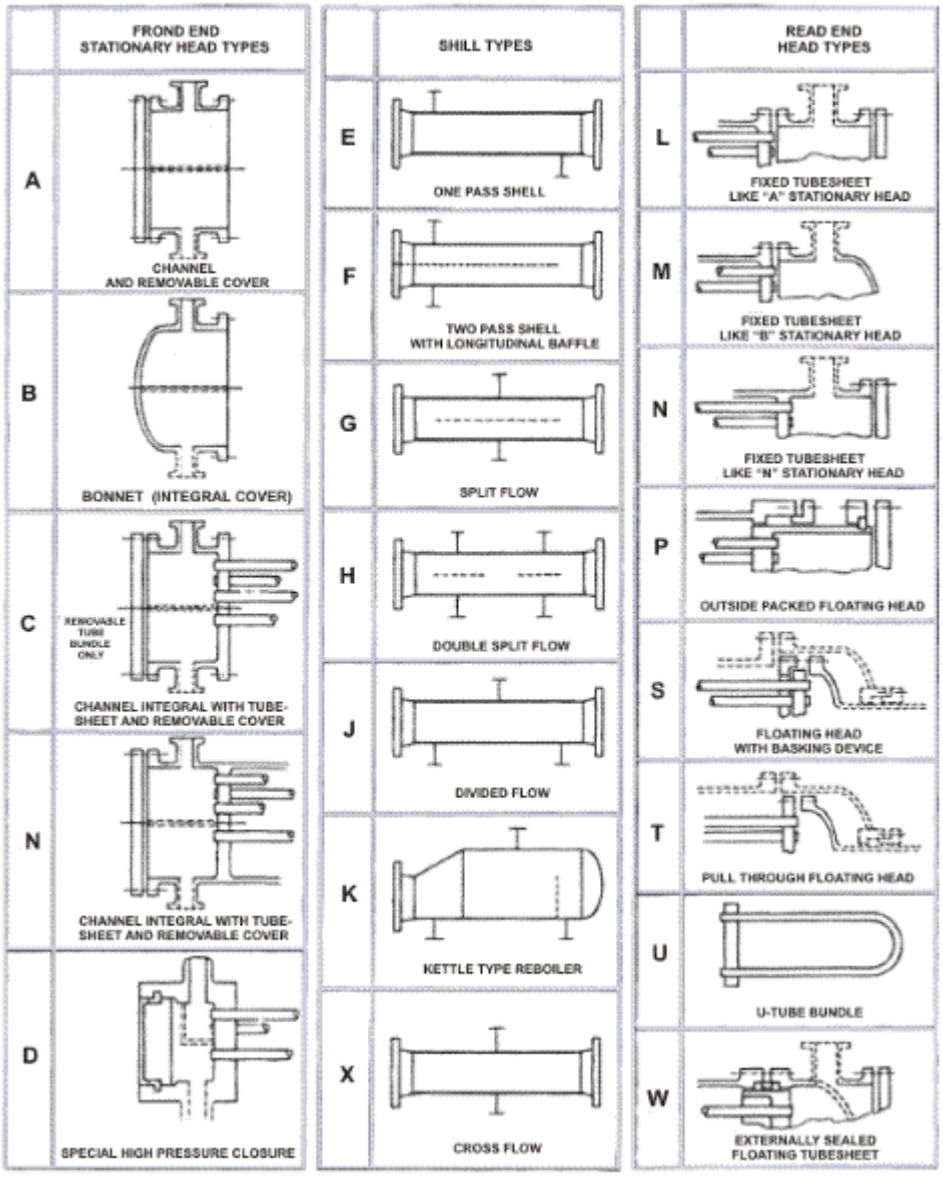

Fonte: TEMA, 2007

1.2.**Heat exchanger calculation**

1.2.1. Logarithmic mean temperature difference method

The main method to describe the steady-state behavior of shell-and-tube heat exchangers is the Logarithmic Mean Temperature Difference method (LMTD). The main variable for design purposes is the heat transfer area and for that, we must know the temperature difference between the two streams that are exchanging heat. However, the temperature is not uniform inside the equipment and a solution is to use the average temperature difference.

The LMTD method indicates the use of the logarithmic mean temperature difference, calculated, for multiple passes and for counter current flow, as (INCROPERA et al., 2006):

$$\widehat{\Delta Tlm} = \frac{(\widehat{Thi} - \widehat{Tco}) - (\widehat{Tho} - \widehat{Tci})}{\ln\left(\frac{(\widehat{Thi} - \widehat{Tco})}{(\widehat{Tho} - \widehat{Tci})}\right)} \quad (1)$$

in which T represents the temperature, the subscript h refers to the hot stream, subscript c to the cold stream, o to the outlet and i to the inlet.

Another important component of this method is the correction factor. Since the flow for multipass exchangers is a mixture of the countercurrent and the co-current flows, it is necessary to calculate a correction factor ($\hat{F}$) for the LMTD method. This correction factor is calculated as (INCROPERA et al., 2006):

$$\hat{F} = \frac{(\hat{R}^2 + 1)^{0.5} \ln\left(\frac{(1-\hat{P})}{(1-\hat{R}\hat{P})}\right)}{(\hat{R}-1)\ln\left(\frac{2-\hat{P}\left(\hat{R}+1-(\hat{R}^2+1)^{0.5}\right)}{2-\hat{P}\left(\hat{R}+1+(\hat{R}^2+1)^{0.5}\right)}\right)} \quad (2)$$

where:

$$\hat{R} = \frac{\widehat{Thi} - \widehat{Tho}}{\widehat{Tco} - \widehat{Tci}} \quad (3)$$

$$\hat{P} = \frac{\widehat{Tco} - \widehat{Tci}}{\widehat{Thi} - \widehat{Tci}} \quad (4)$$

The heat transfer area is then calculated as:

$$\hat{Q} = UA\widehat{\Delta Tlm}F \quad (5)$$

in which $\hat{Q}$ is the heat transfer rate, A is the heat transfer area and U is the overall heat transfer coefficient, calculated using the heat transfer coefficients and fouling resistances, as it will be detailed later.

1.2.2. Tube-side convective heat transfer coefficient

The dimensionless representation of the convective heat transfer coefficient (*ht*) corresponds to the Nusselt number (*Nut*) (INCROPERA et al., 2006):

$$Nut = \frac{htdti}{\widehat{kt}} \tag{6}$$

where $\widehat{kt}$ is the tube-side stream thermal conductivity and *dti* is the inner tube diameter.

The Nusselt number is a dimensionless parameter determined by theoretical models or empirical correlations. The specific model to be applied depends on the flow regime.

One of the correlations that can be used for calculating the Nusselt number for turbulent flow is the Gnielinski correlation (INCROPERA et al., 2006), that can also be used for the transition region ($2300 < Ret < 5 \cdot 10^6$):

$$Nut = \frac{\left(ft/8\right)(Ret-1000)\widehat{Prt}}{1+12.7\left(ft/8\right)^{1/2}\left(\widehat{Pr}^{2/3}-1\right)} \tag{7}$$

where *ft* is the friction factor for the tube-side, *Ret* is the Reynolds number and $\widehat{Prt}$ is the Prandlt number. The friction factor can be calculated by using the Moody diagram.

Another correlation used for turbulent flow is Dittus-Boelter (INCROPERA et al., 2006):

$$Nut = 0.023\, Ret^{0.8}\widehat{Prt}^{n} \tag{8}$$

where *n* is a parameter equal to 0.3 if the tube-side fluid is being cooled, and 0.4 if it is being heated.

Despite the Gnielinski correlation gives more accurate results, Dittus-Boelter type correlations are simpler, allowing the use in more complex problems, like heat exchanger design optimization problems (MIZUTANI et al., 2003).

1.2.3. Shell-side convective heat transfer coefficient

Due to the nature of the shell-and-tube heat exchanger construction, the flow of the shell-side is a complex combination of different flow paths. The main transversal flow path between adjacent baffles is combined with a set of secondary streams that flows through the constructional clearances and gaps.

The next paragraphs describe the main methods available in the literature for evaluation of the thermo-fluid dynamic behavior of the shell-side flow: Kern method (KERN, 1950), Bell-Delaware method (BELL, 1960) and the streams method. The first method is used in the model developed by Gonçalves et al. (2016, 2017) in which this thesis is based on, although this method is simpler it is used as a first approach to the problem, future works will consider the Bell-Delaware method (BELL, 1960).

1.2.3.1. Kern method (KERN, 1950)

The Kern method (KERN, 1950) have once been the most used method in heat exchanger design. Although it does not represent the reality as well as the other two methods mentioned, that will be better explained next, it is the simpler method to implement and therefore the easier one to get results. This method only considers a baffle cut of 25%. The detailed model and its equations will be shown later.

1.2.3.2.Bell-Delaware method (BELL, 1960)

The Bell-Delaware method is more sophisticated than the Kern method (KERN, 1950), it represents reality better, being the most recommended method available in open literature. This method uses several correction factors for the transversal flow to consider flow through the windows, leak flows and bypass flows. Figure 10 shows a schematic representation of the shell-side flow.

Figure 10 – Shell-side flow

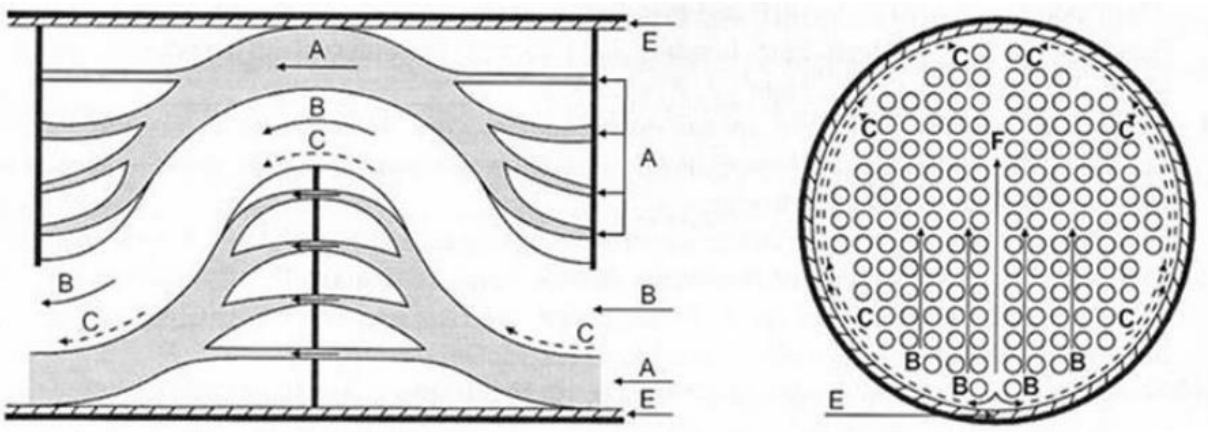

Fonte: Heat Exchanger Design Handbook, 1983.

In Figure 10, stream B is the ideal one, the one that most favors heat transfer. If only stream B existed, the correction factors, shown in Equation 9, would not be necessary:

$$h = h_{ideal} J_c J_l J_b J_r J_s \quad (9)$$

In Equation 9, h_{ideal} is the one calculated for a cross flow through a tube bundle, in which all the stream flows perpendicularly to the tubes. The correction factor J_c is related to the baffle cut and spacing, J_l is the correction factor that considers the shell-baffle and baffle-tube leak streams (streams A and E in Figure 10), J_b is the correction factor due to the different baffle spacing in the inlet and outlet regions of the equipment and J_r is the correction factor for the adverse temperature gradient in laminar flow.

1.2.3.3.Stream analysis method

The streams method details all the streams flowing through the shell-side, calculating each one of them individually (Heat Exchanger Design Handbook, 1983). Tinker (1947) first proposed the detailing of the flow streams.Although the Bell-Delaware method already considers multiple flow streams in the shell-side in the form of correction factors, the streams method is considered to be the most accurate of all.

However, the complete version of this method is not available in open literature. The use if this method is only possible through a commercial software.

1.3. **Fouling**

In heat transfer technology, the fouling phenomenon is the undesirable accumulation of deposits over the heat transfer surfaces and has a big influence on heat exchanger design and its performance over the operating period. These deposits have a deleterious effect over heat transfer and, with time, hinder the heat transfer operation. The growth of the deposits implies in an increase of the resistance to heat transfer, decreasing the overall heat transfer coefficient.

The energy that could not be recovered through heat exchange between two process streams due to fouling will demand an increase of the utility consumption, which penalizes the operational cost and is harmful to the environment, since it implies in more greenhouse effect gases released.

This topic will discuss some theoretical aspects of fouling and the main models used to describe the phenomenon, particularly considering the fouling in crude oil and cooling water streams, systems investigated in the current thesis.

1.3.1. Theoretical aspects

The fouling process, in general, can be described by three different stages (BOTT, 1995):

i. Diffusion of the foulant and/or its precursors across the boundary layer adjacent to the solid heat transfer surface.
ii. Adhesion of the deposit to the surface or to itself.
iii. Removal of the deposits.

Therefore, the fouling phenomenon is described as the difference between the formation rate (i and ii) and the removal rate (iii). It is important to observe that the amount of deposit formed may influence the removal rate; therefore, Figure 11 represents a possible fouling thickness growth curve when the removal of deposits increases with the deposit thickness.

Figure 11 – An example of fouling growth curve

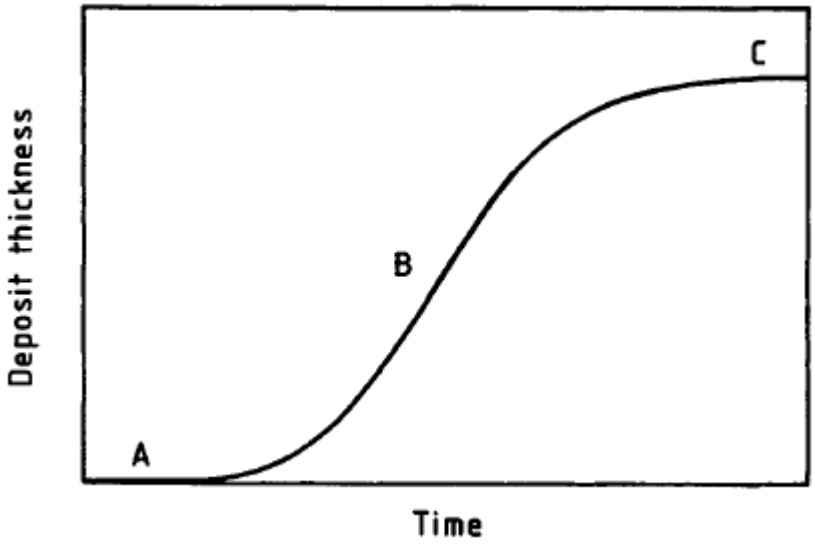

Fonte: BOTT, 1995.

Region A is the induction region, the period of time in which the fouling rate starts as zero and grows, depending on the system this period can be very long (weeks) or very short (minutes or seconds). In Region B, the fouling rate keeps growing and the removal rate starts to grow until they become equal, in Region C. Since the formation and removal rates are equal, the fouling growth will be null.

1.3.2. Crude oil fouling models

The most modern crude oil fouling models are the threshold fouling models. The threshold concept was first proposed by Ebert and Panchal (1995) and since then many other works have been developed based on this concept, those models were summarized by Wilson, Ishiyama and Polley (2015). These models are employed to describe the fouling behavior in crude preheat trains in petroleum distillation units, particularly in the hotter heat exchangers, i.e. downstream the desalter. Fouling in this region is associated to the presence of asphaltenes.

Threshold models describe the fouling rate based on two terms: a formation term and a removal/suppression term (there is a debate in the literature if the deposits can be removed or not during the operation). The nature of the threshold models state that, depending on the temperature and velocity, fouling may occur or not. Therefore, it is possible to establish a

fouling envelope that delimit a fouling region and a no fouling region. Figure 12 shows a scheme of this behavior.

Figure 12 – Fouling envelope

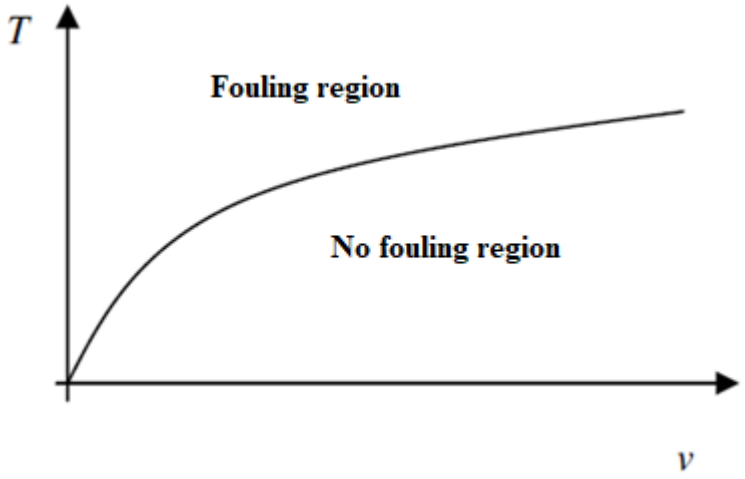

Fonte: A autora, 2018.

The fouling envelope will limit the region where no fouling takes place, this region corresponds to low temperatures and high velocities, because the fouling rate is a function of them. According to what was explained before, if the fouling rate is null (no fouling region) then the removal/suppression rate is larger than the formation rate.

The first threshold fouling model was proposed by Ebert and Panchal (1995), known as the Ebert-Panchal model that introduced the concept and proposed the following fouling rate model:

$$\frac{dRf}{dt} = \alpha Re^{\beta} exp\left(\frac{-Ea}{RT_f}\right) - \gamma'\tau \qquad (10)$$

In Equation 10, α, β and γ are parameters of the model, *Re* is the Reynolds number, *Ea* is the activation energy, *R* is the ideal gas constant, T_f is the film temperature and τ is the shear stress. The first term of the equation is positive, representing the formation rate, and the second term is negative, representing the removal rate.

A few years later, Panchal et al.(1999) proposed a modification, adding the Prandtl (*Pr*) number in the previous model, creating a second model, best known as modified Ebert-Panchal, described by the following:

$$\frac{dRf}{dt} = \alpha Re^{-0.66} Pr^{-0,33} exp\left(\frac{-Ea}{RT_f}\right) - \gamma'\tau \quad (11)$$

The third threshold fouling model was proposed by Polleyet al.(2002a). New parameters were created and it was proposed to replace the shear stress term by a function of the Reynolds number and to use the wall temperature (T_w) instead of the film temperature:

$$\frac{dRf}{dt} = \alpha Re^{-0,8} Pr^{-0,33} exp\left(\frac{-Ea}{RT_w}\right) - \gamma Re^{0,8} \quad (12)$$

Nasr and Givi (2006) also proposed a model based on the previous ones, they used data from literature to estimate the parameters and proposed modifications:

$$\frac{dRf}{dt} = \alpha Re^{\beta} exp\left(\frac{-Ea}{RT_f}\right) - \gamma Re^{0,4} \quad (13)$$

The models displayed here are the most used in the literature in simulation and design problems (WILSON; ISHIYAMA; POLLEY, 2015).

1.3.3. Water fouling models

Water is very common in process industries as cooling water. The cooling water system is always present in process industries. In general, it is a recirculating system in which the water goes through the heat exchangers and then through a cooling tower, to be cooled and afterwards restart the cycle.

The quality of the water used in this system will affect directly the formation of fouling. The mechanisms for fouling in water streams are particulate, crystallization and corrosion fouling that can be mitigate by controlling some parameters as: alkalinity or acidity, hardness, dissolved gases, suspended solids and pH. Another important fouling mechanism in water streams is the biological fouling, that can be mitigate by adjusting the following parameters: microbial population, biological oxygen demand and concentration of organic material.

In literature there are many complex models to predict the fouling rate in systems involving water streams, including different aspects of the phenomenon, such as modeling the ionic equilibrium, mass transfer of the involved species, etc. (BOTT, 1995;CREMASCHI et al., 2011). However, the models are not easily adapted to be included in optimization problems,

such as proposed in this thesis. For this reason, those models will not be explored in this brief review.

Aiming at design purposes, Nesta and Bennett (2004) proposed a simpler model where fouling is a function of velocity and the asymptotic value for the fouling resistance can be used in design problems, and is given by:

$$Rf = \widehat{kRf}\ (v)^{-\widehat{\alpha Rf}} \tag{14}$$

In Equation 14, $\widehat{kRf}$ and $\widehat{\alpha Rf}$ are the model parameters and v is the flow velocity on the tube-side for the water stream. According to the authors, these parameter may assume the following values: 0.00062 and 1.65. The absence of the temperature in this model can be justified due to fixed range usually employed for cooling water streams in the design of coolers.

1.4. **Heat exchanger design considering fouling**

Although fouling is a very important matter and is highly debated and studied in literature (BOTT, 1995), considering its effects during the heat exchanger design in a more detailed way, i.e. using fouling models and not tabled fixed fouling resistances, is not very common. This topic will bring the few works that had the goal of uniting the design and the fouling models, which is the goal of the present thesis.

1.4.1. Recommendations to mitigate fouling

Some works in literature give recommendations of how to design heat exchangers in order to avoid or minimize fouling effects, instead of including the fouling model in the design problem, which is a much more complex task. One of those works is the one by Nesta and Bennett (2004), where they emphasize that if some considerations are made the design can be done without considering the fouling model. They argue that including the fouling resistance in the overall heat transfer coefficient will actually increase the area to compensate the loss related to the fouling resistance, but at the end, this increase in area might lead to a decrease in flow velocity, increasing the fouling rate. Therefore, the additional heat transfer area associated to the inclusion of the fouling resistances might contribute to the effect that it was intended to mitigate, favoring fouling.

The authors showed some preliminary studies made by HTRI (Heat Transfer Research, Inc.). These studies try to find the critical parameters (velocity, wall temperature, etc.) in which fouling does no take place or has a very small rate. The results for a crude oil heat exchanger using those critical parameters were compared to the results obtained by using the traditional design approach (fixed fouling resistance). It was also proposed a model to predict fouling for cooling water on the tube-side where the fouling resistance is a function of velocity. This model was shown before and will be used later in the development of this thesis.

Shilling (2012) presented an analyses of three different alternatives for managing fouling in the design stage. The first option is the traditional approach, in which a fixed fouling resistance is used. A series of critics are presented regarding this approach and its limitations. In the second approach, it is proposed to, instead of using fouling factors, multiply the convective coefficient by a factor to considerate the fouling effect. According to the author, this option would be more appropriate, since the fouling penalization would be associated only to the convective resistance, therefore avoiding high area excesses. Finally, the third option was to use a procedure similar to a risk matrix used to asses risk in industrial process. This method does not take into account the fouling model itself, however it makes a risk analyses to define the percentage of excess of area that must be used considering the analyzed process. It also analyzes the risk of errors in predictive correlations, natural conditions that can degrade performance and uncertainties.

1.4.2. Heat exchanger design considering fouling models

Aiming to contribute in this field not well explored in literature, Polley et al. (2002b) highlighted the importance of considering threshold fouling models when designing heat exchangers in preheat trains and emphasized the importance of the fouling envelope in the design analyses.

The authors proposed to explore the fouling behavior in the design of heat exchangers using the graphical method proposed by Poddar and Polley (2000). This method consists of drawing curves corresponding to the maximum and minimum pressure drop for the tube-side and the shell-side and the constraint for heat load against axes of tube count and tube length. The fouling analysis is conducted through the superposition of the fouling envelope over the graph. Figure 13 shows a typical result of the proposed analysis.

Figure 13 – Poddar plot considering fouling

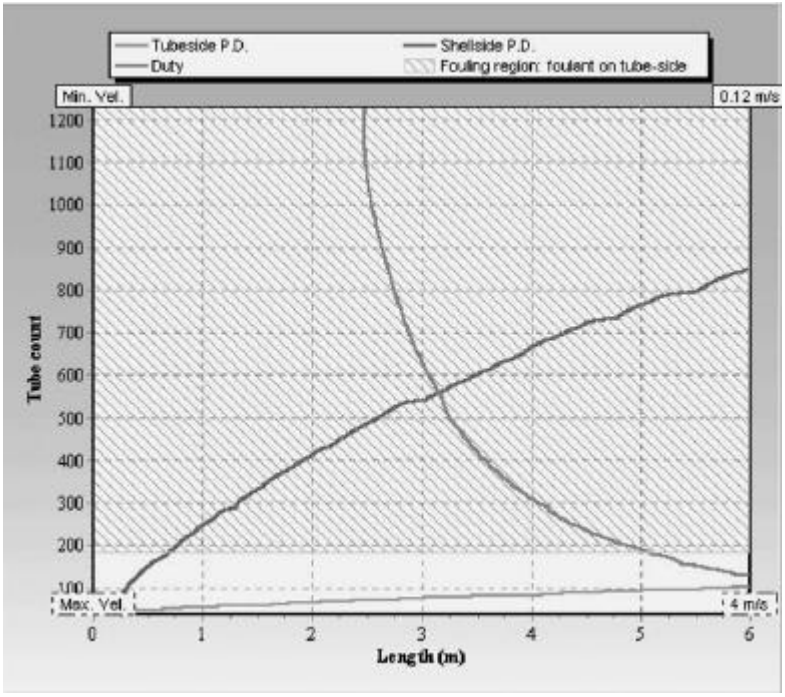

Fonte: POLLEY et al., 2002b

In the original procedure, the optimal result would be where the thermal duty line and the higher of the pressure drop line meet. In this procedure, the heat exchanger would be in the region where fouling occurs. They mention some tactics to change this point, for example modify the baffle cut, in order to get an optimal in the no fouling region or as close as possible, to guarantee a lower fouling rate.

The authors also highlighted that some actions can be taken in order to mitigate fouling. The layout must always avoid that the hottest region of the tube-side flow coincides with the hottest point of the shell-side flow because this will maximize the wall temperature, increasing the fouling rate. This can be observed in Figure 14, where the red circle indicates the two hotter points of the tube and shell-side coincide.

Figure 14 – Heat exchanger with high wall temperature

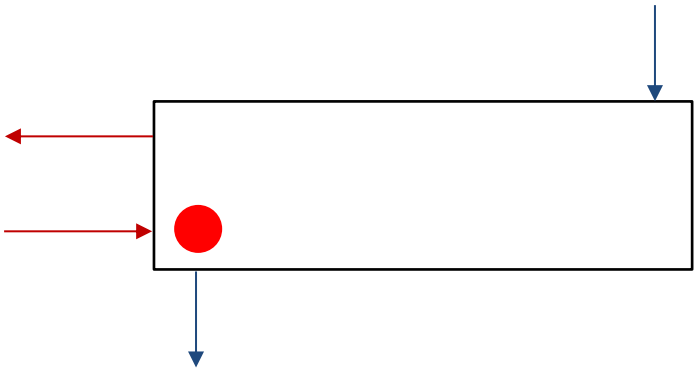

Fonte: A autora, 2018.

Butterworth (2002) treated the problem along with the design problem using a threshold fouling model, highlighting the influence of velocity and temperature. He said that the relation between fouling rate and these parameters was rarely considered during design because of reasons that go from the complexity of the problem until the lack of agreement between the designer and the buyer. The difference between the traditional approach and the proposed approach was emphasized.

In this work, the author referred to a design envelope, similar to the one used by Polley et al. (2002b), that is a graphical method for heat exchanger design. He analyzed five different cases and their influence on the envelope, based on previous works. The first is the base case, assuming null fouling resistance. The second has fixed fouling resistances. In the third case, the resistance changes according to the velocity. The fourth case considered fouling influence on the friction factor. The fifth case assumed fouling resistance raises smoothly with the decreasing of velocity. In each case, the author illustrated how the solution of the heat exchanger design problem was modified. The unprecedented part of this work used the same graphical method from previous works, and considered three new different cases. The first one uses a threshold fouling model to determine the region that contains the heat exchangers in which no fouling occurs. The second used the asymptotic fouling resistance based on a threshold fouling model. The third case considered the fouling resistance at the end of the operating period predicted by a threshold fouling model considering the velocity and the wall temperature to be constant during operation.

Polley et al. (2011) developed another work that explored fouling along with the design problem. The main idea of this paper was to propose a new approach to design heat exchangers that could achieve a predetermined operating period between cleanings. They questioned the

use of fixed fouling resistance values, especially for exchangers located at the end of the preheat trains, in which the fouling rates are higher due to the high wall temperatures.

To execute this task, the heat exchanger was initially designed for the clean condition using the software EXPRESSplus from IHS ESDU. This software employs a graphical analysis similar to that described by Polley et al. (2002b) to identify a heat exchanger with minimum area. Then, the authors proposed to round the tube length to the next commercial available option, which would insert an extra area that may compensate fouling effects. Based on this new design, the amount of fouling the heat exchanger would be able to handle for a certain period was calculated. Finally, the calculated value was compared with the fouling map given by the software. If the heat exchanger is not acceptable for the calculated fouling other possibilities must be tested. Concluding the work it was highlighted that the fouling rate depends more on the wall temperature than on the flow velocity, therefore the available fouling models must be used instead of considering critical values for the parameters, as suggested by Nesta and Bennett (2004).

Caputo et al. (2011) proposed a new approach to heat exchanger design optimization problem considering cleaning. The objective function used included the capital cost, the operation cost, with the pumping cost and maintenance costs related to the cleaning process. The optimization method used was a genetic algorithm, which is a stochastic method.

During the optimization procedure proposed, a fouling model of each heat exchanger design solution is run, such that cleaning costs are evaluated for a given value of maximum fouling resistance. This paper is important for considering the fouling model along with the cleaning in the heat exchanger design problem, which had never been done until then.

Nakao et al. (2017) proposed an iterative approach using a commercial heat exchanger design software (HTRI) in order to include fouling model predictions into the design procedure. In the proposed approach, based on an initial set of fouling resistances, the design of the heat exchanger using HTRI is obtained. Then, a dynamic simulation of the heat exchanger found is run considering a given fouling rate model (the Ebert-Panchal modified model was employed in the examples). The value of the fouling resistances found at the end of the simulation period is then compared with the initial values assumed in the design. If there is no match, the fouling resistances are updated and the procedure is repeated. The procedure stops when convergence is reached. It was observed that the procedure might not converge; in this case, the result will be the smallest heat exchanger found in which the fouling resistance used to design was smaller than the one found in the simulation stage.

2. GLOBAL OPTIMIZATION FOR HEAT EXCHANGER DESIGN

This chapter will present the original nonlinear heat exchanger model (KERN, 1950) and how Gonçalves et al. (2017) used this nonlinear model to formulate the heat exchanger design problem as an ILP problem, able to identify the global optimum. The approach proposed by Gonçalves et al. (2017) is not a linearization of the nonlinear model, but a reformulation that will profit from the fact that the geometric variables to design a heat exchanger have standard values that are commercially available.

The formulation is still based on fixed fouling resistances and it was the starting point for developing the present thesis. Due to its importance to the presentation of the results of the current thesis, a complete description of the optimization formulation of Gonçalves et al. (2017) is presented here. First, the original nonlinear model (KERN, 1950) will be presented, then the reformulation techniques will be explained and later the resultant linear model will be displayed.

2.1. **Original nonlinear model (KERN, 1950)**

To understand the procedure developed by Gonçalves et al. (2016, 2017) used to create a linear heat exchanger model it is necessary to go back to the original nonlinear model. This topic will show the complete model used as a starting point by Gonçalves et al. (2016, 2017). All the parameters will be represented with "^" on top. All the variables and parameters related to the shell-side will have the letter *s* and, to the tube-side, the letter *t*.

The optimization problem solved corresponded to the design of shell-and-tube heat exchangers with a single E-type shell with single segmental baffles, applied for services without phase change, in turbulent flow and the fluid allocation is assumed to be established by the designer and is not included in the optimization.

The geometric variables considered as the decision variables were: number of tube passes (*Npt*), tube diameter (outer and inner: *dte* and *dti*), tube layout (*lay*), tube pitch ratio (*rp*), number of baffles (*Nb*), shell diameter (*Ds*) and tube length (*L*).

2.1.1. Shell-side equations

The Nusselt number for the shell-side is given by (KERN,1950):

$$Nus = 0.36\, Res^{0.55} \widehat{Prs}^{1/3} \quad (15)$$

in which $\widehat{Prs}$ is the dimensionless group Prandtl and *Res* is the Reynolds number for the shell-side. The Nusselt and Reynolds numbers are defined as:

$$Nus = \frac{hsDeq}{\widehat{ks}} \quad (16)$$

$$Res = \frac{Deqvs\widehat{\rho s}}{\widehat{\mu s}} \quad (17)$$

In Equations 16 and 17, $\widehat{ks}$, $\widehat{\rho s}$ and $\widehat{\mu s}$ are the thermal conductivity, the density and the viscosity of the fluid, respectively. Concerning the variables, *hs* is the heat transfer convective coefficient, *Deq* is the equivalent diameter and *vs* is the fluid velocity.

The equivalent diameter is a function of the outer tube diameter (*dte*), the pitch (*ltp*) and the tube layout.

$$Deq = \frac{4\, ltp^2}{\pi dte} - dte \quad \text{(square layout)} \quad (18)$$

$$Deq = \frac{3.46\, ltp^2}{\pi dte} - dte \quad \text{(triangular layout)} \quad (19)$$

The flow velocity is given by:

$$vs = \frac{\widehat{ms}}{\widehat{\rho s} Ar} \quad (20)$$

in which $\widehat{ms}$ is the mass flow rate on the tube side and *Ar* is the flow area between adjacent baffles, which can be calculated as:

$$Ar = DsFARlbc \quad (21)$$

In Equation 21, *Ds* is the shell diameter, *lbc* is the baffle spacing and *FAR* is the free area ratio, given by:

$$FAR = \frac{(ltp - dte)}{ltp} = 1 - \frac{dte}{ltp} = 1 - \frac{1}{rp} \quad (22)$$

where *rp* is the tube pitch ratio ($rp = ltp/dte$).

The pressure drop in the shell-side (ΔPs), not considering the head loss on the nozzles, is described by Equation 23, in which *fs* is the friction factor and *Nb* is the number of baffles:

$$\frac{\Delta Ps}{\widehat{\rho s}\,\hat{g}} = fs\,\frac{Ds(Nb+1)}{Deq}\left(\frac{vs^2}{2\,\hat{g}}\right) \quad (23)$$

The calculation of the friction factor and the relation between the number of baffles and the tube length (*L*) are the following:

$$fs = 1.728\,Res^{-0.188} \quad (24)$$

$$Nb = \frac{L}{lbc} - 1 \quad (25)$$

2.1.2. Tube-side equations

The Nusselt number for the tube-side (*Nut*) is given by the Dittus-Boelter correlation (INCROPERA et al., 2006):

$$Nut = 0.023\,Ret^{0.8}\widehat{Prt}^{n} \quad (8)$$

where:

$$Nut = \frac{htdti}{\widehat{kt}} \quad (6)$$

In Equation 8, the parameter *n* is equal to 0.3 if the fluid flowing on the tube-side is being cooled and 0.4 if the fluid is being heated. In Equation 6, $\widehat{kt}$ is the fluid thermal conductivity. The Reynolds number on the tube-side (*Ret*) is given by:

$$Ret = \frac{dtivt\widehat{\rho t}}{\widehat{\mu t}} \tag{26}$$

The parameters $\widehat{\mu t}$ and $\widehat{\rho t}$ are the viscosity and the density of the tube-side fluid, respectively. The variable *dti* is the inner tube diameter and *vt* represents the tube-side velocity, which is given by Equation 27:

$$vt = \frac{4\widehat{mt}}{Ntp\pi\widehat{\rho t}dti^2} \tag{27}$$

in which $\widehat{mt}$ is the mass flow rate on the tube-side and *Ntp* is the number of tuber per pass.

The pressure drop on the tube-side (ΔPt) is calculated by (SAUNDERS, 1988):

$$\frac{\Delta Pt}{\widehat{\rho t}\hat{g}} = \frac{ftNptLvt^2}{2\,\hat{g}dti} + \frac{\hat{K}Nptvt^2}{2\,\hat{g}} \tag{28}$$

In Equation 28, *ft* is the friction factor on the tube-side. The first term of the equation on the right hand side refers to the head loss over the tube bundle and the second term refers to the loss over the heads. The parameter $\hat{K}$ is defined according to the number of tube passes, it is equal to 0.9 for single pass and 1.6 for two or more passes.

The expression to calculate the friction factor valid for turbulent flow is (SAUNDERS, 1988):

$$ft = 0.014 + \frac{1{,}056}{Ret^{0.42}} \tag{29}$$

2.1.3. Overall heat transfer coefficient

The overall heat transfer coefficient (*U*) is calculated through the following expression:

$$U = \frac{1}{\frac{dte}{dtiht} + \frac{\widehat{Rft}dte}{dti} + \frac{dte\ln(\frac{dte}{dti})}{2\,\widehat{ktube}} + \widehat{Rfs} + \frac{1}{hs}} \tag{30}$$

where$\widehat{Rft}$ e $\widehat{Rfs}$ are the fouling resistances on the tube-side and on the shell-side, respectively, and $\widehat{ktube}$ is the tube thermal conductivity.

2.1.4. Heat transfer rate equation

The LMTD method is based on the logarithmic mean temperature difference ($\widehat{\Delta Tlm}$), which is calculated as:

$$\widehat{\Delta Tlm} = \frac{(\widehat{Thi} - \widehat{Tco}) - (\widehat{Tho} - \widehat{Tci})}{\ln\left(\frac{(\widehat{Thi} - \widehat{Tco})}{(\widehat{Tho} - \widehat{Tci})}\right)} \quad (1)$$

where *T* represents the fluid temperature, the letter *h* refers to the hot fluid, *c* refers to the cold fluid, *o* to the outlet temperature and *i* to the inlet temperature.

The heat transfer rate equation is given by:

$$\hat{Q} = UA\widehat{\Delta Tlm}F \quad (5)$$

Where $\hat{Q}$ is the heat load, *A* is the area and *F* is the correction factor for the LMTD model.

This correction factor is equal to 1 if the exchanger has an unique tube pass in countercurrent flow, otherwise, it is described by Equation 2 for an even number of tube passes:

$$F = \frac{(\hat{R}^2+1)^{0.5}\ln\left(\frac{(1-\hat{P})}{(1-\hat{R}\hat{P})}\right)}{(\hat{R}-1)\ln\left(\frac{2-\hat{P}\left(\hat{R}+1-(\hat{R}^2+1)^{0.5}\right)}{2-\hat{P}\left(\hat{R}+1+(\hat{R}^2+1)^{0.5}\right)}\right)} \quad (2)$$

with:

$$\hat{R} = \frac{\widehat{Thi} - \widehat{Tho}}{\widehat{Tco} - \widehat{Tci}} \quad (3)$$

$$\hat{P} = \frac{\widehat{Tco} - \widehat{Tci}}{\widehat{Thi} - \widehat{Tci}} \quad (4)$$

The heat transfer area (*A*) is given by:

$$A = Nttπdte L \quad (31)$$

where *Ntt* is the total number of tubes.

The heat exchanger area must be higher than the required area aiming to guarantee a design margin according to a certain "excess area" ($\widehat{Aexc}$):

$$A \geq \left(1 + \frac{\widehat{Aexc}}{100}\right) Areq \tag{32}$$

2.1.5. Bounds on pressure drops, flow velocities and Reynolds numbers

The pressure drops and flow velocities are associated to lower and upper bounds, which should be considered in the model:

$$\Delta Ps \leq \Delta\widehat{Psdisp} \tag{33}$$

$$\Delta Pt \leq \Delta\widehat{Ptdisp} \tag{34}$$

$$\widehat{vsmax} \geq vs \geq \widehat{vsmin} \tag{35}$$

$$\widehat{vtmax} \geq vt \geq \widehat{vtmin} \tag{36}$$

The correlations for the convective heat transfer coefficient are only valid for turbulent flow, therefore constraints for the Reynolds number must be considered in the model:

$$Res \geq 2{\cdot}10^3 \tag{37}$$

$$Ret \geq 10^4 \tag{38}$$

2.1.6. Geometric constraints

The baffle spacing must be limited between 20% and 100% of the shell diameter (TABOREK, 2008a):

$$lbc \geq 0.2\ Ds \tag{39}$$

$$lbc \leq 1.0\ Ds \tag{40}$$

The ratio between the tube length and shell diameter must be between 3 and 15 (TABOREK, 2008b):

$$L \geq 3\ Ds \tag{41}$$

$$L \leq 15\ Ds \tag{42}$$

2.1.7. Objective function

In general the objective is to minimize the heat transfer area (A), which has a direct impact over the heat exchanger cost, therefore the objective function will be:

$$min\ A \tag{43}$$

2.2. **Development of the ILP formulation**

This topic will deal with the development of the ILP formulation proposed by Gonçalves et al. (2016, 2017) for the design of heat exchangers, starting from the traditional nonlinear model described previously. Afterwards, in the next chapters of this thesis, this model will be modified to consider different fouling models.

2.2.1. Geometric variables

The geometric variables are the variables that describe the entire heat exchanger. Those variables are discrete, due to their physical nature or due to their standard values commercially

available. This is the basic idea that will lead from the original nonlinear model to the ILP model after the model is rewritten properly.

Each geometric variable (VD) will be considered being associated to a set of parameters (pVD_{sVD}) and a set of binary variables (yVD_{sVD}). Therefore, the original geometric variable will be described by the following equations:

$$VD = \sum_{sVD} \widehat{pVD}_{sVD} yVD_{sVD} \tag{44}$$

$$\sum_{sVD} yVD_{sVD} = 1 \tag{45}$$

The geometric variables and the parameter that represent their available values considered in the model are: inner and outer diameters ($\widehat{pdti}$and$\widehat{pdte}$), shell diameter ($\widehat{pDs}$), number of tube passes ($\widehat{pNpt}$), pitch ratio ($\widehat{prp}$), layout ($\widehat{play}$), tube length ($\widehat{pL}$) and number of baffles ($\widehat{pNb}$).

The constraints that represent each one of the geometric variables as a function of their binary variables are:

$$dte = \sum_{sd=1}^{sdmax} \widehat{pdte}_{sd} yd_{sd} \tag{46}$$

$$dti = \sum_{sd=1}^{sdmax} \widehat{pdti}_{sd} yd_{sd} \tag{47}$$

$$Ds = \sum_{sDs=1}^{sDsmax} \widehat{pDs}_{sDs} yDs_{sDs} \tag{48}$$

$$lay = \sum_{slay=1}^{slaymax} \widehat{play}_{slay} ylay_{slay} \tag{49}$$

$$Npt = \sum_{sNpt=1}^{sNptmax} \widehat{pNpt}_{sNpt} yNpt_{sNpt} \tag{50}$$

$$rp = \sum_{srp=1}^{srpmax} \widehat{prp}_{srp} yrp_{srp} \tag{51}$$

$$L = \sum_{sL=1}^{sLmax} \widehat{pL}_{sL} yL_{sL} \tag{52}$$

$$Nb = \sum_{sNb=1}^{sNbmax} \widehat{pNb}_{sNb} yNb_{sNb} \tag{53}$$

Gonçalves et al. (2017) realized that the developed model was computationally complex and took a long time to solve. Aiming to decrease the computational time, a strategy was proposed through a reorganization of the search space. The idea was to organize the parameters into a unique table, where each row represents a combination of the possible values for the geometric variables, i.e. each row is a different possibility for heat exchanger design. This procedure gave good results in terms of decreasing the computational time to solve the problem. The rows of this big table will be represented by the index *srow*= (*sd, sDs, slay, sNpt, srp, sL, sNb*) (a multi-index one) and the new binary variable that will indicate the selected value for all the geometric variables is *yrow*.

Therefore, the new constraints and new parameters (indexed in *srow*) that represent the geometric variables are:

$$dte = \sum_{srow} \widehat{Pdte}_{srow} yrow_{srow} \tag{54}$$

$$dti = \sum_{srow} \widehat{Pdti}_{srow} yrow_{srow} \tag{55}$$

$$Ds = \sum_{srow} \widehat{PDs}_{srow} yrow_{srow} \tag{56}$$

$$lay = \sum_{srow} \widehat{Play}_{srow} yrow_{srow} \tag{57}$$

$$Npt = \sum_{srow} \widehat{PNpt}_{srow} yrow_{srow} \tag{58}$$

$$rp = \sum_{srow} \widehat{Prp}_{srow} yrow_{srow} \tag{59}$$

$$L = \sum_{srow} \widehat{PL}_{srow} yrow_{srow} \tag{60}$$

$$Nb = \sum_{srow} \widehat{PNb}_{srow} yrow_{srow} \tag{61}$$

To make the visualization of the proposed modification, the structure of this multi-indexed table is presented in Figure 15, where each row represents a combination of the geometric parameters (index *srow*) and each column refers to one of those parameters.

Figure 15 – Multi-indexed table

$$\begin{array}{cccccccc}
\widehat{Pdte_1} & \widehat{Pdti_1} & \widehat{PDs_1} & \ldots & \ldots & \ldots & \widehat{PL_1} & \widehat{PNb_1} \\
\widehat{Pdte_1} & \widehat{Pdti_1} & \widehat{PDs_1} & \ldots & \ldots & \ldots & \widehat{PL_1} & \widehat{PNb_2} \\
\widehat{Pdte_1} & \widehat{Pdti_1} & \widehat{PDs_1} & \cdots & \ldots & \ldots & \widehat{PL_1} & \widehat{PNb_3} \\
\vdots & \vdots & \vdots & \ddots & & & & \\
\vdots & \vdots & \vdots & & \ddots & & \vdots & \vdots \\
\vdots & \vdots & \vdots & & & \ddots & & \\
\widehat{Pdte_{n-1}} & \widehat{Pdti_{n-1}} & \widehat{PDs_n} & \ldots & \ldots & \ldots & \widehat{PL_n} & \widehat{PNb_n} \\
\widehat{Pdte_n} & \widehat{Pdti_n} & \widehat{PDs_n} & \ldots & \ldots & \cdots & \widehat{PL_n} & \widehat{PNb_n}
\end{array}$$

Fonte: A autora, 2018.

Only one row of this table can be chosen in the solution, therefore, we have the following constraint:

$$\sum_{srow} yrow_{srow} = 1 \tag{62}$$

2.2.2. Rewriting the nonlinear model

To rewrite the original nonlinear model in a way to convert it to a linear one, the geometric variables must be replaced in the original constraints. A fundamental aspect of the mathematical manipulations associated to this set of substitutions is the nature of the expressions involving binary variables. In order to illustrate this important aspect, let us consider the expression of the flow area of a tube:

$$Ac = \frac{\pi dti^2}{4} \tag{63}$$

According to the representation of the inner tube diameter through binaries, it yields:

$$Ac = \frac{\pi(\sum_{srow} \widehat{Pdti}_{srow} yrow_{srow})^2}{4} \tag{64}$$

However, since a unique binary variable will assume a nonzero value and the power of a binary does not change its value, this expression is equivalent to:

$$Ac = \frac{\pi \sum_{srow} (\widehat{Pdti}_{srow})^2}{4} yrow_{srow} \tag{65}$$

As can be seen, the substitution of the binaries in the original nonlinear expression of *Ac* yielded a linear expression.

2.2.2.1. Shell-side equations

The replacements must be executed from the most fundamental variables to the more complex ones. The goal is to get an expression to calculate the convective heat transfer coefficient as a function of the geometric variables, now a set of binaries. In this case, we start with the flow area (*Ar*), described previously by Equation 21, in which the baffle spacing (*lbc*) must be replaced by a relation between the tube length and the number of baffles, represented in its binary form by:

$$lbc = \sum_{srow} \frac{\widehat{PL}_{srow}}{\widehat{PNb}_{srow}+1} yrow_{srow} \tag{66}$$

In addition, the free area ratio must be replaced by the following expression:

$$FAR = \sum_{srow} \widehat{PFAR}_{srow} yrow_{srow} \tag{67}$$

where $\widehat{PFAR}_{srow}$ is the parameter for free area ratio, function of the geometric parameter pitch ratio. This parameter is calculated as follows:

$$\widehat{PFAR}_{srow} = 1 - \frac{1}{\widehat{Prp}_{srow}} \tag{68}$$

Replacing these expressions in the flow area constraint (Equation 21) leads to an expression where the flow area is only a function of the binary variable that indicates the chosen heat exchanger:

$$Ar = \sum_{srow} \frac{\widehat{PDs}_{srow} \widehat{PFAR}_{srow} \widehat{PL}_{srow}}{(\widehat{PNb}_{srow}+1)} yrow_{srow} \tag{69}$$

Following the same logic, it is possible to rewrite the shell-side velocity as a function of the binary variable by replacing Equation 69 in Equation 20:

$$vs = \frac{\widehat{ms}}{\widehat{\rho s}} \sum_{srow} \frac{(\widehat{PNb}_{srow}+1)}{\widehat{PDs}_{srow}\widehat{PFAR}_{srow}\widehat{PL}_{srow}} yrow_{srow} \tag{70}$$

The velocity on the shell-side can be replaced in the Reynolds number equation. To write the Reynolds number as a function of the binary variable first we must rewrite the equivalent diameter. For that, the binary representation of the geometric parameters must be replaced in Equations 18 and19, and then the equivalent diameter is written as:

$$Deq = \sum_{srow} \widehat{PDeq}_{srow}\, yrow_{srow} \tag{71}$$

$$\widehat{PDeq}_{srow} = \frac{\widehat{FDeq}_{srow}\widehat{Prp}^2_{srow}\widehat{Pdte}^2_{srow}}{\pi \widehat{Pdte}_{srow}} - \widehat{Pdte}_{srow} \tag{72}$$

In Equation 72, $\widehat{FDeq}_{srow}$ is equal to 4 (Equation 18) for square layout and equal to 3.46 for triangular layout (Equation 19).

Replacing Equations 70 and 71 in Equation 17 we can write the Reynolds number as:

$$Res = \frac{\widehat{ms}}{\widehat{\mu s}} \left(\sum_{srow} \frac{\widehat{PDeq}_{srow}(\widehat{PNb}_{srow}+1)}{\widehat{PDs}_{srow}\widehat{PFAR}_{srow}\widehat{PL}_{srow}} yrow_{srow} \right) \tag{73}$$

With that, it is possible to rewrite the Nusselt number, replacing Equation 73 in Equation 15:

$$Nus = 0{,}36 \left(\frac{\widehat{ms}}{\widehat{\mu s}}\right)^{0{,}55} \left(\sum_{srow} \left(\frac{\widehat{PDeq}_{srow}(\widehat{PNb}_{srow}+1)}{\widehat{PDs}_{srow}\widehat{PFAR}_{srow}\widehat{PL}_{srow}} \right)^{0{,}55} yrow_{srow} \right) \widehat{Prs}^{1/3} \tag{74}$$

Replacing the expression for Nusselt number (Equation 74) in Equation 16, finally we have the following expression for the convective heat transfer coefficient as a function of the binary variables. This equation is important because it will later be inserted in the heat transfer rate equation, along with the tube-side convective heat transfer coefficient, that will be developed in the next section.

$$hs = \sum_{srow} \widehat{Phs}_{srow}\, yrow_{srow} \tag{75}$$

in which:

$$\widehat{Phs}_{srow} = \frac{\widehat{ks}\ 0{,}36\left(\frac{\widehat{ms}}{\widehat{\mu s}}\right)^{0{,}55} \widehat{Prs}^{1/3}}{\widehat{PDeq}_{srow}{}^{0{,}45}} \left(\frac{\widehat{PNb}_{srow}+1}{\widehat{PDs}_{srow}\widehat{PFAR}_{srow}\widehat{PL}_{srow}}\right)^{0{,}55} \tag{76}$$

2.2.2.2. Tube-side equations

Performing the same procedure shown for the shell-side, Equation 27 is rewritten as:

$$vt = \frac{4\widehat{mt}}{\pi\widehat{\rho t}} \sum_{srow} \frac{\widehat{PNpt}_{srow}}{\widehat{PNtt}_{srow}\widehat{Pdti}_{srow}{}^{2}}\, yrow_{srow} \tag{77}$$

The parameter $\widehat{PNtt}_{srow}$ is calculated by the following equation, which represents a counting table data (KAKAÇ; LIU, 2002):

$$\widehat{PNtt}_{srow} = \frac{(\pi\ \widehat{Ds}_{srow}\widehat{Knpt})^2}{4\ \widehat{Pltp}^2\widehat{Klay}} \tag{78}$$

The value obtained for the total number of tubes in Equation 78 must be rounded to its near integer. The parameters in equation are $\widehat{Knpt}$ that depends on the number of passes and is equal to 0.93 for single pass and 0.9 for multiple passes, and $\widehat{Klay}$ that relates to the tube layout and is equal to 0.866 for triangular layout and equal to 1 for square layout.

Replacing Equation 77 in Equation 26, we can write the Reynolds number for the tube-side as a function of the binary variable as:

$$Ret = \frac{4\widehat{mt}}{\pi\widehat{\mu t}} \sum_{srow} \frac{\widehat{PNpt}_{srow}}{\widehat{PNtt}_{srow}\widehat{Pdti}_{srow}}\, yrow_{srow} \tag{79}$$

This expression can be replaced in Equation 8 to give the new expression for Nusselt number:

$$Nut = 0.023 \left(\frac{4\widehat{mt}}{\pi\widehat{\mu t}}\right)^{0{,}8} \widehat{Prt}^{n} \sum_{srow} \left(\frac{\widehat{pNpt}_{srow}}{\widehat{pNtt}_{srow}\widehat{pdti}_{srow}}\right)^{0{,}8} yrow_{srow} \tag{80}$$

Replacing it in in Equation 6 and isolating the convective heat transfer coefficient yields the final expressions:

$$ht = \sum_{srow} \widehat{Pht}_{srow}\, yrow_{srow} \tag{81}$$

$$\widehat{Pht}_{srow} = \frac{\widehat{kt}\ 0{,}023 \left(\frac{4\widehat{mt}}{\pi\widehat{\mu t}}\right)^{0,8} \widehat{Prt}^{n}}{\widehat{Pdti}_{srow}^{1.8}} \left(\frac{\widehat{PNpt}_{srow}}{\widehat{PNtt}_{srow}}\right)^{0,8} \tag{82}$$

2.2.2.3. Overall heat transfer coefficient

Equation 30 also needs to be rewritten as a function of the binary variables:

$$\frac{1}{U} = \sum_{srow} \frac{\widehat{Pdte}_{srow}}{\widehat{Pht}_{srow}\widehat{Pdti}_{srow}} yrow_{srow} + \widehat{Rft} \sum_{srow} \frac{\widehat{Pdte}_{srow}}{\widehat{Pdti}_{srow}} yrow_{srow} + \frac{\sum_{srow} \widehat{Pdte}_{srow} \ln(\frac{\widehat{Pdte}_{srow}}{\widehat{Pdti}_{srow}}) yrow_{srow}}{2\, \widehat{Ktube}} + \widehat{Rfs} + \sum_{srow} \frac{1}{\widehat{Phs}_{srow}} yrow_{srow} \tag{83}$$

In the original model, that is being reported here, the fouling resistances were considered fixed parameters. Later, the proposed modifications, that are the main goal of this work, will allow including the fouling model behavior in this equation.

2.2.2.4. Heat transfer rate equation

The heat transfer rate equation (Equation 5) is the constraint that will incorporate all the heat exchanger model equations. The parameters related to the convective coefficients and the area equation will be included in this constraint. First, the heat transfer area (Equation 31) is rewritten as:

$$A = \pi \sum_{srow} \widehat{PNtt}_{srow} \widehat{Pdte}_{srow} \widehat{PL}_{srow} yrow_{srow} \tag{84}$$

Isolating the area term in the heat transfer rate equation (Equation 5), replacing it in Equation 32 as the required area (*Areq*) and writing the LMTD correction factor using the *srow* concept, we have the following constraint:

$$A \geq \frac{\hat{Q}}{U\widehat{\Delta Tlm}\hat{F}_{srow}}\left(1+\frac{Aexc}{100}\right) \tag{85}$$

$$\hat{F}_{srow} = \begin{cases} \dfrac{\left(\hat{R}^2+1\right)^{0.5}\ln\left(\frac{(1-\hat{P})}{(1-\hat{R}\hat{P})}\right)}{(\hat{R}-1)\ln\left(\frac{2-\hat{P}\left(\hat{R}+1-\left(\hat{R}^2+1\right)^{0.5}\right)}{2-\hat{P}\left(\hat{R}+1+\left(\hat{R}^2+1\right)^{0.5}\right)}\right)} & \text{if } \widehat{PNpt}_{srow} \neq 1 \\ 1 & \text{if } \widehat{PNpt}_{srow} = 1 \end{cases} \tag{86}$$

Rearranging:

$$\frac{\hat{Q}}{U} \leq A\left(\frac{100}{100+\widehat{Aexc}}\right)\widehat{\Delta Tlm}\hat{F}_{srow} \tag{87}$$

Finally, replacing Equation 87 in Equation 83, we have:

$$\hat{Q}\left(\sum_{srow}\frac{\widehat{Pdte}_{srow}}{\widehat{Pht}_{srow}\widehat{Pdti}_{srow}}yrow_{srow} + \widehat{Rft}\sum_{srow}\frac{\widehat{Pdte}_{srow}}{\widehat{Pdti}_{srow}}yrow_{srow} + \frac{\sum_{srow}\widehat{Pdte}_{srow}\ln(\frac{\widehat{Pdte}_{srow}}{\widehat{Pdti}_{srow}})yrow_{srow}}{2\,\widehat{Ktube}} + \widehat{Rfs} + \sum_{srow}\frac{1}{\widehat{Phs}_{srow}}yrow_{srow}\right) \leq A\left(\frac{100}{100+\widehat{Aexc}}\right)\widehat{\Delta Tlm}\hat{F}_{srow} \tag{88}$$

The final formulation will only contain the constraint represented by Equation 88, since the calculations of the convective heat transfer coefficients are represented by the parameters $\widehat{Pht}_{srow}$ (Equation 82) and $\widehat{Phs}_{srow}$ (Equation 76) that multiplies the binary variable ($yrow_{srow}$).

2.2.2.5. Bounds on pressure drops, flow velocities and Reynolds numbers

The constraints for pressure drop will undergo the same reformulation process. Replacing the Reynolds number (Equation 73) in the friction factor equation for the shell-side (Equation 24), we have:

$$fs = 1.728\left(\frac{\widehat{ms}}{\widehat{\mu s}}\right)^{-0.188}\left(\sum_{srow}\frac{\widehat{PDeq}_{srow}(\widehat{PNb}_{srow}+1)}{\widehat{PDs}_{srow}\widehat{PFAR}_{srow}\widehat{PL}_{srow}}yrow_{srow}\right)^{-0.188} \tag{89}$$

Replacing the equations for friction factor for the shell-side (Equation 89), shell diameter (Equation 56), number of baffles (Equation 61), equivalent diameter (Equation 71) and shell-side velocity (Equation 70) in the pressure drop equation for the shell-side (Equation 23), we write:

$$\Delta Ps_{srow} = \sum_{srow} \widehat{P\Delta Ps}_{srow}\, yrow_{srow} \tag{90}$$

$$\widehat{P\Delta Ps}_{srow} = 0.864 \frac{\widehat{ms}^{1.812}\widehat{\mu s}^{0.188}}{\widehat{\rho s}} \left(\frac{(\widehat{PNb}_{srow}+1)^{2.812}}{\widehat{PDs}_{srow}^{\,0.812}(\widehat{PFAR}_{srow}\widehat{PL}_{srow})^{1.812}(\widehat{PDeq}_{srow})^{1.188}} \right) \tag{91}$$

Finally, the constraint for maximum shell-side pressure drop is:

$$\sum_{srow} \widehat{P\Delta Ps}_{srow} yrow_{srow} \leq \widehat{\Delta Psdisp} \tag{92}$$

The parameter $\widehat{\Delta Psdisp}$ is the available pressure drop in the system and must be defined by the designer according to the project specifications. This constraint (Equation 92) will be part of the final model that will be entirely organized and displayed later.

The development of the constraint for the maximum tube-side pressure drop will also start by reformulating the friction factor for the tube-side. Replacing the tube-side Reynolds number equation (Equation 79) in the tube-side friction factor equation (Equation 29).

$$ft = 0.014 + 1{,}056 \left(\frac{\pi \widehat{\mu t}}{4\widehat{mt}} \right)^{0.42} \sum_{srow} \left(\frac{\widehat{PNtt}_{srow}\widehat{Pdti}_{srow}}{\widehat{PNpt}_{srow}} \right)^{0.42} yrow_{srow} \tag{93}$$

Replacing the equations for friction factor for the tube-side (Equation 93), number of tube passes (Equation 58), tube length (Equation 60), inner tube diameter (Equation 55) and tube-side velocity (Equation 77) in the pressure drop equation for the tube-side (Equation 28), we write:

$$\Delta Pt_{srow} = \sum_{srow} \left(P\Delta \widehat{Pttur}b1_{srow} + P\Delta \widehat{Pttur}b2_{srow} + P\Delta \widehat{Ptcab}_{srow}\widehat{K}_{srow} \right) yrow_{srow} \tag{94}$$

where $\widehat{K}_{srow}$ is a parameter of the pressure drop model, which values have already been specified.

The two first terms in the right hand side of Equation 94 refer to the pressure drop along the tubes, while the third and the last terms refer to the pressure drop in the heads. These terms are determined by the following equations:

$$P\widehat{\Delta Pttur}b1_{srow} = \left(\frac{0.112\,\widehat{mt}^2}{\pi^2 \rho t}\right)\left(\frac{\widehat{PNpt}^3_{srow}\widehat{PL}_{srow}}{\widehat{PNtt}^2_{srow}\widehat{Pdti}_{srow}{}^5}\right) \tag{95}$$

$$P\widehat{\Delta Pttur}b2_{srow} = (0.528)\left(\frac{4^{1.58}\widehat{mt}^{1.58}\widehat{\mu t}^{0.42}}{\pi^{1.58}\widehat{\rho t}}\right)\frac{\widehat{PNpt}^{2.58}_{srow}\widehat{PL}_{srow}}{\widehat{PNtt}^{1.58}_{srow}\widehat{Pdti}^{4.58}_{srow}} \tag{96}$$

$$P\widehat{\Delta Ptcab}_{srow} = \frac{8\widehat{mt}^2}{\pi^2\widehat{\rho t}^2}\left(\frac{\widehat{PNpt}^3_{srow}}{\widehat{PNtt}^2_{srow}\widehat{Pdti}_{srow}{}^4}\right) \tag{97}$$

At the end, the constraint for maximum pressure drop will be:

$$\sum_{srow} P\widehat{\Delta Pttur}b1_{srow}yrow_{srow} + \sum_{srow} P\widehat{\Delta Pttur}b2_{srow}yrow_{srow} + \sum_{srow} P\widehat{\Delta Ptcab}_{srow}\widehat{K}_{srow}yrow_{srow} \leq \widehat{\Delta Ptdisp} \tag{98}$$

where $\widehat{\Delta Ptdisp}$ is analogous to $\widehat{\Delta Psdisp}$.

The Reynolds number on the tube-side, as explained before, must be bounded for the model considered here, since the correlations to calculate Nusselt numbers and friction factors are only valid for turbulent flow. Therefore, for the Reynolds number (Equation 79) we will have the following bounds:

$$\frac{\widehat{ms}}{\widehat{\mu s}}\sum_{srow}\frac{\widehat{PDeq}_{srow}(\widehat{PNb}_{srow}+1)}{\widehat{PDs}_{srow}\widehat{PFAR}_{srow}\widehat{PL}_{srow}}yrow_{srow} \geq 2{\cdot}10^3 \tag{99}$$

$$\frac{4\widehat{mt}}{\pi\widehat{\mu t}}\sum_{srow}\frac{\widehat{PNpt}_{srow}}{\widehat{PNtt}_{srow}\widehat{Pdti}_{srow}}yrow_{srow} \geq 10^4 \tag{100}$$

It is usual when designing a heat exchanger to assume bounds for maximum and minimum velocity. The maximum values are related to avoiding vibration and erosion inside the equipment, the minimum values are considered to avoid rapid fouling growth, since fouling

rate is a function of velocity and increases with its decrease. Then, the maximum and minimum bounds for the tube-side (Equation 77) and shell-side (Equation 70) velocities are:

$$\widehat{vsmin} \leq \frac{\widehat{ms}}{\widehat{\rho s}} \sum_{srow} \frac{(\widehat{PNb}_{srow}+1)}{\widehat{PDs}_{srow}\widehat{PFAR}_{srow}\widehat{PL}_{srow}} yrow_{srow} \quad (101)$$

$$\widehat{vsmax} \geq \frac{\widehat{ms}}{\widehat{\rho s}} \sum_{srow} \frac{(\widehat{PNb}_{srow}+1)}{\widehat{PDs}_{srow}\widehat{PFAR}_{srow}\widehat{PL}_{srow}} yrow_{srow} \quad (102)$$

$$\widehat{vtmin} \leq \frac{4\widehat{mt}}{\pi\widehat{\rho t}} \sum_{srow} \frac{\widehat{PNpt}_{srow}}{\widehat{PNtt}_{srow}\widehat{Pdti}_{srow}{}^2} yrow_{srow} \quad (103)$$

$$\widehat{vtmax} \geq \frac{4\widehat{mt}}{\pi\widehat{\rho t}} \sum_{srow} \frac{\widehat{PNpt}_{srow}}{\widehat{PNtt}_{srow}\widehat{Pdti}_{srow}{}^2} yrow_{srow} \quad (104)$$

2.2.2.6. Geometric constraints

Replacing the equation for baffle spacing (Equation 66) and for shell diameter (Equation 56) into the constraints represented in Equations 39 and 40, we have:

$$\sum_{srow} \frac{\widehat{PL}_{srow}}{(\widehat{PNb}_{srow}+1)} yrow_{srow} \geq 0.2 \sum_{srow} \widehat{PDs}_{srow} yrow_{srow} \quad (105)$$

$$\sum_{srow} \frac{\widehat{PL}_{srow}}{(\widehat{PNb}_{srow}+1)} yrow_{srow} \leq 1.0 \sum_{srow} \widehat{PDs}_{srow} yrow_{srow} \quad (106)$$

The same can be done for the length-shell diameter ratio, replacing its equations (Equations 60 and 56) in the constraints presented by Equations 41 and 42:

$$\sum_{srow} \widehat{PL}_{srow} yrow_{srow} \geq 3 \sum_{srow} \widehat{PDs}_{srow} yrow_{srow} \quad (107)$$

$$\sum_{srow} \widehat{PL}_{srow} yrow_{srow} \leq 15 \sum_{srow} \widehat{PDs}_{srow} yrow_{srow} \quad (108)$$

2.2.2.7. Additional constraints

The constraints presented in this topic aim to reduce the search space, with the goal to accelerate the processing time, making the problem faster to solve. These constraints will make the binary variable equal to zero for the exchangers that do not obey the relations considered.

Velocity bounds

$$yrow_{srow} = 0 \text{ for } srow \in (Svsminout \cup Svsmaxout) \tag{109}$$

$$yrow_{srow} = 0 \text{ for } srow \in (Svtminout \cup Svtmaxout) \tag{110}$$

Svsminout, *Svsmaxout*, *Svtminout* and *Svtmaxout* are the subsets of *srow* given by:

$$Svsminout = \{srow \mid \frac{\widehat{ms}}{\widehat{\rho s}} \frac{(\widehat{PNb}_{srow}+1)}{\widehat{PDs}_{srow}\widehat{PFAR}_{srow}\widehat{PL}_{srow}} \leq \widehat{vsmin} - \varepsilon\} \tag{111}$$

$$Svsmaxout = \{srow \mid \frac{\widehat{ms}}{\widehat{\rho s}} \frac{(\widehat{PNb}_{srow}+1)}{\widehat{PDs}_{srow}\widehat{PFAR}_{srow}\widehat{PL}_{srow}} \geq \widehat{vsmax} + \varepsilon\} \tag{112}$$

$$Svtminout = \{srow \mid \frac{4\widehat{mt}}{\pi\widehat{\rho t}} \frac{\widehat{PNpt}_{srow}}{\widehat{PNtt}_{srow}\widehat{Pdti}_{srow}^{\,2}} \leq \widehat{vtmin} - \varepsilon\} \tag{113}$$

$$Svtmaxout = \{srow \mid \frac{4\widehat{mt}}{\pi\widehat{\rho t}} \frac{\widehat{PNpt}_{srow}}{\widehat{PNtt}_{srow}\widehat{Pdti}_{srow}^{\,2}} \geq \widehat{vtmax} + \varepsilon\} \tag{114}$$

with ε being a small positive number used to not exclude the heat exchanger that obeys the constraint being equal to it.

Maximum pressure drop for the shell-side

$$yrow_{srow} = 0 \text{ for } srow \in SDPsmaxout \tag{115}$$

where *SDPsmaxout* is a subset of *srow* given by:

$$SDPsmaxout = \{srow \mid \widehat{P\Delta Ps}_{srow} \geq \widehat{\Delta Psdisp} + \varepsilon\} \tag{116}$$

Bounds for baffle spacing

$$yrow_{srow} = 0 \text{for} srow \in (SLNbminout \cup SLNbmaxout) \quad (117)$$

where *SLNbminout* and *SLNbmaxout* are subsets of *srow* given by:

$$SLNbminout = \{srow \mid \frac{\widehat{PL}_{srow}}{\widehat{PNb}_{srow}+1} \leq 0.2\widehat{PDs}_{srow} - \varepsilon\} \quad (118)$$

$$SLNbmaxout = \{srow \mid \frac{\widehat{PL}_{srow}}{\widehat{PNb}_{srow}+1} \geq 1.0\widehat{PDs}_{srow} + \varepsilon\} \quad (119)$$

Tube length-shell diameter ratio

$$yrow_{srow} = 0 \text{ for } srow \in (SLDminout \cup SLDmaxout) \quad (120)$$

where *SLDminout* and *SLDmaxout* are subsets of *srow* given by:

$$SLDminout = \{srow \mid \widehat{PL}_{srow} \leq 3\widehat{PDs}_{srow} - \varepsilon\} \quad (121)$$

$$SLDmaxout = \{srow \mid \widehat{PL}_{srow} \geq 15\widehat{PDs}_{srow} + \varepsilon\} \quad (122)$$

Minimum heat transfer area

$$yrow_{srow} = 0 \text{ for } srow \in SAminout \quad (123)$$

where *SAminout* is a subset of *srow* given by:

$$SAminout = \{srow \mid \pi\widehat{PNtt}_{srow}\widehat{Pdte}_{srow}\widehat{PL}_{srow} \leq \widehat{Amin} - \varepsilon\} \quad (124)$$

The lower bound for heat transfer area ($\widehat{Amin}$) is defined as the required heat transfer area considering the maximum overall heat transfer coefficient, which is calculated using the maximum convective heat transfer coefficients for the tube and shell sides ($\widehat{htmax}$ and

$\widehat{hsmax}$)and the minimum inner tube diameter-outer tube diameter ratio ($\widehat{drmin}$). Those parameters are calculated as follows:

$$\widehat{Umax} = \frac{1}{\frac{1}{\widehat{htmax}}\widehat{drmin} + \widehat{Rft}\cdot\widehat{drmin} + \frac{\widehat{Pdte}_{srow}\ln(\widehat{drmin})}{2\,\widehat{ktube}} + \widehat{Rfs} + \frac{1}{\widehat{hsmax}}} \quad (125)$$

$$\widehat{htmax} = \max(\widehat{Pht}_{srow}) \quad (126)$$

$$\widehat{hsmax} = \max(\widehat{Phs}_{srow}) \quad (127)$$

$$\widehat{drmin} = \min(\widehat{Pdte}_{srow}/\widehat{Pdti}_{srow}) \quad (128)$$

Finally, the minimum heat transfer area is:

$$\widehat{Amin} = \frac{\hat{Q}}{\widehat{Umax}\widehat{\Delta Tlm}} \quad (129)$$

2.2.2.8. Objective function

The heat exchanger area is calculated as a function of the total number of tubes (*Ntt*), the outer tube diameter (*dte*) and the tube length (*L*) as follows:

$$A = \pi Nttdte L \quad (130)$$

The total number of tubes is determined, as the other geometric variables, by the following equation:

$$Ntt = \sum_{srow} \widehat{PNtt}_{srow}\, yrow_{srow} \quad (131)$$

Therefore, the objective function, which is the minimization of the area, will be rewritten by replacing the equations for total number of tubes (Equation 106), outer tube diameter (Equation 53) and length (Equation 59) in Equation 104:

$$\min \pi \sum_{srow} \widehat{PNtt}_{srow}\widehat{Pdte}_{srow}\widehat{PL}_{srow} yrow_{srow} \quad (132)$$

2.3. **The complete ILP model**

There are no nonlinear terms or continuous variables in the final model; it only has binary variables in linear functions. Therefore, the reformulation of the nonlinear model is an ILP model that can be solved to its global optimum. This ILP model is composed by the objective function (Equation 132) and the following constraints:

- Heat transfer rate equation (Equation 88);
- Summation of binaries (Equation 62);
- Bounds on velocity for the tube-side (Equation 103 and 104) and for the shell-side (Equation 101 and 102);
- Bounds on Reynolds number for the tube-side (Equation 100) and for the shell-side (Equation 99);
- Constraint for maximum pressure drop on the tube-side side (Equation 98) and on the shell-side (Equation 92);
- Geometric constraints (Equations 105-108);
- Additional constraints (Equations 109, 110, 115, 117, 120 and 123).

The following sections will propose modifications for this model in order to consider fouling models in the optimization problem. The modification will focus on the heat transfer rate equation, particularly in the terms for fouling resistance on the tube-side, that in this model were considered constant. The fouling models explored here show that fouling can be described as a function of velocity and/or wall temperature, depending on the model.

3. OPTIMIZATION OF HEAT EXCHANGER DESIGN CONSIDERING FOULING MODELS: VELOCITY EFFECT

This section encompasses the insertion of the fouling model proposed by Nesta and Bennett (2004) for cooling water into the ILP model described previously. The resultant model will be another ILP model with the fouling resistance being defined by the mentioned fouling model, in which it is a function of velocity. The value found for fouling resistance according to the fouling model is the asymptotic value, the highest value it can achieve.

3.1. **Insertion of the fouling model**

The fouling model considered here is a power law in which the fouling resistance is inversely proportional to a power of velocity:

$$Rft = \widehat{kRft}\ (vt)^{-\widehat{\alpha Rft}} \tag{133}$$

Originally, this model was proposed for cooling water flowing in the tube-side, however this thesis considers that the model can be applied to other fluids and for the shell-side, as proposed by Caputo et al. (2011). Therefore, it is possible to write the following equation for fouling resistance on the shell-side:

$$Rfs = \widehat{kRfs}\ (vs)^{-\widehat{\alpha Rfs}} \tag{134}$$

In Equations 133 and 134, *Rft* and *Rfs* are the fouling resistances on the tube-side and on the shell-side, respectively, $\widehat{kRft}$ and $\widehat{\alpha Rft}$ are the model parameters for the tube-side, and $\widehat{kRfs}$ and $\widehat{\alpha Rfs}$ are the model parameters for the shell-side.

To insert the fouling model in the ILP model we have to replace Equations 134 and 133 in the heat transfer rate constraint (Equation 88), however if we replace them directly as they are we will have nonlinear terms in our model, related to the variables representing the velocities. Therefore, the fouling model equations must undergo the same reformulation procedure described in Chapter 2.

Replacing the tube-side velocity (Equation 77) and the shell-side velocity (Equation 70) in Equations 133 and 134 we have:

$$Rft = \widehat{kRft}\left(\frac{4\widehat{mt}}{\pi\widehat{\rho t}}\sum_{srow}\frac{\widehat{PNpt}_{srow}}{\widehat{PNtt}_{srow}\widehat{Pdti}_{srow}{}^{2}}\right)^{-\widehat{\alpha Rft}} yrow_{srow} \quad (135)$$

$$Rfs = \widehat{kRfs}\left(\frac{\widehat{ms}}{\widehat{\rho s}}\sum_{srow}\frac{\left(\widehat{PNb}_{srow}+1\right)}{\widehat{PDs}_{srow}\widehat{PFAR}_{srow}\widehat{PL}_{srow}}\right)^{-\widehat{\alpha Rfs}} yrow_{srow} \quad (136)$$

These equations are replaced in the heat transfer rate constraint (Equation 88), giving the following linear constraint:

$$\hat{Q}\left(\sum_{srow}\frac{\widehat{Pdte}_{srow}}{\widehat{Pht}_{srow}\,\widehat{Pdti}_{srow}}yrow_{srow} + \widehat{kRft}\left(\frac{4\,\widehat{mt}}{\pi\,\widehat{\rho t}}\right)^{-\widehat{\alpha Rft}}\sum_{srow}\left(\frac{\widehat{PNpt}_{srow}}{\widehat{PNtt}_{srow}\widehat{Pdti}_{srow}{}^{2}}\right)^{-\widehat{\alpha Rft}}\frac{\widehat{Pdte}_{srow}}{\widehat{Pdti}_{srow}}yrow_{srow} + \frac{\sum_{srow}\widehat{Pdte}_{srow}\,yrow_{srow}\ln\left(\frac{\widehat{Pdte}_{srow}}{\widehat{Pdti}_{srow}}\right)}{2\,\widehat{Ktube}} + \widehat{kRfs}\left(\frac{\widehat{ms}}{\widehat{\rho s}}\sum_{srow}\frac{\left(\widehat{PNb}_{srow}+1\right)}{\widehat{PDs}_{srow}\widehat{PFAR}_{srow}\widehat{PL}_{srow}}\right)^{-\widehat{\alpha Rfs}} yrow_{srow} + \sum_{srow}\frac{1}{\widehat{Phs}_{srow}}yrow_{srow}\right) \leq \left(\frac{100}{100+\widehat{Aexc}}\right)\left(\pi\sum_{srow}\widehat{PNtt}_{srow}\widehat{Pdte}_{srow}\,\widehat{PL}_{srow}yrow_{srow}\right)\widehat{\Delta Tlm}\;\hat{F}_{srow} \quad (137)$$

3.2. **Complete ILP model**

To facilitate the visualization of the resultant ILP model, this topic will display all the constraints and the objective function. Numerical investigations indicated that replacing the original constraints (Equations 103, 104, 101, 102, 92, 105, 106, 107 and 108) by the additional constraints (Equations 109, 110, 115, 117, 120 and 123) allows a performance gain (SOUZA; COSTA; BAGAJEWICZ, 2018), therefore, in the proposed formulation, only the auxiliary constraints are displayed.

3.2.1. Objective function

$$\min \pi\sum_{srow}\widehat{PNtt}_{srow}\widehat{Pdte}_{srow}\widehat{PL}_{srow}yrow_{srow} \quad (132)$$

3.2.2. Constraints

Heat transfer rate equation

$$\hat{Q}\left(\sum_{srow}\frac{\widehat{Pdte}_{srow}}{\widehat{Pht}_{srow}\,\widehat{Pdti}_{srow}}yrow_{srow}+\right.$$
$$\widehat{kRft}\left(\frac{4\,\widehat{mt}}{\pi\,\widehat{\rho t}}\right)^{-\widehat{\alpha Rft}}\sum_{srow}\left(\frac{\widehat{PNpt}_{srow}}{\widehat{PNtt}_{srow}\widehat{Pdti}_{srow}{}^{2}}\right)^{-\widehat{\alpha Rft}}\frac{\widehat{Pdte}_{srow}}{\widehat{Pdti}_{srow}}yrow_{srow}+$$
$$\frac{\sum_{srow}\widehat{Pdte}_{srow}\,yrow_{srow}\ln\left(\frac{\widehat{Pdte}_{srow}}{\widehat{Pdti}_{srow}}\right)}{2\,\widehat{Ktube}}+\widehat{kRfs}\left(\frac{\widehat{ms}}{\widehat{\rho s}}\sum_{srow}\frac{\left(\widehat{PNb}_{srow}+1\right)}{\widehat{PDs}_{srow}\widehat{PFAR}_{srow}\widehat{PL}_{srow}}\right)^{-\widehat{\alpha Rfs}}yrow_{srow}+$$
$$\left.\sum_{srow}\frac{1}{\widehat{Phs}_{srow}}yrow_{srow}\right)\leq$$
$$\left(\frac{100}{100+\widehat{Aexc}}\right)\left(\pi\sum_{srow}\widehat{PNtt}_{srow}\widehat{Pdte}_{srow}\,\widehat{PL}_{srow}yrow_{srow}\right)\widehat{\Delta Tlm}\;\hat{F}_{srow} \quad (133)$$

Summation of binaries

$$\sum_{srow}yrow_{srow}=1 \quad (62)$$

Maximum pressure drop for the tube-side

$$\sum_{srow}P\widehat{\Delta Pturb1}_{srow}yrow_{srow}+\sum_{srow}P\widehat{\Delta Pturb2}_{srow}yrow_{srow}+$$
$$\sum_{srow}P\widehat{\Delta Pcab}_{srow}\hat{K}_{srow}yrow_{srow}\leq\widehat{\Delta Pdisp} \quad (98)$$

Maximum pressure drop for the shell-side

$$yrow_{srow}=0 \text{ for } srow\in SDPsmaxout \quad (115)$$

where *SDPsmaxout* is a subset of *srow* given by:

$$SDPsmaxout=\{srow\mid\widehat{P\Delta Ps}_{srow}\geq\widehat{\Delta Psdisp}+\varepsilon\} \quad (116)$$

Reynolds number bounds

$$\frac{\widehat{ms}}{\widehat{\mu s}}\sum_{srow}\frac{\widehat{PDeq}_{srow}(\widehat{PNb}_{srow}+1)}{\widehat{PDs}_{srow}\widehat{PFAR}_{srow}\widehat{PL}_{srow}}yrow_{srow} \geq 2{\cdot}10^{3} \tag{99}$$

$$\frac{4\widehat{mt}}{\pi\widehat{\mu t}}\sum_{srow}\frac{\widehat{PNpt}_{srow}}{\widehat{PNtt}_{srow}\widehat{Pdti}_{srow}}yrow_{srow} \geq 10^{4} \tag{100}$$

Velocity bounds

$$yrow_{srow} = 0 \text{ for } srow \in (Svsminout \cup Svsmaxout) \tag{109}$$

$$yrow_{srow} = 0 \text{ for } srow \in (Svtminout \cup Svtmaxout) \tag{110}$$

Svsminout, *Svsmaxout*, *Svtminout* and *Svtmaxout* are the subsets of *srow* given by:

$$Svsminout = \{srow \mid \frac{\widehat{ms}}{\widehat{\rho s}}\frac{(\widehat{PNb}_{srow}+1)}{\widehat{PDs}_{srow}\widehat{PFAR}_{srow}\widehat{PL}_{srow}} \leq \widehat{vsmin} - \varepsilon\} \tag{111}$$

$$Svsmaxout = \{srow \mid \frac{\widehat{ms}}{\widehat{\rho s}}\frac{(\widehat{PNb}_{srow}+1)}{\widehat{PDs}_{srow}\widehat{PFAR}_{srow}\widehat{PL}_{srow}} \geq \widehat{vsmax} + \varepsilon\} \tag{112}$$

$$Svtminout = \{srow \mid \frac{4\widehat{mt}}{\pi\widehat{\rho t}}\frac{\widehat{PNpt}_{srow}}{\widehat{PNtt}_{srow}\widehat{Pdti}_{srow}^{\,2}} \leq \widehat{vtmin} - \varepsilon\} \tag{113}$$

$$Svtmaxout = \{srow \mid \frac{4\widehat{mt}}{\pi\widehat{\rho t}}\frac{\widehat{PNpt}_{srow}}{\widehat{PNtt}_{srow}\widehat{Pdti}_{srow}^{\,2}} \geq \widehat{vtmax} + \varepsilon\} \tag{114}$$

with ε being a small positive number.

Bounds for baffle spacing

$$yrow_{srow} = 0 \text{ for } srow \in (SLNbminout \cup SLNbmaxout) \tag{117}$$

where *SLNbminout* and *SLNbmaxout* are subsets of *srow* given by:

$$SLNbminout = \{srow \mid \frac{\widehat{PL}_{srow}}{\widehat{PNb}_{srow}+1} \leq 0.2\widehat{PDs}_{srow} - \varepsilon\} \quad (118)$$

$$SLNbmaxout = \{srow \mid \frac{\widehat{PL}_{srow}}{\widehat{PNb}_{srow}+1} \geq 1.0\widehat{PDs}_{srow} + \varepsilon\} \quad (119)$$

Tube length-shell diameter ratio

$$yrow_{srow} = 0 \text{ for } srow \in (SLDminout \cup SLDmaxout) \quad (120)$$

where *SLDminout* and *SLDmaxout* are subsets of *srow* given by:

$$SLDminout = \{srow \mid \widehat{PL}_{srow} \leq 3\widehat{PDs}_{srow} - \varepsilon\} \quad (121)$$

$$SLDmaxout = \{srow \mid \widehat{PL}_{srow} \geq 15\widehat{PDs}_{srow} + \varepsilon\} \quad (122)$$

Minimum heat transfer area

$$yrow_{srow} = 0 \text{ for } srow \in SAminout \quad (127)$$

where *SAminout* is a subset of *srow* given by:

$$SAminout = \{srow \mid \pi\widehat{PNtt}_{srow}\widehat{Pdte}_{srow}\widehat{PL}_{srow} \leq \widehat{Amin} - \varepsilon\} \quad (128)$$

In this case, the fouling resistances are not fixed, then the minimum fouling resistances for the tube-side and for the shell-side must be calculated according to the fouling model considered:

$$\widehat{Umax} = \frac{1}{\frac{1}{\widehat{htmax}}\widehat{drmin} + \widehat{Rftmin}\cdot\widehat{drmin} + \frac{\widehat{Pdte}_{srow}\ln(\widehat{drmin})}{2\,\widehat{ktube}} + \widehat{Rfsmin} + \frac{1}{\widehat{hsmax}}} \quad (134)$$

$$\widehat{Rftmin} = \widehat{kRft}(\widehat{vtmax})^{-\widehat{\alpha Rft}} \quad (135)$$

$$\widehat{Rfsmin} = \widehat{kRfs}(\widehat{vsmax})^{-\widehat{\alpha Rfs}} \quad (136)$$

3.3. Results

In this section, we will present the results for the proposed ILP approach for designing heat exchangers considering a fouling model, in which the fouling is a function of velocity. To illustrate the use of this approach for the proposed problem, we also present the results for the traditional approach, using fixed fouling resistances. The values adopted for the fixed fouling resistances were based on the model, considering the values calculated for minimum velocity (overestimated resistance) and maximum velocity (underestimated resistance). Additionally, we also considered an iterative scheme that can be used for the design of heat exchangers considering fixed fouling resistances based on Nakao et al. (2017).

3.3.1. Problem data

The investigated problem considers that the fluids flowing in the heat exchanger in the tube-side as well as in the shell-side are water, and the cold fluid flows in the tubes. Table 2 presents the physical properties for those fluids and Table 3 presents the characteristics of the thermal task.

Table 2 – Physical properties

Density (kg/m^3)	Viscosity (Pa·s)	Conductivity (W/mK)	Heat capacity (J/kgK)
1000	0.000695	0.628	4178

Table3 –Thermal task

Stream	Cold	Hot
Mass flow rate (kg/s)	200	100
Inlet temperature (ºC)	32	70
Outlet temperature (ºC)	40	54
Maximum pressure drop (kPa)	60	60
Velocity bounds (m/s)	1.0 – 3.0	0.5 – 2.0

The values used for the fouling model parameters were the same used reported by Nesta and Bennett (2004). The parameters for the shell-side and for the tube-side were considered the

same, with $\widehat{kRft}$ and $\widehat{kRft}$ equal to 0.00062, and $\widehat{\alpha Rft}$ and $\widehat{\alpha Rfs}$ equal to 1.65. The minimum area excess was 11%.The problems were solved using software GAMS with the solver CPLEX using computer with Intel Core i7 processor with 8 Mb of RAM memory. The commercial values used for the geometric variables are displayed in Table 4.

Table 4 – Commercial values for the geometric variables

Variables	Values
Outer tube diameter, $\widehat{pdte}_{sd}$ (m)	0.01905,0.02540,0.03175,0.03810,0.05080
Inner tube diameter,$\widehat{pdti}_{sd}$(m)	0.01575, 0.02210, 0.02845, 0.03480, 0.04750
Tube length, $\widehat{pL}_{sL}$ (m)	1.2195, 1.8293, 2.4390, 3.0488, 3.6585, 4.8768, 6.0976
Baffle number, $\widehat{pNb}_{sNb}$	1, 2, … , 20
Number of tube passes, $\widehat{pNpt}_{sNpt}$	1, 2, 4, 6
Pitch ratio, $\widehat{prp}_{srp}$	1.25, 1.33, 1.50
Shell diameter, $\widehat{pDs}_{sDs}$ (m)	0,7874;0,8382;0,889;0,9398; 0,9906; 1,0668; 1,143; 1.2192; 1.3716; 1.524
Tube layout, $\widehat{play}_{slay}$	1 = square, 2 = triangular

3.3.2. Case 1: ILP problem with fixed fouling resistances related to the minimum velocities

In this case, the fouling resistances for the tube-side and for the shell-side were overestimated using the fouling model to calculate the maximum fouling resistances that correspond to the minimum velocities. In Equations 133 and 134,it is shown that the fouling resistance is inversely proportional to the power of velocity, therefore using the minimum velocities, we obtain the maximum fouling resistances for the example considered.

The fouling resistances are calculated through Equations 133 and 134, for the tube and shell sides, respectively.The values calculated for the resistances are $6.20 \cdot 10^{-4}$ m^2K/W for the tube-side and $1.95 \cdot 10^{-3}$ m^2K/W for the shell-side. The problem is then solved for these fixed fouling resistances and the results obtained are shown in Table 5.

Table 5 – Case 1: results

Variable	Value	Variable	Value
dte (m)	0.01905	*Deq* (m)	0.01375
dti (m)	0.01575	*Res*	10647
L (m)	4.8768	*Nus*	98.38
Nb	7	*hs* (W/m^{2}K)	4494.0
Npt	4	*vt* (m/s)	1.23
rp	1.25	*Ret*	27857.9
Ds (m)	1.524	*Nut*	152.6
lay	2	*ht* (W/m^{2}K)	6086.4
ltp	0.02381	*U* (W/m^{2}K)	317.14
Ntt	3342	*A* (m^2)	974.9
Ntp	835.5	*fs*	0.3023
lbc(m)	0.6096	*ft*	0.02835
Ar (m^2)	0.1858	ΔPs(Pa)	38822
vs (m/s)	0.538	ΔPt(Pa)	31364

Assuming that the model proposed by Nesta and Bennett (2004) can represent well the reality; we can calculate the fouling resistances through this model for the velocities found for the optimization problem. Summarizing, to find the fouling resistances we must replace the values found for the velocities (Table 5) in Equations 133 and 134.

By performing this procedure we can recalculate the overall heat transfer coefficient using the calculated fouling resistances (*vs* = 0.538 m/s e *vt* = 1.23 m/s). Table 6 shows the values obtained.

Table 6 – Case 1: recalculated values

Variable	Recalculated value
Rft (m^{2}K/W)	$4.41 \cdot 10^{-4}$
Rfs (m^{2}K/W)	$1.72 \cdot 10^{-3}$
U (W/m^{2}K)	363.42

The recalculated values for fouling resistance are smaller than the fixed ones considered during the optimization procedure; therefore, the new overall heat transfer coefficient is bigger than the one obtained by the optimization. Concluding, the heat exchanger designed by the

optimization is viable for proposed thermal service; however, we still do not know if the area indicated by the optimization is close to the minimum area, since we used fixed fouling resistances and not the fouling resistance model during the optimization.

3.3.3. Case 2: ILP problem with fixed fouling resistances related the maximum velocities

This section approaches the problem the same way it was described in the previous section. However, instead of using an overestimated value for fouling resistance it uses an underestimated value. The value is calculated through the use of the maximum velocity and is equal to $1.01 \cdot 10^{-4}$ m^2K/W for the tube-side and $1.97 \cdot 10^{-4}$ m^2K/W for the shell-side. Table 7 shows the results and Table 8 shows the values recalculated through the same procedure described for Case 1.

Table 7 – Case 2: results

Variable	Value	Variable	Value
dte (m)	0.01905	*Deq* (m)	0.01375
dti (m)	0.01575	*Res*	17168.4
L (m)	3.6585	*Nus*	127.9
Nb	4	*hs* (W/m^2K)	5844.6
Npt	2	*vt* (m/s)	2.303
rp	1.25	*Ret*	52186.7
Ds (m)	0.7874	*Nut*	252.2
lay	2	*ht* (W/m^2K)	10056.6
ltp	0.02381	*U* (W/m^2K)	1544.3
Ntt	892	*A* (m^2)	195.2
Ntp	446	*fs*	0.2763
lbc(m)	0.7317	*ft*	0.02502
Ar (m^2)	0.1152	ΔPs (Pa)	29796
vs (m/s)	0.868	ΔPt (Pa)	39309

Table 8 – Case 2: recalculated values

Variable	Value
Rft (m^2K/W)	$1.56 \cdot 10^{-4}$
Rfs (m^2K/W)	$7.83 \cdot 10^{-4}$
U (W/m^2K)	775.8

In this case, the fouling resistances calculated through the fouling model were smaller than the ones calculated for the designed exchanger;therefore, the overall heat transfer coefficient given by the optimization is smaller than the real one. In this case the heat exchanger will not be able promote the necessary heat transfer through the entire operating time; the equipment will need to go through a cleaning process earlier during the operation. Stopping the heat exchanger during operation might only be possible by reducing the flow rate, what would lead to production losses.

3.3.4. Case 3: ILP iterative problem updating fouling resistance

In this section another alternative will be explored to design heat exchangers, where a iterative procedure is performed in which the fouling resistance values are updated according to the model considered in this part of the thesis (Equations 133 and 134). This procedure involves solving ILP optimization problems consecutively using fixed fouling resistances calculated with the velocities obtained in the previous ILP optimization problem, similar to what was proposed by Nakao et al. (2017).

The iterative procedure was performed using three different values of fouling resistance as initial points. The first initial point considered the medium velocities, calculated using the maximum and minimum bounds, to calculate the fouling resistance values. The other two initial points were calculated using the maximum and minimum velocities. Figure 16 shows a scheme of the iterative procedure used.

Figure 16 – Iterative procedure scheme

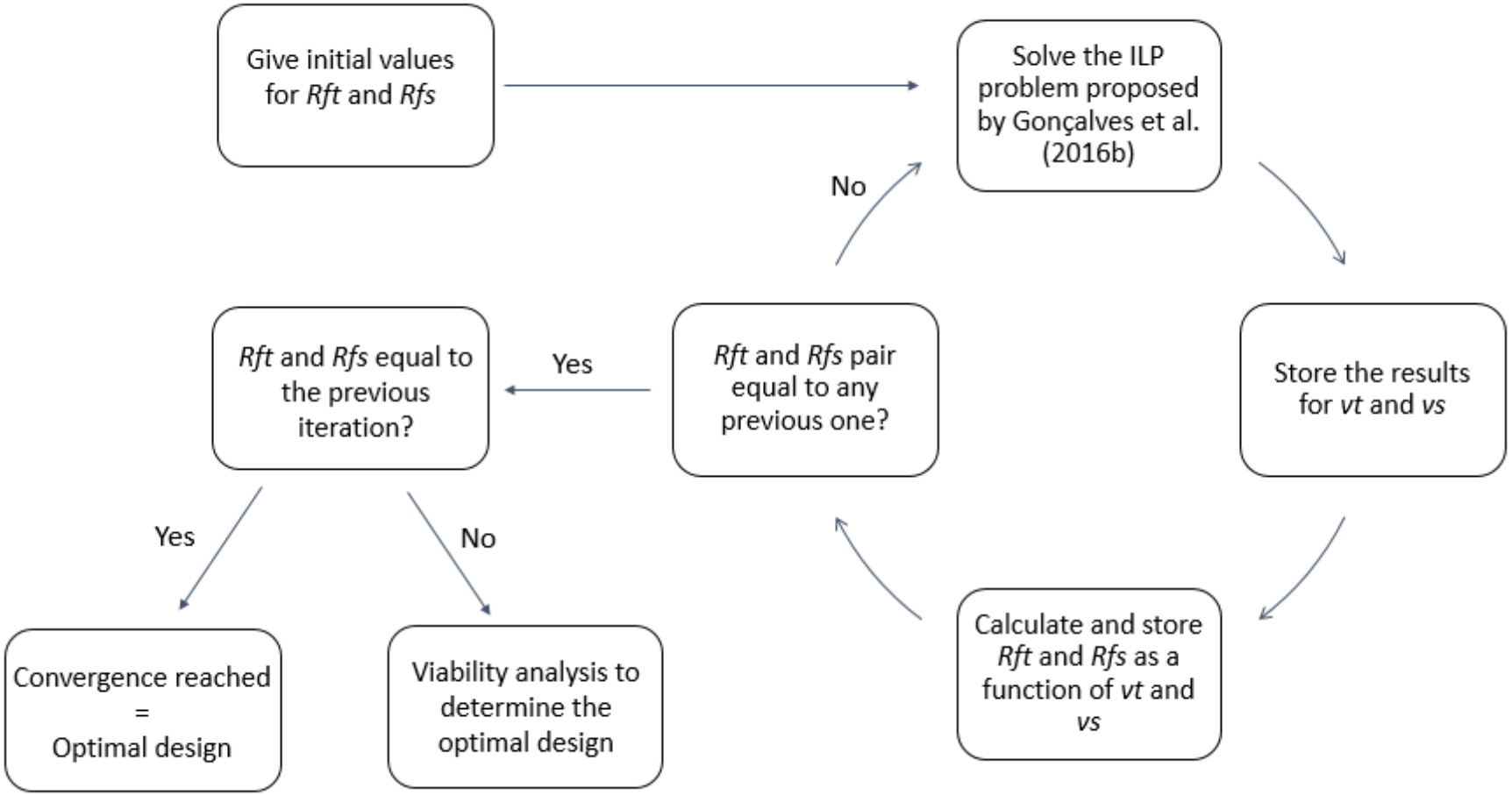

Fonte: A autora, 2018

The fouling resistance values calculated to each one of the iterations, and the corresponding velocity values are presented in Tables 9, 10 and 11 to each initial point related to the medium velocity (Case 3A), the maximum velocity (Case 3B) and the minimum velocity (Case 3C), respectively.

Table 9– Case 3A: iterative procedure results

Iteration	*Rft*(m^2K/W)	*Rfs*(m^2K/W)	*vt*(m/s)	*vs*(m/s)	*Area*(m^2)
1	$1.98 \cdot 10^{-4}$	$4.29 \cdot 10^{-4}$	1.97	0.957	308.4
2	$2.02 \cdot 10^{-4}$	$6.67 \cdot 10^{-4}$	1.90	0.801	393.9
3	$2.15 \cdot 10^{-4}$	$8.95 \cdot 10^{-4}$	1.62	0.611	463.6
4	$2.81 \cdot 10^{-4}$	$14.0 \cdot 10^{-4}$	1.55	0.723	654.1
5	$3.00 \cdot 10^{-4}$	$10.6 \cdot 10^{-4}$	1.45	0.813	559.3
6	$3.35 \cdot 10^{-4}$	$8.72 \cdot 10^{-4}$	1.81	0.875	506.6
7	$2.32 \cdot 10^{-4}$	$7.73 \cdot 10^{-4}$	1.68	0.828	446.1
8	$2.64 \cdot 10^{-4}$	$8.47 \cdot 10^{-4}$	1.62	0.698	463.6
9	$2.81 \cdot 10^{-4}$	$11.2 \cdot 10^{-4}$	1.79	0.819	566.6
10	$2.37 \cdot 10^{-4}$	$8.62 \cdot 10^{-4}$	1.62	0.611	463.6
11	$2.81 \cdot 10^{-4}$	$14.0 \cdot 10^{-4}$	1.55	0.723	654.1

Table 10 – Case 3B: iterative procedure results

Iteration	*Rft*(m^2K/W)	*Rfs*(m^2K/W)	*vt*(m/s)	*vs* (m/s)	*Area*(m^2)
1	$1.01 \cdot 10^{-4}$	$1.97 \cdot 10^{-4}$	2.30	0.868	195.2
2	$1.57 \cdot 10^{-4}$	$7.83 \cdot 10^{-4}$	1.87	0.872	401.2
3	$2.21 \cdot 10^{-4}$	$7.76 \cdot 10^{-4}$	1.68	0.828	446.1
4	$2.63 \cdot 10^{-4}$	$8.47 \cdot 10^{-4}$	1.62	0.698	463.6
5	$2.80 \cdot 10^{-4}$	$11.2 \cdot 10^{-4}$	1.79	0.819	566.6
6	$2.37 \cdot 10^{-4}$	$8.62 \cdot 10^{-4}$	1.62	0.611	463.6
7	$2.80 \cdot 10^{-4}$	$14.0 \cdot 10^{-4}$	1.55	0.723	654.1
8	$3.00 \cdot 10^{-4}$	$10.6 \cdot 10^{-4}$	1.45	0.813	559.3
9	$3.35 \cdot 10^{-4}$	$8.72 \cdot 10^{-4}$	1.81	0.875	506.6
10	$2.32 \cdot 10^{-4}$	$7.73 \cdot 10^{-4}$	1.68	0.828	446.1

Table 11 – Case 3C: iterative procedure results

Iteration	*Rft*(m^2K/W)	*Rf*(m^2K/W)	*vt*(m/s)	*vs* (m/s)	*Area* (m^2)
1	$6.2 \cdot 10^{-4}$	$19.0 \cdot 10^{-4}$	1.23	0.538	974.91
2	$4.41 \cdot 10^{-4}$	$17.2 \cdot 10^{-4}$	1.42	0.673	844.22
3	$3.48 \cdot 10^{-4}$	$11.9 \cdot 10^{-4}$	1.51	0.753	609.12
4	$3.14 \cdot 10^{-4}$	$9.90 \cdot 10^{-4}$	1.71	0.781	538.36
5	$2.56 \cdot 10^{-4}$	$9.34 \cdot 10^{-4}$	1.86	0.837	493.86
6	$2.23 \cdot 10^{-4}$	$8.32 \cdot 10^{-4}$	1.68	0.828	446.08
7	$2.64 \cdot 10^{-4}$	$8.47 \cdot 10^{-4}$	1.62	0.698	463.58
8	$2.80 \cdot 10^{-4}$	$11.2 \cdot 10^{-4}$	1.79	0.819	566.56
9	$2.37 \cdot 10^{-4}$	$8.63 \cdot 10^{-4}$	1.62	0.611	463.58
10	$2.81 \cdot 10^{-4}$	$14.0 \cdot 10^{-4}$	1.55	0.723	654.10
11	$3.00 \cdot 10^{-4}$	$10.6 \cdot 10^{-4}$	1.45	0.813	559.32
12	$3.35 \cdot 10^{-4}$	$8.72 \cdot 10^{-4}$	1.81	0.875	506.61
13	$2.32 \cdot 10^{-4}$	$7.73 \cdot 10^{-4}$	1.68	0.828	446.08

Analyzing the tables we can observe that the iterative procedure do not converge, reaching a pattern that will repeat infinitely. This pattern is observed to all three initial points for the data considered here, highlighting the importance of the approach developed in this thesis, in which it is possible to consider the fouling model together with the heat exchanger design, without any external iterative procedures.

Similarly to what was performed by Nakao et al. (2017), we can assume a viable result for the iterative procedure, considering the best result obtained in which the values calculated for the fouling resistances using the velocities (fixed values of the next loop) are smaller than the ones considered fixed in that iteration. The results for Case 3A, 3B and 3C are the ones in iterations 6, 9 and 9, respectively. The complete results for each case are shown in Tables 12, 13 and 14.

Table 12 – Case 3A: viable heat exchanger

Variable	Value	Variable	Value
dte (m)	0.03175	*Deq* (m)	0.0314
dti (m)	0.02845	*Res*	39571.5
L (m)	4.8768	*Nus*	202.5
Nb	12	*hs* (W/m^{2}K)	4044.9
Npt	6	*vt* (m/s)	1.81
rp	1.25	*Ret*	74195.4
Ds (m)	1.524	*Nut*	334.2
lay	1	*ht* (W/m^{2}K)	7377.4
ltp	0.0397	*U* (W/m^{2}K)	595.4
Ntt	1042	*A* (m^2)	506.6
Ntp	173.67	*fs*	0.236
lbc(m)	0.3751	*ft*	0.0235
Ar (m^2)	0.1143	Δ*Ps* (Pa)	56904
vs (m/s)	0.875	Δ*Pt* (Pa)	55484

Table 13 – Case 3B: viable heat exchanger

Variable	Value	Variable	Value
dte (m)	0.03175	*Deq* (m)	0.0314
dti (m)	0.02845	*Res*	39571.5
L (m)	4.8768	*Nus*	202.5
Nb	12	*hs* (W/m^{2}K)	4044.9
Npt	6	*vt* (m/s)	1.81
rp	1.25	*Ret*	74195.4
Ds (m)	1.524	*Nut*	334.2
lay	1	*ht* (W/m^{2}K)	7377.4
ltp	0.0397	*U* (W/m^{2}K)	595.4
Ntt	1042	*A* (m^2)	506.6
Ntp	173.67	*fs*	0.236
lbc(m)	0.3751	*ft*	0.0235
Ar (m^2)	0.1143	Δ*Ps*(Pa)	56904
vs (m/s)	0.875	Δ*Pt*(Pa)	55484

Table 14 – Case 3C: viable heat exchanger

Variable	Value	Variable	Value
dte (m)	0.01905	*Deq* (m)	0.0137
dti (m)	0.01575	*Res*	12082.6
L (m)	6.0976	*Nus*	105.5
Nb	6	*hs* (W/m^{2}K)	4817.7
Npt	2	*vt* (m/s)	1.62
rp	1.25	*Ret*	36625.1
Ds (m)	0.9398	*Nut*	190.0
lay	2	*ht* (W/m^{2}K)	7575.8
ltp	0.0238	*U* (W/m^{2}K)	644.5
Ntt	1271	*A* (m^2)	463.6
Ntp	635.50	*fs*	0.295
lbc(m)	0.8711	*ft*	0.02679
Ar (m^2)	0.1637	Δ*Ps*(Pa)	26344
vs (m/s)	0.611	Δ*Pt*(Pa)	31270

3.3.5. Case 4: ILP model considering fouling as a function of velocity (current proposal)

Case 4 is the proposed approach of this thesis for designing heat exchangers. The approach considers the fouling model in which fouling resistance is a function of velocity (NESTA; BENNETT, 2004). This model is able to identify the global optimum because of its linear nature. The results are displayed in Table 15.

Table 15 – Case 4: results

Variable	Value	Variable	Value
dte (m)	0.0254	*Deq* (m)	0.02516
dti (m)	0.0221	*Res*	33483.6
L (m)	4.8768	*Nus*	184.8
Nb	10	*hs* (W/m^{2}K)	4612.3
Npt	4	*vt* (m/s)	2.00
rp	1.25	*Ret*	63676
Ds (m)	1.2192	*Nut*	295.7
lay	1	*ht* (W/m^{2}K)	8403.7
ltp	0.03175	*U* (W/m^{2}K)	757.2
Ntt	1042	*A* (m^2)	405.3
Ntp	260.5	*fs*	0.2437
lbc(m)	0.4433	*ft*	0.02414
Ar (m^2)	0.1081	ΔPs(Pa)	55584
vs (m/s)	0.925	ΔPt(Pa)	55551

The results obtained using the proposed model gives an area equal to 405.29 m² which presents a reduction of 58% compared to the more conservative approach (fixed fouling resistances calculated using the minimum velocities).

3.3.6. Comparing the results

In this section, some comparative analyses will be made in order to summarize the results, facilitating the visualization of the gain related to using the proposed approach (Case 4) and not the others. Table 16 shows some of the results for the cases previously presented.

Table 16 – Comparing the proposed approach with the others

	Computational time (s)	Area(m^2)	Viability	Excess of area compared to Case 4 (%)
Case 1	1.06	974.8	Viable	140.05
Case 2	1.14	191.6	Not viable	-
Case 3A	198.2	506.6	Viable	25.0
Case 3B	303.3	506.6	Viable	25.0
Case 3C	126.5	463.6	Viable	14.4
Case 4	23.12	405.3	Viable	0

The column related to the viability of the heat exchanger in Table 16 indicates whether the result is viable during the entire operating time. The only result that is not viable is the one for Case 2, which uses the value for fouling resistance calculated with the maximum velocity possible for flow in both sides.

Comparing the computational times it is easy to observe that Cases 1 and 2 took much less time to solve. However, as mentioned before, Case 2 presents a not viable result and Case 1 has an area excess larger than 140% compared to the area of the proposed approach (Case 4). Due to their iterative nature, cases 3 demanded larger computational times when compared to the other ones, where the ILP problem must be solved many times to achieve the final result. Case 4 has a computational time considerably smaller than the ones for Cases 3.

Regarding the resultant areas, Case 3C was the one that got closer to the results from the proposed approach, however, it still has an area excess of almost 15%, besides the larger computational time. Therefore, it is possible to say that the proposed approach presented in this thesis has advantages when compared to the other ones explored here.

4. OPTIMIZATION OF HEAT EXCHANGER DESIGN CONSIDERING FOULING MODELS: VELOCITY AND WALL TEMPERATURE EFFECTS

This chapter will introduce a new approach regarding the inclusion of threshold fouling models in the original ILP model. This type of semi-empirical model is highly applied to describe fouling in crude oil streams flowing in the tube-side in refinery preheat trains. As usually considered in this scenario, the fouling resistance in the shell-side will be considered negligible. The way the fouling model is considered in this approach, the complete resultant MILP model and the results will be presented next.

4.1. **MILP model development**

This section will be divided in three parts, the first one will present the idea of this approach to include the fouling model into the ILP model, the second part regards the fouling behavior modeling using mathematical logic and the third one shows the development of the model including the reformulation of the nonlinear terms through the mathematical techniques used before.

4.1.1. Modelling fouling resistance

There are severalthreshold fouling models described in literature, the formulation proposed here was developed using the model proposed by Polley et al. (2002a), that was already shown in the section regarding the review of literature.

Here, the model will be represented by the following equation:

$$\frac{dRf}{dt} = \alpha Ret^{-0,8} Prt^{-0.33} exp\left(\frac{-Ea}{RT_s}\right) - \gamma Ret^{0,8} \quad (137)$$

in which $\frac{dRf}{dt}$ is the fouling rate, α, Ea and γ are the empirical parameters, R is the gas universal constant and T_s is the surface temperature at the interface between wall/fouling layer and the cold stream. Other models of this type have a similar mathematical structure; therefore, the proposed approach can be adapted to consider other threshold fouling models (WILSON; ISHIYAMA; POLLEY, 2015).

In a more compact form, the model can be represented as:

$$\frac{dRf}{dt} = \widehat{Af} Ret^{-0,8} exp\left(\frac{-\widehat{\psi f}}{T_s}\right) - \widehat{Bf} Ret^{0,8} \quad (138)$$

where:

$$\widehat{Af} = \alpha Prt^{-0,33} \quad (139)$$

$$\widehat{Bf} = \gamma \quad (140)$$

$$\widehat{\psi f} = \frac{Ea}{R} \quad (141)$$

In this type of model, there is a term regarding the formation rate, positive term, and another regarding the removal/suppression rate, negative term. The interpretation of the negative term in the threshold fouling model as suppression or removal is still in debate in the literature. The suppression hypothesis assumes that the thermo-fluid dynamic conditions may suppress the accumulation of deposits, but it cannot remove them once they are installed over the thermal surface, i.e. according to this interpretation, the net fouling rate would be never negative (negative values predicted by the model would be overrun by zero) (ISHIYAMA, PATERSON, WILSON, 2008). The proposition of the optimization model developed in this thesis will not be affected by the difference between these two interpretations, therefore, we will identify this term from now on as “suppression”, without loss of generality.

At the beginning of the campaign, if the suppression rate term is equal or bigger than the formation rate, the fouling rate is null and the heat exchanger will remain clean over the operating period. In this scenario the exchanger will be in the “no fouling” region, presented in Figure 12.

If the opposite situation occurs, there will be accumulation of deposits over the operation. As the deposits accumulate, the surface temperature drops and, as the Arrhenius term shows, there is a gradual reduction of the fouling rate. Depending on the values of the fouling model parameters and the cold stream temperature, this progressive reduction of rate can go to zero (i.e. asymptotic pattern) or go to a constant not null value (i.e. linear pattern). As consequence, considering a finite operating time, the fouling resistance value at the end of the

campaign, that will be used to design the heat exchanger, will be the minimum between its asymptotic value (Rf^{∞}) and a maximum value established by the designer ($\widehat{Rf}^{max}$).

Therefore:

$$\widehat{Af}Ret^{-0,8}e^{-\widehat{\psi f}/T_{w0}} \leq \widehat{Bf}Ret^{0,8} \qquad then, Rf = 0 \tag{142}$$

$$\widehat{Af}Ret^{-0,8}e^{-\widehat{\psi f}/T_{w0}} > \widehat{Bf}Ret^{0,8} \qquad then, Rf = \min(\widehat{Rf}^{max}, Rf^{\infty}) \tag{143}$$

In the previous equations, T_{w0} is the wall temperature for the clean heat exchanger (Rf= 0), at the beginning of the operation.

The formulation of the optimization problem demands an expression for the asymptotic fouling condition (Rf^{∞}). This value can be calculated by analyzing the fouling rate model equation when the rate is null.

First, we need to get the expression for wall/interface temperature because it is present at the Arrhenius term of the rate equation. The evaluation of the surface temperature is based on the thermal circuit between the hot and cold streams depicted in Figure 17. Equation 144presents the corresponding mathematical expression that relates the rates of both sides of the circuit.

Figure 17 – Thermal circuit between hot and cold streams

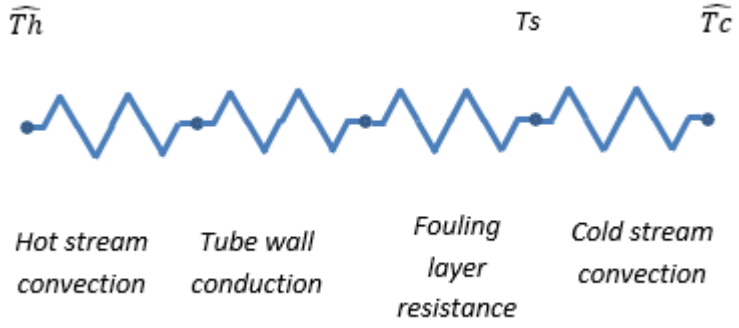

Fonte: A autora, 2017.

$$\frac{\widehat{Th} - Ts}{\frac{1}{hs} + \frac{dte\ ln(dte/dti)}{2\widehat{ktube}} + Rft\left(\frac{dte}{dti}\right)} = \frac{Ts - \widehat{Tc}}{\frac{1}{ht}\left(\frac{dte}{dti}\right)} \tag{144}$$

in which $\widehat{Th}$ and $\widehat{Tc}$ are the hot and cold stream temperatures, respectively. Isolating *Ts* from the expression, it yields:

$$Ts = \frac{(\widehat{Th}-\widehat{Tc})\frac{1}{h_t}\frac{dte}{dti}}{\frac{1}{hs}+\frac{dteln(dte/dti)}{2k\widehat{tube}}+\frac{1}{ht}\left(\frac{dte}{dti}\right)+Rft\left(\frac{dte}{dti}\right)} + \widehat{Tc} \quad (145)$$

This equation can be expressed in a more compact form using the overall heat transfer coefficient at a clean condition (*Uc*):

$$Ts = \frac{(\widehat{Th}-\widehat{Tc})\frac{1}{h_t}\frac{dte}{dti}}{\frac{1}{Uc}+Rf\left(\frac{dte}{dti}\right)} + \widehat{Tc} \quad (146)$$

The heat transfer along the thermal surface implies that $\widehat{Th}$ and $\widehat{Tc}$ vary along the tube length. However, the design procedure does not rely on local temperatures and properties (they are not modeled), but rather on average values, therefore, we need to rely on average values as well. Assuming average values to apply this equation to the entire equipment:

$$Ts = \frac{\widehat{\Delta T}^{av}\frac{1}{h_t}\frac{dte}{dti}}{\frac{1}{Uc}+Rf\left(\frac{dte}{dti}\right)} + \widehat{Tc}^{av} \quad (147)$$

The extreme values that the surface temperature can reach will be important in the analysis of the fouling condition in the design, because they are associated to the limiting values of the formation rate (higher surface temperatures implies higher formation rates).

The highest value of the surface temperature occurs at the clean condition (e.g. $Rf = 0$ at the start-up):

$$Ts_{max} = \frac{\widehat{\Delta T}^{av}\frac{1}{h_t}\frac{dte}{dti}}{\frac{1}{Uc}} + \widehat{Tc}^{av} \quad (148)$$

The corresponding maximum fouling formation rate (*FR*) becomes:

$$FR_{max} = \widehat{Af} Re^{-0.8} exp\left(\frac{-\widehat{\psi f}}{\frac{\widehat{\Delta T}^{av} \frac{1}{h_t} \frac{dte}{dti}}{\frac{1}{Uc}} + \widehat{Tc}^{av}}\right) \quad (149)$$

The lowest value that the surface temperature can reach is the cold stream temperature:

$$Ts_{min} = \widehat{Tc}^{av} \quad (150)$$

The corresponding fouling formation rate becomes:

$$FR_{min} = \widehat{Af} Re^{-0.8} exp\left(\frac{-\widehat{\psi f}}{\widehat{Tc}^{av}}\right) \quad (151)$$

The suppression rate will always be the same, since we are not considering the hydraulic impact of fouling that would change the flow velocity and, therefore, the Reynolds number.

$$SR = \widehat{Bf} Ret^{0,8} \quad (152)$$

The following subsections explore the three fouling conditions employed in the formulation of the design optimization: no fouling condition, fouling continuous growth, and asymptotic fouling resistance.

4.1.1.1.No fouling condition

If the suppression rate is higher than the formation rate at the clean condition (FR_{max}), then the fouling rate will be always equal to zero and no fouling layer will be formed in the heat exchanger.

The mathematical expression for the no fouling condition is:

$$FR_{max} \leq SR \quad (153)$$

This condition must be associated to a null fouling resistance in the design procedure:

$$Rft = 0 \quad (154)$$

Analyzing the situation, we have the following figure that represents the curves for suppression rate and formation rate according to the fouling resistance. As we can see, the suppression rate will always be bigger than the formation rate; hence, no fouling will occur for this case.

Figure 18 – No fouling condition

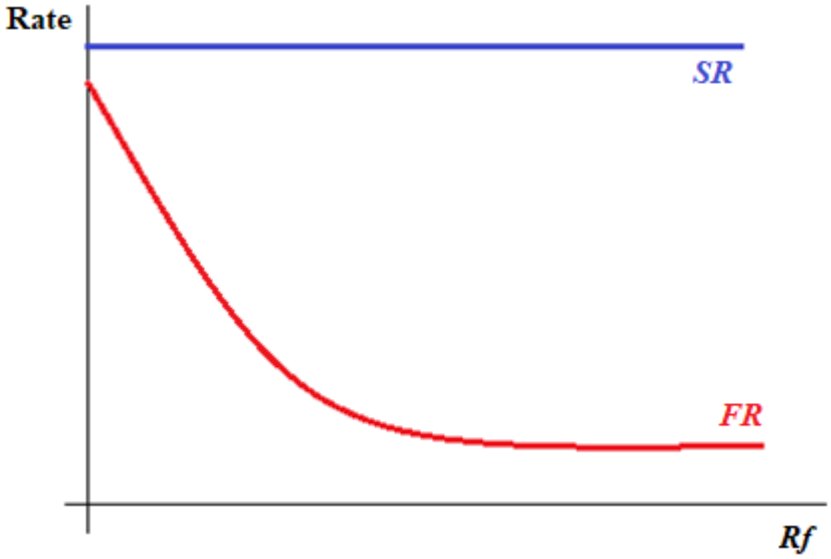

Fonte: A autora, 2018.

4.1.1.2.Continuous growth

If the formation rate is higher than the suppression rate, then a fouling layer will be formed over the thermal surface. In this case, the following mathematical relation holds:

$$FR_{max} > SR \tag{155}$$

The growth of the fouling layer reduces the surface temperature gradually and consequently, the fouling rate reduces due to the decrease of the formation rate. However, instead of considering that the formation rate will reach a value equivalent to the suppression rate (i.e. zero fouling rate), the formation rate can be limited by a constant value higher than the suppression rate, hence there is a continuous growth. This condition is identified by:

$$FR_{min} > SR \tag{156}$$

Since, in this condition, the fouling resistance always increases, the design procedure can adopt a maximum fouling resistance previously established, i.e. when this value is reached during the operation, this heat exchanger must be cleaned to regain its initial effectiveness. Therefore, in this case:

$$Rft = \widehat{Rf}^{max} \tag{157}$$

This case is illustrated by the curves in Figure 19:

Figure 19 – Continuous growth condition

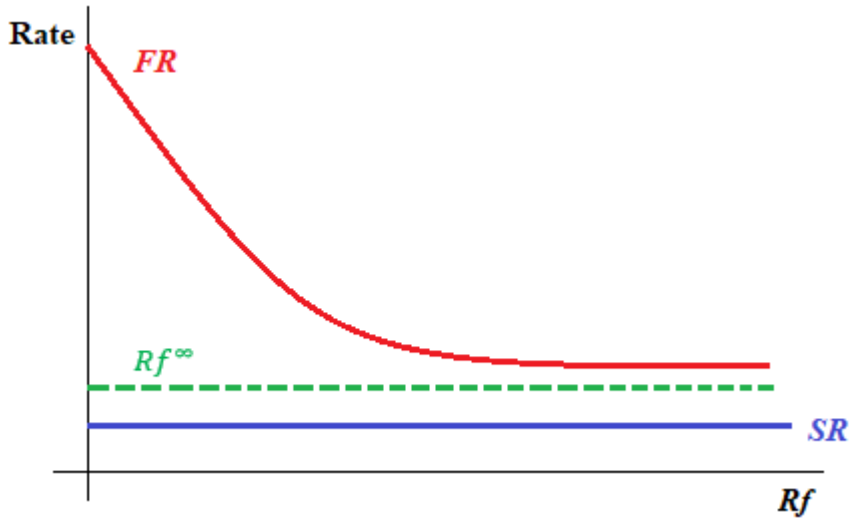

Fonte: A autora, 2018

4.1.1.3.Asymptotic fouling condition

Differently from the previous condition, the fouling growth can reduce the formation rate until it reaches the suppression rate. In this case, fouling resistance assumes an asymptotic value. The corresponding mathematical condition is:

$$FR_{min} \leq SR \tag{158}$$

The corresponding value for the asymptotic fouling resistance (Rf^{∞}) can be found by matching the formation (FR) and suppression (SR) rates.

$$\widehat{Af}Re^{-0.8}exp\left(\frac{-\widehat{\psi f}}{T_s}\right) = \widehat{Bf}Re^{0.8} \tag{159}$$

Figure 20 shows the curves for the formation and suppression rates in this case. Now, replacing Equation 147 in Equation 159 for the asymptotic fouling resistance, and isolating it, we have:

$$Rf^{\infty} = \frac{\widehat{\Delta T}^{av}\left(\frac{1}{h_t}\right)}{\left[\frac{\widehat{\psi f}}{ln\left(\frac{\widehat{Af}\widehat{Ret}^{-1.6}}{\widehat{Bf}}\right)}\right]-\widehat{Tc}^{av}} - \frac{1}{Uc}\frac{dti}{dte} \tag{160}$$

Figure 20 – Asymptotic fouling condition

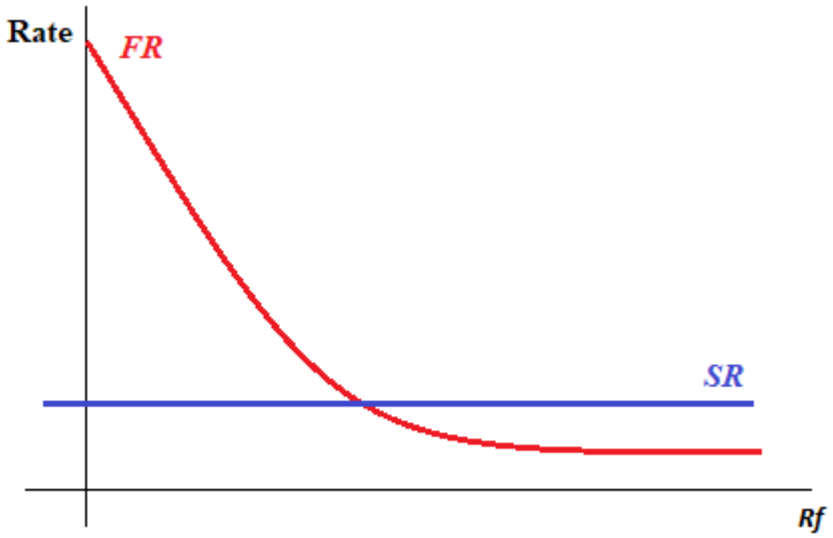

Fonte: Aautora, 2018.

Going back to the design problem, in this condition, the fouling resistance value to be adopted in the design solution procedure must be the lowest value between the asymptotic fouling resistance and the maximum value imposed by the designer:

$$Rft = \min(\widehat{Rf}^{max}, Rf^{\infty}) \tag{161}$$

4.1.1.4.Binary representation of fouling conditions

The three fouling conditions identified above can be inserted into the optimization model using a set of binary variables related to a corresponding set of propositions, as shown in Table 17 (if the proposition is true, the corresponding binary variable is equal to 1).

Table 17 - Propositions and corresponding binary variables

Proposition	Binary variable
$\boldsymbol{FR_{max} \leq SR}$	y_1
$\boldsymbol{FR_{min} \leq SR}$	y_2
$\boldsymbol{Rf^{\infty} \leq \widehat{Rf}^{max}}$	y_3

The mathematical relations among the binary variables and the corresponding propositions are:

$$\widehat{L1}y1 + \varepsilon \leq FR_{max} - SR \leq \widehat{U1}(1 - y1) \quad (162)$$

$$\widehat{L2}y2 + \varepsilon \leq FR_{min} - SR \leq \widehat{U2}\,(1 - y2) \quad (163)$$

$$\widehat{L3}y3 + \varepsilon \leq Rf^{\infty} - \widehat{Rf}^{max} \leq \widehat{U3}\,(1 - y3) \quad (164)$$

where ε is a small positive number, $\widehat{U1}$ and $\widehat{L1}$ are upper and lower bounds for the difference $FR_{max} - SR$, $\widehat{U2}$ and $\widehat{L2}$ are upper and lower bounds for the difference $FR_{min} - SR$, and $\widehat{U3}$ and $\widehat{L3}$ are upper and lower bounds for the difference $Rf^{\infty} - \widehat{Rf}^{max}$.

Based on this set of binary variables, each of the fouling conditions is identified by a certain combination of 0-1 values, as shown in Table 18.

Table 18 - Relation among the binary variables and the fouling conditions

Variable	No fouling	Continuous fouling growth	Asymptotic resistance with $\boldsymbol{Rf^{\infty} \leq \widehat{Rf}^{max}}$	Asymptotic resistance with $\boldsymbol{Rf^{\infty} > \widehat{Rf}^{max}}$
*y*1	1	0	0	0
y2	1	0	1	1
y3	1	1	1	0
Rft	0	$\widehat{Rf}^{max}$	$\widehat{Rf}^{\infty}$	$\widehat{Rf}^{max}$

The different combinations for values of the binary variables can be organized for the evaluation of the fouling resistance according to each condition identified in Table 18:

$$Rft = y3Rf^{\infty} - Rf^{\infty} + y2Rf^{\infty} - y1Rf^{\infty} + (1 - y2 + 1 - y3)\,\widehat{Rf}^{max} \quad (165)$$

This equation presents nonlinearities that will be reformulated in order to make the final model a MILP model.

4.2.**The MILP model**

The development regarding the fouling model shown in the previous section will be included in the ILP model developed by Gonçalves et al (2017), proper mathematical manipulations will be applied to keep the linear nature of the model.

4.2.1. Inclusion of the fouling model in the original ILP model

In order to include the fouling model in the original model, first we have to make the fouling resistance in the tube-side (*Rft*) a variable, for that we must rewrite Equation 88 as Equation 166with no fouling in the shell-side, the other original constraints of the model will remain unchanged, for they are not affected by fouling.

$$\hat{Q}\left(\sum_{srow}\frac{\widehat{Pdte_{srow}}}{\widehat{Pht_{srow}}\widehat{Pdti_{srow}}}yrow_{srow}+\sum_{srow}\frac{\widehat{Pdte_{srow}}}{\widehat{Pdti_{srow}}}Rft\,yrow_{srow}+\frac{\sum_{srow}\widehat{Pdte_{srow}}yrow_{srow}\ln\left(\frac{\widehat{Pdte_{srow}}}{\widehat{Pdti_{srow}}}\right)}{2\,\widehat{ktube}}+\sum_{srow}\frac{1}{\widehat{Phs_{srow}}}yrow_{srow}\right)\leq$$

$$\left(\frac{100}{100+\widehat{Aexc}}\right)(\pi\sum_{srow}\widehat{PNtt_{srow}}\widehat{Pdte_{srow}}\widehat{PL_{srow}}yrow_{srow})\widehat{\Delta Tlm}\hat{F}_{srow} \quad (166)$$

The second step is to include Equations 149, 151, 152, 160 and 162-165. However, we must rewrite Equations 149, 151, 152 and 160 using the same techniques explained earlier, that consist of replacing the geometric variables by their corresponding binary representation. The rewritten equations are:

$$FR_{max}=\widehat{Af}\left(\frac{4\,\widehat{mt}}{\pi\,\widehat{\mu t}}\right)^{-0.8}\sum_{srow}\left(\frac{\widehat{PNpt}_{srow}}{\widehat{PNtt}_{srow}\widehat{Pdti}_{srow}}\right)^{-0.8}$$

$$exp\left(\frac{-\widehat{\psi f}}{\widehat{Tc}^{av}+\frac{\widehat{\Delta T}^{av}\frac{\widehat{pdte}_{srow}}{\widehat{pht}_{srow}\widehat{pdti}_{srow}}}{\left[\frac{\widehat{Pdte}_{srow}}{\widehat{Pht}_{srow}\widehat{Pdti}_{srow}}+\frac{\widehat{Pdte}_{srow}\ln(\frac{\widehat{Pdte}_{srow}}{\widehat{Pdti}_{srow}})}{2\,\widehat{ktube}}+\frac{1}{\widehat{Phs}_{srow}}\right]}}\right)yrow_{srow} \quad (167)$$

$$FR_{min}=\widehat{Af}\left(\frac{4\,\widehat{mt}}{\pi\,\widehat{\mu t}}\right)^{-0.8}exp\left(\frac{-\widehat{\psi}}{\widehat{Tc}^{av}}\right)\sum_{srow}\left(\frac{\widehat{PNpt}_{srow}}{\widehat{PNtt}_{srow}\widehat{Pdti}_{srow}}\right)^{-0.8}yrow_{srow} \quad (168)$$

$$SR=\widehat{Bf}\left(\frac{4\widehat{mt}}{\pi\widehat{\mu t}}\right)^{0.8}\sum_{srow}\left(\frac{\widehat{PNpt}_{srow}}{\widehat{PNtt}_{srow}\widehat{Pdti}_{srow}}\right)^{0.8}yrow_{srow} \quad (169)$$

$$Rf^{\infty} = \sum_{srow} \left[\frac{\widehat{\Delta T}^{av} / \widehat{pht}_{srow}}{\left[\frac{\widehat{\psi f}}{ln\left[\frac{\widehat{Af}\left(\frac{4\widehat{mt}}{\pi \widehat{\mu t}\, \widehat{PNtt}_{srow} \widehat{Pdtl}_{srow}} \right)^{-(1.6)}}{\widehat{Bf}} \right]} - \widehat{Tc}^{av} \right]} \right] yrow_{srow} -$$

$$\sum_{srow} \left[\frac{\widehat{Pdtl}_{srow}}{\widehat{Pdte}_{srow}} \left(\frac{\widehat{Pdte}_{srow}}{\widehat{Pht}_{srow} \widehat{Pdtl}_{srow}} + \frac{\widehat{Pdte}_{srow} \ln\left(\frac{\widehat{Pdte}_{srow}}{\widehat{Pdtl}_{srow}} \right)}{2\ \widehat{ktube}} + \frac{1}{\widehat{Phs}_{srow}} \right) \right] yrow_{srow} \quad (170)$$

Equations 165 and 166 have bilinear terms that must be rewritten as linear terms so that the final model can be a MILP model.

4.2.1.1.Reformulation of bilinear terms

The bilinear terms presented above contains the multiplication of a continuous variable and a binary variable. Therefore, they can be replaced by a set of linear inequalities, as described below (FLOUDAS, 1995).

Let *x* be a continuous variables, *y* a binary variable and *w* the continuous variable that represents the bilinear term *y* times *x*:

$$w = yx \quad (171)$$

This bilinear term is represented by:

$$x - Ux(1 - y) \leq w \leq x - Lx(1 - y) \quad (172)$$

$$Lxy \leq w \leq Uxy \quad (173)$$

where *Lx* and *Ux* are the lower and upper bounds for *x*, respectively.

If *y* is equal to zero then the new variable *w* will also be zero and this condition must be repected by Equations 172 and 173 that will be:

$$x - Ux \leq w \leq x - Lx \quad (174)$$

$$0 \leq w \leq 0 \tag{175}$$

and equation 175 (Equation 173 for *y* equal to zero) guarantees that *w*is equal to zero.

If *y* is equal to one, then *w* must be equal to *x*:

$$x - Ux(1-1) \leq w \leq x - Lx(1-1) \tag{176}$$

$$x \leq w \leq x \tag{177}$$

$$Lx \leq w \leq Ux \tag{178}$$

In this case, Equation 177 guarantees that *w* is equal to *x*. Therefore, the viability of the constraints is showed.

In this subsection, we will use those techniques to rewrite Equations 165 and 166. Equation 165 have 3 bilinear terms, the first one is $y3Rf^{\infty}$, that will be replaced by $w3Rf^{\infty}$, the second one is $y2Rf^{\infty}$, that will be replaced by $w2Rf^{\infty}$, and the final one if $y1Rf^{\infty}$, replaced by $w1Rf^{\infty}$. Besides replacing the bilinear terms, inequalities must be added; therefore, Equation 165 is replaced by Equations 179-186:

$$Rft = w3Rf^{\infty} - Rf^{\infty} + w2Rf^{\infty} - w1Rf^{\infty} + (1 - y2 + 1 - y3)\,\widehat{Rf}^{max} \tag{179}$$

$$L\widehat{Rfinf} \leq Rf^{\infty} \leq U\widehat{Rfinf} \tag{180}$$

$$Rf^{\infty} - U\widehat{Rfinf}(1-y1) \leq w1Rf^{\infty} \leq Rf^{\infty} - L\widehat{Rfinf}(1-y1) \tag{181}$$

$$L\widehat{Rfinf}\ y1 \leq w1Rf^{\infty} \leq U\widehat{Rfinf}\ y1 \tag{182}$$

$$Rf^{\infty} - U\widehat{Rfinf}(1-y2) \leq w2Rf^{\infty} \leq Rf^{\infty} - L\widehat{Rfinf}(1-y2) \tag{183}$$

$$L\widehat{Rfinf}\ y2 \leq w2Rf^{\infty} \leq U\widehat{Rfinf}\ y2 \tag{184}$$

$$Rf^{\infty} - U\widehat{Rfinf}(1-y3) \leq w3Rf^{\infty} \leq Rf^{\infty} - L\widehat{Rfinf}(1-y3) \tag{185}$$

$$\widehat{LRf\imath nf}\ y3 \leq w3Rf^{\infty} \leq \widehat{URf\imath nf}\ y3 \tag{186}$$

Equation 166 has only one bilinear term, that is $Rftyrow_{srow}$ and will be replaced by wRf_{srow}. Therefore, Equation 166 is replaced by the following equations:

$$\hat{Q}\left(\sum_{srow}\frac{\widehat{Pdte_{srow}}}{\widehat{Pht_{srow}}\widehat{Pdt\imath_{srow}}}yrow_{srow} + \sum_{srow}\frac{\widehat{Pdte_{srow}}}{\widehat{Pdt\imath_{srow}}}wRf_{srow} + \frac{\sum_{srow}\widehat{Pdte_{srow}}\ln\left(\frac{\widehat{Pdte_{srow}}}{\widehat{Pdt\imath_{srow}}}\right)yrow_{srow}}{2\ \widehat{ktube}} + \sum_{srow}\frac{1}{\widehat{Phs_{srow}}}yrow_{srow}\right) \leq \left(\frac{100}{100+\widehat{Aexc}}\right)\left(\pi\sum_{srow}\widehat{PNtt_{srow}}\widehat{Pdte_{srow}}\widehat{PL_{srow}}yrow_{srow}\right)\widehat{\Delta Tlm}\hat{F}_{srow} \tag{187}$$

$$\widehat{LRf} \leq Rft \leq \widehat{URf} \tag{188}$$

$$Rft - \widehat{URf}(1 - yrow_{srow}) \leq wRf_{srow} \leq Rft - \widehat{LRf}(1 - yrow_{srow}) \tag{1891}$$

$$\widehat{LRf}yrow_{srow} \leq wRf_{srow} \leq \widehat{URf}yrow_{srow} \tag{190}$$

4.2.2. The complete model

In this subsection, in order to facilitate the visualization, all the constraints and the objective function for the MILP model will be presented again without further explanation.

4.2.2.1.Objective function

$$\min \pi\sum_{srow}\widehat{PNtt_{srow}}\widehat{Pdte_{srow}}\widehat{PL_{srow}}yrow_{srow} \tag{132}$$

4.2.2.2. Constraints

Heat transfer rate equation

$$\hat{Q}\left(\sum_{srow}\frac{\widehat{Pdte}_{srow}}{\widehat{Pht}_{srow}\widehat{Pdti}_{srow}}yrow_{srow}+\sum_{srow}\frac{\widehat{Pdte}_{srow}}{\widehat{Pdti}_{srow}}wRf_{srow}+\frac{\sum_{srow}\widehat{Pdte}_{srow}\ln\left(\frac{\widehat{Pdte}_{srow}}{\widehat{Pdti}_{srow}}\right)yrow_{srow}}{2\,\widehat{ktube}}+\sum_{srow}\frac{1}{\widehat{Phs}_{srow}}yrow_{srow}\right)\leq\left(\frac{100}{100+\widehat{Aexc}}\right)(\pi\sum_{srow}\widehat{PNtt}_{srow}\widehat{Pdte}_{srow}\widehat{PL}_{srow}yrow_{srow})\widehat{\Delta Tlm}\hat{F}_{srow} \quad (187)$$

$$\widehat{LRf}\leq Rft\leq\widehat{URf} \quad (188)$$

$$Rft-\widehat{URf}(1-yrow_{srow})\leq wRf_{srow}\leq Rft-\widehat{LRf}(1-yrow_{srow}) \quad (189)$$

$$\widehat{LRf}yrow_{srow}\leq wRf_{srow}\leq\widehat{URf}yrow_{srow} \quad (190)$$

Summation of binaries

$$\sum_{srow}yrow_{srow}=1 \quad (62)$$

Maximum pressure drop for the tube-side

$$\sum_{srow}P\Delta\widehat{Pttur}b1_{srow}yrow_{srow}+\sum_{srow}P\Delta\widehat{Pttur}b2_{srow}yrow_{srow}+\sum_{srow}P\widehat{\Delta Ptcab}_{srow}\hat{K}_{srow}yrow_{srow}\leq\widehat{\Delta Ptdisp} \quad (98)$$

Maximum pressure drop for the shell-side

$$yrow_{srow}=0 \text{ for } srow\in SDPsmaxout \quad (115)$$

where *SDPsmaxout* is a subset of *srow* given by:

$$SDPsmaxout = \{srow \mid \widehat{P\Delta Ps}_{srow} \geq \widehat{\Delta Psdisp} + \varepsilon\} \quad (116)$$

Reynolds number bounds

$$\frac{\widehat{ms}}{\widehat{\mu s}} \sum_{srow} \frac{\widehat{PDeq}_{srow}(\widehat{PNb}_{srow}+1)}{\widehat{PDs}_{srow}\widehat{PFAR}_{srow}\widehat{PL}_{srow}} yrow_{srow} \geq 2{\cdot}10^3 \quad (99)$$

$$\frac{4\widehat{mt}}{\pi\widehat{\mu t}} \sum_{srow} \frac{\widehat{PNpt}_{srow}}{\widehat{PNtt}_{srow}\widehat{Pdti}_{srow}} yrow_{srow} \geq 10^4 \quad (100)$$

Velocity bounds

$$yrow_{srow} = 0 \text{ for } srow \in (Svsminout \cup Svsmaxout) \quad (109)$$

$$yrow_{srow} = 0 \text{ for } srow \in (Svtminout \cup Svtmaxout) \quad (110)$$

Svsminout, *Svsmaxout*, *Svtminout* and *Svtmaxout* are the subsets of *srow* given by:

$$Svsminout = \{srow \mid \frac{\widehat{ms}}{\widehat{\rho s}} \frac{(\widehat{PNb}_{srow}+1)}{\widehat{PDs}_{srow}\widehat{PFAR}_{srow}\widehat{PL}_{srow}} \leq \widehat{vsmin} - \varepsilon\} \quad (111)$$

$$Svsmaxout = \{srow \mid \frac{\widehat{ms}}{\widehat{\rho s}} \frac{(\widehat{PNb}_{srow}+1)}{\widehat{PDs}_{srow}\widehat{PFAR}_{srow}\widehat{PL}_{srow}} \geq \widehat{vsmax} + \varepsilon\} \quad (112)$$

$$Svtminout = \{srow \mid \frac{4\widehat{mt}}{\pi\widehat{\rho t}} \frac{\widehat{PNpt}_{srow}}{\widehat{PNtt}_{srow}\widehat{Pdti}_{srow}^{\,2}} \leq \widehat{vtmin} - \varepsilon\} \quad (113)$$

$$Svtmaxout = \{srow \mid \frac{4\widehat{mt}}{\pi\widehat{\rho t}} \frac{\widehat{PNpt}_{srow}}{\widehat{PNtt}_{srow}\widehat{Pdti}_{srow}^{\,2}} \geq \widehat{vtmax} + \varepsilon\} \quad (114)$$

with ε being a small positive number.

Bounds for baffle spacing

$$yrow_{srow} = 0 \text{ for } srow \in (SLNbminout \cup SLNbmaxout) \quad (117)$$

where *SLNbminout* and *SLNbmaxout* are subsets of *srow* given by:

$$SLNbminout = \{srow \mid \frac{\widehat{PL}_{srow}}{\widehat{PNb}_{srow}+1} \leq 0.2\widehat{PDs}_{srow} - \varepsilon\} \quad (118)$$

$$SLNbmaxout = \{srow \mid \frac{\widehat{PL}_{srow}}{\widehat{PNb}_{srow}+1} \geq 1.0\widehat{PDs}_{srow} + \varepsilon\} \quad (119)$$

Tube length-shell diameter ratio

$$yrow_{srow} = 0 \text{ for } srow \in (SLDminout \cup SLDmaxout) \quad (120)$$

where *SLDminout* and *SLDmaxout* are subsets of *srow* given by:

$$SLDminout = \{srow \mid \widehat{PL}_{srow} \leq 3\widehat{PDs}_{srow} - \varepsilon\} \quad (121)$$

$$SLDmaxout = \{srow \mid \widehat{PL}_{srow} \geq 15\widehat{PDs}_{srow} + \varepsilon\} \quad (122)$$

Minimum heat transfer area

$$yrow_{srow} = 0 \text{ for } srow \in SAminout \quad (127)$$

where *SAminout* is a subset of *srow* given by:

$$SAminout = \{srow \mid \pi\widehat{PNtt}_{srow}\widehat{Pdte}_{srow}\widehat{PL}_{srow} \leq \widehat{Amin} - \varepsilon\} \quad (128)$$

In this case, fouling only occurs in the tube-side and the minimum value for it is zero, the no fouling case. Therefore, the maximum overall heat transfer coefficient must be calculated as:

$$\widehat{Umax} = \frac{1}{\frac{1}{\widehat{htmax}}\widehat{drmin} + 0 + \frac{\widehat{Pdte}_{srow}\ln(\widehat{drmin})}{2\,\widehat{ktube}} + \frac{1}{\widehat{hsmax}}} \quad (191)$$

Fouling resistance evaluation

$$Rft = w3Rf^{\infty} - Rf^{\infty} + w2Rf^{\infty} - w1Rf^{\infty} + (1 - y2 + 1 - y3)\,\widehat{Rf}^{max} \quad (179)$$

$$L\widehat{Rfinf} \le Rf^{\infty} \le U\widehat{Rfinf} \quad (180)$$

$$Rf^{\infty} - U\widehat{Rfinf}(1 - y1) \le w1Rf^{\infty} \le Rf^{\infty} - L\widehat{Rfinf}(1 - y1) \quad (181)$$

$$L\widehat{Rfinf}\ y1 \le w1Rf^{\infty} \le U\widehat{Rfinf}\ y1 \quad (182)$$

$$Rf^{\infty} - U\widehat{Rfinf}(1 - y2) \le w2Rf^{\infty} \le Rf^{\infty} - L\widehat{Rfinf}(1 - y2) \quad (183)$$

$$L\widehat{Rfinf}\ y2 \le w2Rf^{\infty} \le U\widehat{Rfinf}\ y2 \quad (184)$$

$$Rf^{\infty} - U\widehat{Rfinf}(1 - y3) \le w3Rf^{\infty} \le Rf^{\infty} - L\widehat{Rfinf}(1 - y3) \quad (185)$$

$$L\widehat{Rfinf}\ y3 \le w3Rf^{\infty} \le U\widehat{Rfinf}\ y3 \quad (186)$$

Fouling conditions

$$\widehat{L1}y1 + \varepsilon \le FR_{max} - SR \le \widehat{U1}(1 - y1) \quad (162)$$

$$\widehat{L2}y2 + \varepsilon \le FR_{min} - SR \le \widehat{U2}\,(1 - y2) \quad (163)$$

$$\widehat{L3}y3 + \varepsilon \le Rf^{\infty} - \widehat{Rf}^{max} \le \widehat{U3}\,(1 - y3) \quad (164)$$

$$FR_{max} = \widehat{Af}\left(\frac{4\,\widehat{mt}}{\pi\,\widehat{\mu t}}\right)^{-0.8}\sum_{srow}\left(\frac{\widehat{PNpt}_{srow}}{\widehat{PNtt}_{srow}\widehat{Pdti}_{srow}}\right)^{-0.8}$$

$$exp\left(\frac{-\widehat{\psi f}}{\widehat{Tc}^{av}+\frac{\widehat{\Delta T}^{av}\frac{\widehat{pdte}_{srow}}{\widehat{pht}_{srow}\widehat{pdti}_{srow}}}{\left[\frac{\widehat{Pdte}_{srow}}{\widehat{Pht}_{srow}\widehat{Pdti}_{srow}}+\frac{\widehat{Pdte}_{srow}\ln(\frac{\widehat{Pdte}_{srow}}{\widehat{Pdti}_{srow}})}{2\,\widehat{ktube}}+\frac{1}{\widehat{Phs}_{srow}}\right]}}\right)yrow_{srow} \quad (167)$$

$$FR_{min} = \widehat{Af}\left(\frac{4\,\widehat{mt}}{\pi\,\widehat{\mu t}}\right)^{-0.8}exp\left(\frac{-\widehat{\psi}}{\widehat{Tc}^{av}}\right)\sum_{srow}\left(\frac{\widehat{PNpt}_{srow}}{\widehat{PNtt}_{srow}\widehat{Pdti}_{srow}}\right)^{-0.8}yrow_{srow} \quad (168)$$

$$SR = \widehat{Bf}\left(\frac{4\widehat{mt}}{\pi\widehat{\mu t}}\right)^{0.8}\sum_{srow}\left(\frac{\widehat{PNpt}_{srow}}{\widehat{PNtt}_{srow}\widehat{Pdti}_{srow}}\right)^{0.8}yrow_{srow} \quad (169)$$

$$Rf^{\infty} = \sum_{srow}\frac{\widehat{\Delta T}^{av}/\widehat{pht}_{srow}}{\left[\frac{\widehat{\psi f}}{ln\left[\frac{\widehat{Af}\left(\frac{4\widehat{mt}}{\pi\widehat{\mu t}}\frac{\widehat{PNpt}_{srow}}{\widehat{PNtt}_{srow}\widehat{Pdti}_{srow}}\right)^{-(1.6)}}{\widehat{Bf}}\right]}-\widehat{Tc}^{av}\right]}yrow_{srow} -$$

$$\sum_{srow}\left[\frac{\widehat{Pdti}_{srow}}{\widehat{Pdte}_{srow}}\left(\frac{\widehat{Pdte}_{srow}}{\widehat{Pht}_{srow}\widehat{Pdti}_{srow}}+\frac{\widehat{Pdte}_{srow}\ln(\frac{\widehat{Pdte}_{srow}}{\widehat{Pdti}_{srow}})}{2\,\widehat{ktube}}+\frac{1}{\widehat{Phs}_{srow}}\right)\right]yrow_{srow} \quad (170)$$

4.3.**Results**

Three examples are used to illustrate the differences of our proposed approach as compared to the use of recommended fixed fouling resistances. These examples explore different situations involving a no fouling case, the fouling resistance equal to $\widehat{Rf}^{MAX}$, and the fouling resistance equal to Rf^{∞}. In addition, three case studies are also presented considering

the relation between the heat exchanger design and fouling aspects, involving crude oil type, pressure drop manipulation, and energy integration.

Table 19 presents the physical properties of the streams, associated to average values calculated along the temperature operating range. Table 20 displays the characteristics of the thermal task. These values are taken from a real pre-heat train, where the hot stream flows in the shell-side and the cold stream, crude oil, flows in the tubes. The discrete values used as parameters related to the geometric variables are the same used in the previous model (Table 4). The thermal conductivity of the tube wall is equal to 50 W/m·K.

Table 19 - Physical properties

	Density (kg/m^3)	Viscosity (Pa·s)	Conductivity (W/m·K)	Heat capacity (J/kgK)
Cold stream	768.9	$5.36 \cdot 10^{-4}$	0.09	2742.5
Hot stream	898.0	$1.87 \cdot 10^{-3}$	0.13	2754.0

Table 20 - Thermal task

	Cold stream	Hot stream
Mass flow rate (kg/s)	91.9	40.0
Inlet temperature (ºC)	288.4	343.8
Outlet temperature (ºC)	305.0	305.4
Maximum pressure drop (kPa)	80	80
Flow velocity bounds (m/s)	1.0 – 3.0	0.5 – 2.0

The fouling resistance used for the traditional approach is $7.04 \cdot 10^{-4} m^2K/W$, which corresponds to the TEMA (2007) indication for the crude oil flowing in the conditions depicted in Table 20. This value will be also used as the maximum fouling resistance in the proposed design procedure ($\widehat{Rf}^{MAX}$).

The values of the empirical parameters of the fouling rate model are displayed in Table 21, close to the values reported by Polley et al. (2007), with the exception of the activation energy that was modified in each example so that all the three different possibilities could be achieved through the same service. The identification of fouling model parameters can be

conducted using a parameter estimation procedure based on laboratory or process data (POLLEY et al., 2007; ASOMANING; PANCHAL; LIAO, 2000; COSTA et al., 2013).

Table 21 - Parameters of the fouling model

α (m^2K/J)	γ(m^2K/J)
0.2798	$4.17 \cdot 10^{-13}$

The optimization problems were solved using the software GAMS with the solver CPLEX. The computational time, which corresponds to the elapsed time using a computer with Intel Core i7 processor with 8 Mb of RAM memory, was less than 40 seconds to all of the examples and case studies displayed here.

4.3.1. Example 1

The results obtained using the proposed approach for an activation energy of 40000 J/mol are displayed in Tables 22 and 23.

Table 22 - Results for Example 1 – Design variables

Variable	Value	Variable	Value
A (m^2)	585	*rp*	1.25
dte (m)	0.0254	*Ds* (m)	1.22
dti (m)	0.0221	*lay*	2
L (m)	6.10	*ltp*(m)	0.0317
Nb	19	*Ntt*	1203
Npt	6	*lbc*(m)	0.305

Table 23 - Results for Example 1 – Thermo-fluid dynamic variables

Variable	Value
ΔPs (Pa)	74001
ΔPt (Pa)	47833
hs (W/m^{2}K)	984
ht (W/m^{2}K)	1638
U (W/m^{2}K)	390
vs (m/s)	0.60
vt (m/s)	1.55

This case leads to a fouling resistance value that is equal to $\widehat{Rf}^{MAX}$, which means that the design fouling resistance will be the same proposed by TEMA (2007). In this particular scenario, the results obtained by the proposed approach are exactly the same as the ones obtained with the traditional approach, since the fouling resistance values are the same.

4.3.2. Example 2

The results obtained for the proposed approach with an activation energy of 41000 J/mol are displayed in Tables 24 and 25.

Table 24 - Results for Example 2 – Design variables

Variable	Value	Variable	Value
A (m^2)	412	rp	1.25
dte (m)	0.03175	Ds (m)	1.14
dti (m)	0.02845	lay	2
L (m)	6.10	ltp(m)	0.0397
Nb	17	Ntt	677
Npt	6	lbc(m)	0.339

Table 25 - Results for Example 2 – Thermo-fluid dynamic variables

Variable	Value
ΔPs (Pa)	44483
ΔPt (Pa)	43046
hs (W/m^{2}K)	870
ht (W/m^{2}K)	1646
U (W/m^{2}K)	527
vs (m/s)	0.58
vt (m/s)	1.67

The proposed approach leads to a solution associated to an asymptotic fouling resistance (Rf^{∞}) equal to $3.22 \cdot 10^{-5}$m^{2}K/W, lower than the value adopted by TEMA (2007) ($7.04 \cdot 10^{-4}$m^{2}K/W). Therefore, the proposed design procedure could identify an alternative associated to a smaller fouling resistance and, consequently, with a smaller area. Indeed, our optimal heat exchanger has an area of 412 m^2 and the corresponding result with the TEMA fixed fouling resistance (shown in Example 1) is 585 m^2, i.e. the optimization could achieve a reduction in the heat transfer area of 29 %.

4.3.3. Example 3

In this last example, the value of the activation energy is 48000 J/mol. The corresponding optimization results are displayed in Tables 26 and 27.

Table 26 - Results for Example 3 – Design variables

Variable	Value	Variable	Value
A (m^2)	321	*rp*	1.25
dte (m)	0.01905	*Ds* (m)	0.940
dti (m)	0.01575	*lay*	1
L (m)	4.88	*ltp*(m)	0.02381
Nb	15	*Ntt*	1100
Npt	4	*lbc* (m)	0.305

Table 27 - Results for Example 3 – Thermo-fluid dynamic variables

Variable	Value
ΔPs (Pa)	70706
ΔPt (Pa)	71992
hs (W/m^{2}K)	1121
ht (W/m^{2}K)	2340
U (W/m^{2}K)	692
vs (m/s)	0.78
vt (m/s)	2.23

This case leads to a no fouling condition, which allowed a considerable increase of the overall heat transfer coefficient, and consequently, a reduction of the heat transfer area. Comparing with the traditional approach, this solution allowed a reduction of 45 % in the heat exchanger area.

The no fouling behavior can be illustrated by the envelope of fouling threshold (Equation 159) represented in Figure 12, where it can be observed the position corresponding to the optimal heat exchanger inside the no fouling region.

Figure 21 - Example 3: Threshold fouling and optimal heat exchanger solution

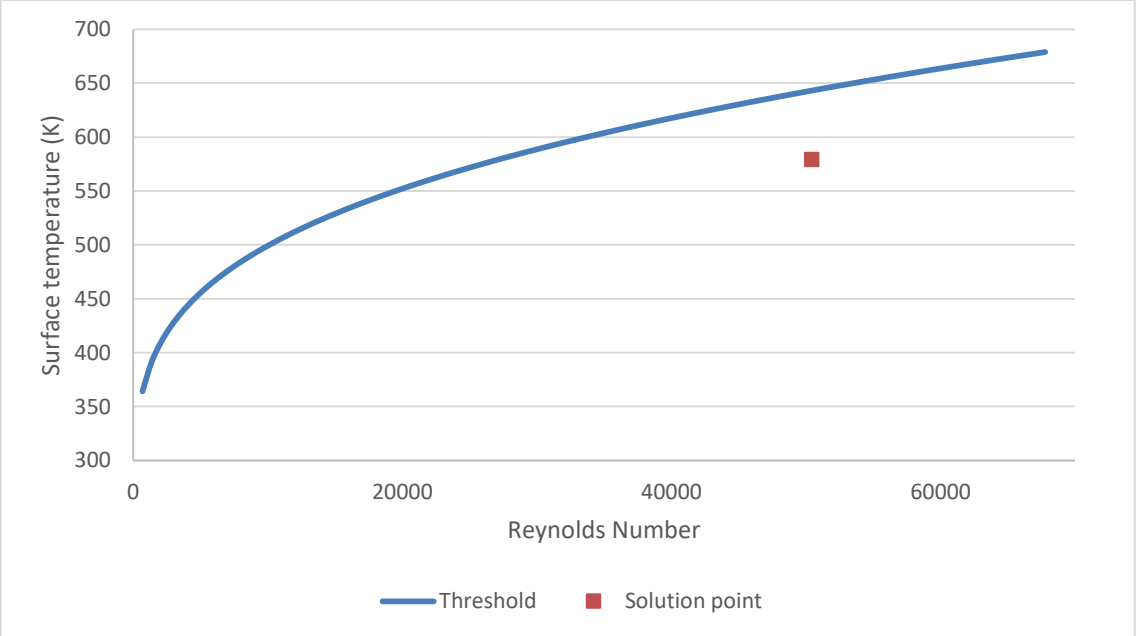

Fonte: A autora, 2018.

4.3.4. Case Study 1: Crude oil selection

Different crudes can be more or less prone to fouling. The introduction of fouling modeling in the heat exchanger design procedure can bring a better understanding of the impact of the crude oil selection on the design of the crude preheat train.

Example 3 showed a crude oil associated to an activation energy of 48000 J/mol that was associated to an optimal exchanger with a heat transfer area of 321 m^2 and no fouling behavior. The utilization of an alternative crude oil with activation energy of 43000 J/mol would imply that the previous optimal solution would not be feasible anymore. The application of the design procedure finds a solution in this new condition associated to an increase of the heat transfer area of 8 %, according to the solution depicted in Tables 28 and 29. This solution alternative is inside the no fouling region of the alternative crude oil stream, but the original heat exchanger would be located outside the no fouling envelope.

Table 28 - Results for Case Study 1 – Design variables

Variable	Value	Variable	Value
A (m^2)	348	*rp*	1.25
dte (m)	0.0254	*Ds* (m)	0.940
dti (m)	0.0221	*lay*	2
L (m)	6.10	*ltp*(m)	0.03175
Nb	18	*Ntt*	715
Npt	4	*lbc* (m)	0.321

Table 29 - Results for Case Study 1 – Thermo-fluid dynamic variables

Variable	Value
Δ*Ps* (Pa)	79138
Δ*Pt* (Pa)	39435
hs (W/m^2K)	1104
ht (W/m^2K)	1795
U (W/m^2K)	632
vs (m/s)	0.74
vt (m/s)	1.74

4.3.5. Case study 2: Pressure drop manipulation

An important parameter in the design of a heat exchanger is the available pressure drop. This parameter represents a tradeoff between pumping operational costs and heat exchanger capital costs. However, a more complete analysis of this issue must also consider fouling aspects.

Tables 30 and 31 show the result of the application of the design procedure in relation to Example 2, but allowing a 25 % increase in the available pressure drop for the crude oil.

Table 30 - Results for Case Study 2 – Design variables

Variable	Value	Variable	Value
A (m^2)	396	*rp*	1.33
dte (m)	0.0254	*Ds* (m)	1.07
dti (m)	0.0221	*lay*	2
L (m)	6.10	*ltp*(m)	0.0338
Nb	18	*Ntt*	814
Npt	6	*lbc* (m)	0.321

Table 31 - Results for Case Study 2 – Thermo-fluid dynamic variables

Variable	Value
ΔPs (Pa)	34889
ΔPt (Pa)	98734
hs (W/m^2K)	808
ht (W/m^2K)	2238
U (W/m^2K)	560
vs (m/s)	0.52
vt (m/s)	2.30

The analysis of the new solution indicates that the increase of the available pressure drop brought a reduction of the heat transfer area from 412 m^2 to 396 m^2. This area reduction occurred because the higher available pressure drop allowed an increase of the tube-side heat

transfer coefficient, from 1646 W/m^{2}K to 2238 W/m^{2}K, and there was a total fouling suppression, i.e. the heat exchanger associated to a higher pressure drop is inside the no fouling region.

This result indicates that the manipulation of the pressure drop can be a variable employed to mitigate fouling. Besides the possibility of capital costs reduction, the possibility to operate inside the no fouling region also has other advantages: elimination of costs associated to heat exchanger cleaning, elimination of environmental problems associated to the discard of the deposits, longer operational runs, etc.

4.3.6. Case study 3: Energy integration

The selection of the optimal set of heat exchanges in crude preheat trains is fundamental for the reduction of the fuel consumption in the fired heater located at the end of the train. This case study illustrates that fouling aspects may affect the problem of energy integration.

We use a design problem equivalent to Example 2, but all stream temperatures presented in Table 20 are increased by 20 ºC, thus representing a similar service that would be located at a different position along the crude preheat train. Because all temperatures were modified simultaneously, the temperature approach is the same, and a conventional design procedure with fixed fouling resistances would yield the same result (dismissing possible modifications of physical properties).

However, the increase of the temperatures in the heat exchange task implies an increase on the surface temperature that intensifies the fouling problem. This effect is illustrated in Tables 32 and 33, where it is depicted the solution of the Example 2 with higher temperatures.

Table 32 - Results for Case Study 3 – Design variables

Variable	Value	Variable	Value
A (m^2)	585	*rp*	1.25
dte (m)	0.0254	*Ds* (m)	1.219
dti (m)	0.0221	*lay*	2
L (m)	6.10	*ltp*(m)	0.03175
Nb	19	*Ntt*	1203
Npt	6	*lbc* (m)	0.305

Table 33 - Results for Case Study 3 – Thermo-fluid dynamic variables

Variable	Value
ΔPs (Pa)	74001
ΔPt (Pa)	47833
hs (W/m^{2}K)	984
ht (W/m^{2}K)	1638
U (W/m^{2}K)	390
vs (m/s)	0.60
vt (m/s)	1.55

The original solution of Example 2 presents an area of 412 m^2 associated to a fouling resistance of $3.22 \cdot 10^{-5}$ m^{2}K/W (asymptotic fouling condition). The increase of the stream temperatures elevated the area to 585 m^2 and the fouling resistance to $7.04 \cdot 10^{-4}$ m^{2}K/W (maximum fouling condition).

The considerable difference in the heat exchanger area of similar thermal tasks, but associated to different temperature levels, is an indication of the importance of the inclusion of fouling modeling in the heat exchanger network synthesis. An example of the discussion of the relation between network synthesis and fouling modeling can be found in Wilson et al. (2002).

CONCLUSIONS AND SUGGESTIONS

Fouling is an unsolved problem in heat transfer technology. The intensity of the fouling problem depends on the thermo-fluid dynamic conditions associated to the heat exchanger design. However, this aspect of the problem is ignored by the conventional design approach, which is based on the adoption of fixed values of fouling resistances. Therefore, the opportunity to include fouling models at the design phase is the central point of this thesis. An important additional aspect of the proposed approach is the utilization of linear models, which guarantees the identification of the global optimum and avoid the need to identify good initial estimates.

The analysis presented in this thesis involved two types of fouling models. The first model describes the fouling resistance as a function of the temperature and it is typically employed for cooling water streams. The second model describes the fouling rate in relation to the temperature and velocity and it is particularly applied for crude oil streams in distillation units in refineries.

The first model results in an ILP formulation. Numerical tests demonstrate that when compared to other design proceduresusing fixed fouling resistances oriterative schemes, the solution of the proposed ILP problem can reach results associated to lower capital costs.

The second approach yields a MILP formulation. The comparison between the proposed optimization scheme and the optimization using fixed fouling resistances also indicated that the proposed approach can reach solutions associated to lower capital costs. Additional tests using the MILP model also illustrated that the inclusion of the fouling model to the heat exchanger design may help to explore issues related to crude selection, pressure drop optimization, and heat exchanger network synthesis.

Suggestions for continuation of the research presented here may be directed to apply the models developed for the synthesis of heat exchanger networks. Since, the traditional solutions of energy integration problems ignore fouling modelling, the possibility to extend heat exchanger network synthesis models to encompass the relation of each stream match to the corresponding fouling effect would be an important achievement for the state-of-the-art of the process systems engineering literature.

REFERÊNCIAS

ASOMANING, S.; PANCHAL, C. B.; LIAO, C. F. Correlating field and laboratory data for crude oil fouling. *Heat Transfer Eng*., v. 21, p. 17-23, 2000.

BELL, K. J. Exchanger design: based on the Delaware research report. *Petro/Chem*, v. 32, 1960.

BOTT, T. R. *Fouling of Heat Exchangers*. Amsterdam: Elsevier, 1995.

BUTTERWORTH, D. Design of shell-and-tube heat exchangers when the fouling depends on local temperature and velocity. *Applied Thermal Engineering,* v. 22, p. 789-801, 2002.

CAPUTO, A. C. et al. Joint economic optimization of heat exchanger design and maintenance policy. *Applied Thermal Engineering,* v. 31, p. 1381-1392, 2011.

COSTA, A. L. H. et al..Parameter estimation of fouling models in crude preheat trains. *Heat Transfer Eng*., v. 34, p. 683-691, 2013.

CREMASCHI, L. et al. Waterside fouling performance in brazed-plate-type condensers for cooling tower applications. *HVAC&R Research*, v. 17 n.2, p. 198-217, 2011.

EBERT, W.; PANCHAL, C. B. Analysis of Exxon crude-oil-slip stream coking, *Proceedings of mitigation of fouling in industrial heat exchangers*, San Luis Obispo, 1995.

FLOUDAS, C. A. *Nonlinear and mixed-integer optimization*: fundamentals and applications. 1st ed. New York: Oxford University Press, 1995.

GONÇALVES, C. O.; COSTA, A. L. H.; BAGAJEWICZ, M. J. Alternative MILP formulations for shell and tube heat exchanger optimal design. *Ind. Eng. Chem. Res.*, v. 56, p. 5970-5979, 2017.

GONÇALVES, C. O.; COSTA, A. L. H.; BAGAJEWICZ, M. J. Shell and tube heat exchanger design using mixed-integer linear programming. *AIChE J*., v. 63, p. 1907-1922, 2016.

INCROPERA, F.P. et al. *Fundamentals of heat and mass transfer*. 6th.ed. New York: John Wiley & Sons, 2006.

ISHIYAMA, E. M.; PATERSON, W. R.; WILSON, D. I. Thermo-hydraulic channelling in parallel heat exchangers subject to fouling. *ChemEng Sci*. v. 63, n. 13, p. 3400-3410, 2008.

KAKAÇ, S.; LIU, H. Heat Exchanger Selection, Rating and Thermal Design. 2nd ed. Miami: CRC Press. 2002.

KERN, D. Q. Process heat transfer. New York: McGraw-Hill, 1950.

MIZUTANI, F. T. et al.. Mathematical Programming Model for Heat-Exchanger Network Synthesis Including Detailed Heat-Exchanger Designs. 1. Shell-and-Tube Heat-Exchanger Design. *Ind. Eng. Chem. Res,* v. 42, n.17, p. 4009-4018, 2003.

NAKAO, A. et al. Incorporating fouling modeling into shell-and-tube heat exchanger design. *Ind. Eng. Chem. Res,* v. 56, p. 4377-4385, 2017.

NASR, M. R. J.; GIVI, M. M. Modeling of crude oil fouling in preheat exchangers of refinery distillation units. *Applied Thermal Engineering*, v. 26, p. 1572–1577, 2006.

NESTA, J.; BENNETT, C. A. Reduce fouling in shell-and-tube heat exchangers. *Hydrocarbon Processing,* p. 77-82, july, 2004.

PANCHAL, C. B., et al. Threshold conditions for crude oil fouling, In: BOOT, T. R. et al. *Understanding heat exchanger fouling and mitigation*. New York: Begell House, 1999. p. 273–279.

PODDAR, T.K.; POLLEY, G.T. Optimising the design of shell-and-tube heat exchangers, *Chemical Engineering Progress*, September, 2000.

POLLEY, G. T. et al. Design of shell-and-tube heat exchangers to achieve a specified operating period in refinery preheat trains. *Heat Transfer Engineering,* v. 32, n. 3-4, p. 314-319, 2011.

_____. Evaluation of laboratory crude oil threshold fouling data for application to refinery pre-heat Trains. *Applied Thermal Engineering*, v. 22, n. 7, p. 777–788, 2002a.

_____. Use of crude oil fouling threshold data in heat exchanger design. *Applied Thermal Engineering*, v. 22, p. 763-776, 2002b.

_____. Extraction of crude oil fouling model parameters from plant exchanger monitoring. *Heat Transfer Eng.*, v. 28, p. 185-192, 2007.

SAUNDERS, E. A. D. Heat exchangers. New York: John Wiley and Sons Inc., 1988.

SERTH, R. W. *Process heat transfer*: principles and applications. Oxford: Elsevier, 2007.

SHILLING, R. L. Fouling and uncertainty margins in tubular heat exchanger design: an alternative. *Heat Transfer Engineering*, v. 33, n. 13, p. 1094-1104, 2012.

SOUZA, P. A.; COSTA, A. L. H.; BAGAJEWICZ, M. J. Globally optimal linear approach for the design of process equipment: The case of air coolers. *AIChE J.*, v. 64, p. 886-903, 2018.

TABOREK, J. Shell-and-tube heat exchangers:single-phase flow. In: Hewitt, G. F. (Ed.) *Heat exchanger design handbook*. New York: Begell House, 2008a.

TABOREK, J. Survey of shell-side flow correlations. In: Hewitt, G. F. (Ed.) *Heat exchanger design handbook*. New York: Begell House, 2008b.

TEMA. Standards of the tubular exchangers manufactures association. Tubular Exchanger Manufacturers Association, 9th ed., New York, 2007

WILSON, D. I; ISHIYAMA, E. M.; POLEY, G. T. *Twenty years of Ebert and Panchal – what next?*In: International Conference on Heat Exchanger Fouling and Cleaning, 2015.

WILSON, D. I. et al. Mitigation of crude oil Preheat Train Fouling by Design. *Heat Transfer Engineering*, v. 23, p. 24-37, 2002.

APENDIX: SCIENTIFIC PRODUCTION

The scientific production developed during the period of this thesis is showed in this section. Only the first page of the works will be displayed in the same order they are listed.

Conference: XXI Congresso Brasileiro de Engenharia Química – COBEQ 2016. FromSeptember 25th -29th, 2016. Fortaleza, CE, Brasil.

⇒ Title: Otimização da síntese de redes de trocadores de calor considerando o impacto dinâmico da deposição. Authors: Julia C. Lemos, André L. H. Costa, Miguel J. Bagajewicz.

Conference: 27th European Symposium on Computer Aided Process Engineering – ESCAPE 27. October 1st - 5th, 2017, Barcelona, Spain.

⇒ Title: Heat Exchanger Design Optimization Considering Threshold Fouling Modelling. Authors: Julia C. Lemos, André L. H. Costa, Miguel J. Bagajewicz.

Periodic: Applied Thermal Engineering (Elsevier Editorial System), 2017.

⇒ Title: Linear Method for the Design of Shell and Tube Heat Exchangers Including Fouling Modeling. Authors: Julia C. Lemos, André L. H. Costa, Miguel J. Bagajewicz.

Periodic: AICHE JOURNAL, 2018.

⇒ Title: Globally optimal linear approach to the design of heat exchangers using threshold fouling modeling. Authors: Julia C. Lemos, André L. H. Costa, Miguel J. Bagajewicz.

XXI Congresso Brasileiro de Engenharia Química
Fortaleza/CE
25 a 29 de setembro
COBEQ 2016
ENBEQ 2016
XVI Encontro Brasileiro sobre o Ensino de Engenharia Química
Fortaleza/CE
25 a 29 de setembro

OTIMIZAÇÃO DA SÍNTESE DE REDES DE TROCADORES DE CALOR CONSIDERANDO O IMPACTO DINÂMICO DA DEPOSIÇÃO

J. C. LEMOS1, A. L. H. COSTA1 e M. J. BAGAJEWICZ2

[1]Universidade do Estado do Rio de Janeiro, Programa de Pós-Graduação em Engenharia Química
[2]Universityof Oklahoma
E-mail para contato: ju_1512@hotmail.com

RESUMO – *A síntese de redes de trocadores de calor é uma das principais etapas no projeto de uma planta industrial. Estas redes são importantes tanto do ponto de vista econômico, como ambiental, levando a redução de custos, assim como emissões de CO2. Muitos trabalhos foram desenvolvidos visando otimizar sua síntese, porém há vários aspectos ainda não devidamente solucionados no problema. Uma das questões cuja análise ainda é limitada corresponde à avaliação do impacto da deposição na síntese. Neste sentido, o presente trabalho explora técnicas de programação matemática, baseadas no modelo de superestrutura proposto por Yee e Grossmann (1990), modificado para considerar o efeito da deposição ao longo do tempo. O problema a ser resolvido é um problema de programação não-linear inteira mista (MINLP). Devido à sua natureza não-linear, para garantir uma boa convergência é discutida também a aplicação de procedimentos de inicialização.*

1. INTRODUÇÃO

A síntese de redes de trocadores de calor é um dos problemas mais estudados na engenharia química, pois através destas estruturas é promovida a integração energética possibilitando um menor consumo de utilidades. Porém a síntese é um problema complexo devido à sua natureza combinatorial, não-linear e não convexa com múltiplos ótimos locais.

Atualmente a maioria dos projetos de redes de trocadores de calor são realizados utilizando a Tecnologia Pinch, método que pode levar a ótimos locais e excluir alguns arranjos de rede possíveis da região viável, porém coma vantagem de sempre obter um resultado.

Ao longo das décadas de 80 e 90 a Tecnologia Pinch foi discutida de acordo com a sua dependência em relação à localização do pinch. Como alternativa, foram propostas outras abordagens mais complexas utilizando programação matemática, capazes de levar à melhores resultados.

Floudas e Ciric (1989)utilizaram uma abordagem envolvendo a resolução de um problema de

Antonio Espuña, MoisèsGraells and Luis Puigjaner (Editors), Proceedings of the 27th European Symposium on Computer Aided Process Engineering – ESCAPE 27
October 1st - 5th, 2017, Barcelona, Spain

Heat Exchanger Design Optimization Considering Threshold Fouling Modelling

André L. H. Costa[a], Julia C. Lemos[a], Miguel J. Bagajewicz[b*]

[a]*Rio de Janeiro State University (UERJ), Rua São Francisco Xavier, 524, Maracanã, CEP20550-900, Rio de Janeiro, RJ, Brazil*
[b]*School of Chemical, Biological and Materials Engineering, University of Oklahoma, Norman, Oklahoma 73019, USA*
bagajewicz@ou.edu

Abstract

In heat exchangers, fouling is the undesired accumulation of deposits over the equipment thermal surface. This phenomenon causes agradual reduction of the overall heat transfer coefficient. The traditional approach to handle the fouling problem during the design consistsin the introduction of fouling factors in the evaluation of the (dirty) overall heat transfer coefficient. However, this approach ignores the factthat the fouling rate is dependent on the flow velocity and temperature. Aiming to fill thisgap, this paper investigates the optimization of the design of heat exchangers including fouling modelling. Among the many fouling manifestations, this investigation focuses on chemical reaction fouling in crude oil streams associated to the presence of asphaltenes, modelled by a threshold model (EbertPanchalmodel and its variants). According to this model, there are conditions of surface (or film) temperature and flow velocitywhere there is no fouling. The developed formulation of the designproblem employs a mixed integer linear programing approach, where the geometry-related design variables are defined based on standard values. The results are compared with a traditionalapproach with fixed fouling factor, which indicates a potential reduction of capital costs.

Keywords: heat exchangers, design, optimization, fouling.

1. Introduction

In heat exchangers, fouling is the undesired accumulation of deposits over the heat transfer surface, which causes a reduction in the overall heat transfer coefficient. The traditional approach to include the fouling impact in the heat exchanger model during the design phase consists in the insertion of fouling factors into the expression of the (dirty) overall heat transfer coefficient. Tables of fouling factors are available in the literature for different process streams and utilities. However, these values are associated to a considerable level of uncertainty.

Because these limitations, some authors have proposed the utilization of fouling models in the design equations. Butteworth (2002) and Polley et al. (2002a) proposed the identification of the design solution considering the fouling behaviour based on the Ebert-Panchal model (Wilson et al., 2017) using a graph relating the number of tubes and tube length of the available candidate options (Poddar plot).

The focus of the current paper is to present a mathematical programming alternative for shell-and-tube heat exchanger design optimization including fouling modelling. In the

Linear Method for the Design of Shell and Tube Heat Exchangers Including Fouling Modeling

Julia C. Lemos[a], André L. H. Costa[a,], Miguel J. Bagajewicz[b]*

[a]Rio de Janeiro StateUniversity (UERJ), Rua São Francisco Xavier, 524, Maracanã, CEP20550-900, Rio de Janeiro, RJ, Brazil

[b]School of Chemical, Biological and Materials Engineering, University of Oklahoma, Norman, Oklahoma USA 73019

ABSTRACT

Typical heat exchanger design procedures are based on the use of fixed values of fouling factors, mostly based on estimates coming from practice. However, fouling depends on thermofluidynamic conditions (e.g. flow velocity) which values are consequence of the selection of design variables (e.g. baffle spacing). Therefore, the inclusion of fouling models into an optimal design procedure may yield better solutions. In this article, we extend a recent globally optimal linear formulation for the design of shell and tube heat exchangers (Gonçalves et al., 2017) [Ind. Eng. Chem. Res. DOI: 10.1021/acs.iecr.6b04950]. Our extension leads to a linear model and consists on adding velocity dependent fouling factors. A comparison with design examples based on fixed

* Corresponding author.
E-mail address: andrehc@uerj.br (A. Costa)

Globally Optimal Linear Approach to the Design of Heat Exchangers Using Threshold Fouling Modeling

Julia C. Lemos and André L. H. Costa
Institute of Chemistry, Rio de Janeiro State University (UERJ) Rua São Francisco Xavier, 524, Maracanã, Rio deJaneiro. RJ, CEP 20550-900 Brazil

Miguel J. Bagajewicz
School of Chemical, Biological and Materials Engineering, University of Oklahoma, Norman Oklahoma 73019

This article presents a method for the mathematical optimization of the design of heat exchangers including fouling rate modeling for the tube-side. The description of the fouling rate in crude preheat trains of petroleum distillation units is commonly based on threshold models (Ebert-Panchal model and its variants). Our formulation of the design problem employs a mixed integer linear programing approach; therefore the solution is the global optimum and common nonconvergence drawbacks of mixed-integer nonlinear programming models are totally avoided. Three different examples are employed to compare the proposed approach with an optimization procedure using fixed fouling resistances. The results indicate that in two problems was possible to obtain design solutions associated to smaller heat exchangers. Additionally, three case studies are also explored to discuss how fouling is related to crude types, pressure drop manipulation, and energy integration.

Correspondence concerning this article should be addressed to A. L. H. Costa at andrehc@uerj.br